

**Aus dem Zentrum für Tumor- und Immunbiologie
des Fachbereichs Medizin der Philipps-Universität Marburg**

Geschäftsführender Direktor: Prof. Dr. Rolf Müller

Titel der Dissertation:

Role of BCAM in ovarian cancer metastasis

zur Erlangung des Doktorgrades der Naturwissenschaften
(Dr. rer. nat.)

vorgelegt von

Suresh Sivakumar
aus Puducherry, Indien

Marburg, 2023

Angenommen vom Fachbereich Medizin der Philipps-Universität Marburg am:
19.07.2023

Gedruckt mit Genehmigung des Fachbereichs Medizin

Dekanin: Prof. Dr. Denise Hilfiker-Kleiner

Referent: Prof. Dr. Rolf Müller

1. Korreferent: Dr. Jörg - Walter Bartsch

Table of Contents

• CHAPTER 1 - ABSTRACT	5
1.1 English abstract.....	5
1.2 German abstract.....	6
• CHAPTER 2 - INTRODUCTION	8
2.1 Ovarian cancer.....	8
2.2 Tumor microenvironment	9
2.3 Mediators and proteases in TME	9
2.4 Structural and functional features of BCAM	10
2.5 BCAM in cancer	11
2.6 Aim of the thesis.....	12
• CHAPTER 3 – PUBLICATION SUMMARY	14
3.1 Basal cell adhesion molecule promotes metastasis-associated processes in ovarian cancer	14
3.2 Results	14
3.2.1 Association of OC progression with BCAM expression and the ascites levels of its soluble form	14
3.2.2 Inhibition of OC cell adhesion, migration and motility by membrane-bound and soluble BCAM	15
3.2.3 Expression of metalloproteinases in OC cells	16
3.2.4 Role of ADAM 10 and ADAM 17 ectodomain shedding of BCAM.....	17
3.2.5 Identification of ADAM 10 cleavage sites in BCAM.....	17

3.2.6 Immunohistochemical staining of BCAM, LAMA5 and collagens in OC metastases and matched spheroids	18
3.2.7 Inhibition of OC cell spheroid compaction by membrane-bound and soluble BCAM.....	19
3.2.8 Interference of BCAM with LN-511 – integrin β 1 interaction in spheroids ...	20
3.2.9 Promotion of spheroid dispersion and mesothelial clearance by BCAM	20
3.2.10 BCAM-mediated enhancement of spheroid invasion into the omentum.....	21
3.3 Discussion.....	22
3.3.1 BCAM as a key mediator of HGSC progression in ascites.....	22
3.3.2 ADAM 10 and ADAM 17 mediated shedding of BCAM	22
3.3.3 Role of BCAM in metastasis.....	23
3.3.4 Function of BCAM as a decoy receptor	25
3.3.5 BCAM as a novel target for translational approaches in cancer therapy	26
3.4 My contributions	28
• CHAPTER 4 – ABBREVIATIONS.....	29
• CHAPTER 5 – REFERENCES.....	31
• CHAPTER 6 – APPENDICES.....	38
• CHAPTER 7 – MANUSCRIPT	44

1.1 English abstract

Ovarian cancer (OC) is one of the deadliest gynecological malignancies due to its early and wide-spread peritoneal dissemination, with the omentum being the preferred site of metastasis. The underlying molecular mechanisms are not yet fully understood. Basal cell adhesion molecule (BCAM) is a laminin $\alpha 5$ (LAMA5) binding protein. BCAM is expressed in multiple forms in OC, including the full-length protein (BCAM1), a splicing variant lacking the cytoplasmic domain (BCAM2) and soluble BCAM (sBCAM). Although BCAM is associated with a poor survival of OC, its contribution to peritoneal metastasis remains elusive.

In this study, we identified ADAM10 as a major BCAM sheddase produced by OC cells and determined the proteolytic cleavage sites. All BCAM forms interfered with the interaction of LAMA5 with integrin $\beta 1$ to inhibit the adhesion and migration of tumor cells on a LAMA5-containing matrix, indicating the functionality of both membrane-bound and soluble BCAM. It is, however, unlikely that this effect of BCAM on adherent tumor cells significantly affects peritoneal dissemination of OC cells, as suggested by several lines of evidence: (i) the known essential function of collagen I (COL1) rather than laminins in the adhesion of OC cells to peritoneal organs; (ii) our observation that BCAM had no detectable effect on COL1-dependent OC cell adhesion; and (iii) the known pivotal role of tumor cell spheroids rather than single cells in metastatic dissemination.

We discovered, however, that all forms of BCAM negatively regulate the compactness of LAMA5-rich tumor cell spheroids, thereby promoting their dispersion in a three-dimensional collagen matrix, which in turn facilitates the clearance of mesothelial cells and promotes their trans-mesothelial invasion into the omentum. Importantly, we also observed a significant association between BCAM expression and a poor clinical outcome in OC, highlighting the potential translational relevance of these findings.

In summary, our study provides new mechanistic insights into the role of BCAM in ovarian cancer progression and highlights its potential as a therapeutic target for peritoneal metastasis.

1.2 German abstract

Das Ovarialkarzinom ist eine der tödlichsten gynäkologischen Krebserkrankungen aufgrund seiner frühen peritonealen Ausbreitung mit dem Omentum als primärem Ort der Metastasierung. Die zugrunde liegenden molekularen Mechanismen sind noch nicht vollständig geklärt. Das *Basal Cell Adhesions Molecule* (BCAM) ist ein Laminin $\alpha 5$ (LAMA5)-bindendes Protein. BCAM wird im OC in mehreren Formen exprimiert, darunter das Volllängenprotein (BCAM1), eine Spleißvariante, der die zytoplasmatische Domäne fehlt (BCAM2) und lösliches BCAM (sBCAM). Obwohl BCAM mit einem schlechten Überleben des OC assoziiert ist, war sein Beitrag zur Peritonealmetastasierung zu Beginn der vorliegenden Arbeit ungeklärt.

In dieser Studie wurde ADAM10 als eine wichtige von OC-Zellen produzierte BCAM-Sheddase identifiziert und die proteolytischen Spaltstellen bestimmt. Alle BCAM-Formen beeinträchtigten die Interaktion von LAMA5 mit Integrin $\beta 1$. Dies führte zur Hemmung der Adhäsion und Migration von Tumorzellen auf einer LAMA5-haltigen Matrix, was die Funktionalität sowohl der membrangebundenen als auch der löslichen BCAM-Formen aufzeigt. Es ist jedoch unwahrscheinlich, dass diese Wirkung von BCAM auf adhärenzte Tumorzellen die peritoneale Disseminierung von OC-Zellen signifikant beeinflusst, was nahelegt wird durch: (i) die bekannte essentielle Funktion von Kollagen I (COL1) und nicht von Lamininen bei der Adhäsion von OC-Zellen an peritoneale Organe; (ii) unsere Beobachtung einer nicht nachweisbaren Wirkung von BCAM auf die COL1-abhängige OC-Zelladhäsion; und (iii) die etablierte zentrale Rolle von Tumorzell-Sphäroiden (im Gegensatz zu Einzelzellen) bei der metastatischen Dissemination.

Wir entdeckten jedoch, dass alle Formen von BCAM die Kompaktheit von LAMA5-reichen Tumorzell-Sphäroiden negativ regulieren und dadurch ihre Dispersion in einer dreidimensionalen Kollagenmatrix fördern. Dies erleichterte wiederum die Disruption eines Mesothelzell-Monolayers und förderte die trans-mesotheliale Invasion von Tumorzellen in das Omentum. Darüber hinaus beobachteten wir einen signifikanten Zusammenhang zwischen BCAM-Expression und einem schlechten klinischen Ergebnis, was die potenzielle translationale Relevanz dieser Ergebnisse unterstreicht.

Zusammenfassend lässt sich sagen, dass die vorliegende Arbeit neue mechanistische Erkenntnisse über die Rolle von BCAM bei der Progression des OCs liefert und sein Potenzial als therapeutisches Ziel für Peritonealmetastasen hervorhebt.

2.1 Ovarian cancer

Ovarian cancer (OC) is one of the deadliest forms of gynecological cancer in women [Worzfeld et al., 2017]. Every year, 239,000 new cases are reported worldwide [Reid et al., 2017]. As a result of its low survival rate, it is responsible for 5% of cancer-related fatalities in women [Torre et al., 2018]. Often, diagnosis occurs at a later stage of the disease. Around 70% of cases are detected after the disease has progressed to stage III or IV [Stewart et al., 2019]. Current screening approaches are not sensitive enough to detect OC at an early stage [Buys et al., 2011]. Although it is termed OC, its cellular origin is still in debate [Auersperg et al., 2008]. Earlier, it was thought that cancer might develop from cells in the epithelial surface layer of the ovary. However, recent studies have suggested that cancer cells rather originate from cells of the fallopian tubes [Dubeau, 2011].

High-grade serous ovarian cancer (HGSC) is the most common form of OC. It alone reports 70 to 80% of OC deaths [Bowtell et al., 2015]. HGSC cells are aggressive, and often they have metastasized at the time of diagnosis [Kim et al., 2012]. The standard treatment procedure for HGSC includes a combination of platinum-based chemotherapy (cisplatin and carboplatin) and surgery [Strandmann et al., 2017; Kleih et al., 2019]. Even though the majority of HGSC patients respond well to the initial treatment, most of them relapse and become resistant to chemotherapy [Lisio et al., 2019].

For most cancer cells to metastasize, they must undergo a series of cellular transformations to migrate, invade, extravasate, and re-initiate themselves as a colony at a distant site. This type of metastasis requires dissemination via the blood and/or lymphatic vessel system. In contrast, in HGSC the primary route of metastasis occurs passively by peritoneal spread rather than lymphatic or hematogenous dissemination [Lengyel et al., 2010]. Tumor cells and spheroids detach from the primary site and float in the peritoneal fluid to disseminate and attach to the organs in the peritoneal cavity with the omentum as the preferential site [Kim et al., 2012].

2.2 Tumor microenvironment

The tumor microenvironment (TME) in the peritoneal cavity of OC is unique and complex. It consists of both liquid-state ascites and solid-state metastatic niches [Mei et al., 2023]. It comprises extracellular matrix components and various cell types of both cancerous and non-cancerous origins, the latter including host stromal cells and immune cells, which interact to promote OC progression [Yang et al., 2020].

Malignant ascites is an accumulation of peritoneal fluid within the peritoneal cavity to a larger volume. It is present in more than 90% of patients with advanced stages of OC, and it is considered as a major hallmark of this malignancy [Ford et al., 2020; Kim et al., 2016]. Upregulation of vascular endothelial growth factor (VEGF) causes blood vessel dilation and permeability, driving ascites fluid accumulation [Ford et al., 2020]. Most OC metastases occurs via the peritoneal cavity. Ascites fluid is rich in cellular and acellular factors as well as extracellular vesicles (EVs), playing essential roles in tumor metastasis, chemoresistance, and immune evasion [Finkernagel et al., 2019; Piché. 2018]. Ascites promotes metastasis by downregulating tight-junction proteins (E-cadherin, occludin, etc.) of mesothelial cells, thereby supporting transmesothelial invasion by tumor cells [Mikula et al., 2017]. Accumulating evidence suggests that ascites promotes epithelial-to-mesenchymal transition (EMT) of tumor cells. EMT drives tumor cells to acquire features of mesenchymal cells, which are essential for invasion and metastasis [Pakula et al., 2019].

Tumor cells in ascites are primarily present as spheroids [Wintzell et al., 2012]. Their interaction with peritoneal mesothelial cells (HPMCs) in ascites is essential for OC metastasis [Pasquet et al., 2010]. HPMCs also produce factors that promote chemoresistance in OC cells [Matte et al., 2014].

2.3 Mediators and proteases in TME

The cells of the TME interact with each other and secrete a range of mediators, which play a critical role in tumor growth, metastasis, and immune suppression. These mediators include cell adhesion molecules, proteases, cytokines, chemokines, growth factors and extracellular vesicles [Worzfeld et al., 2017]. However, traditional mass-spectrometry-based proteomics faces limitations in studying unfractionated ascites or

plasma samples due to the high abundance of blood proteins, in particular albumins and globulins. This has hindered a comprehensive understanding of the mediators impacting HGSC progression until the recent development of more appropriate technologies [Finkernagel et al., 2019].

In previous studies, our group utilized advanced affinity proteomics technologies such as the aptamer-based SOMAscan platform and the antibody-based "Proximity Extension Assay" (PEA) technology to overcome these limitations [Finkernagel et al., 2019; Graumann et al., 2019]. Analysis of the proteome of ascites and plasma samples from HGSC patients identified important mediators that play critical roles in HGSC progression, including secreted proteins, membrane receptors, and intracellular proteins. The generated datasets provided valuable insights into the tumor microenvironment of HGSC and the roles of various mediators in promoting tumor growth, metastasis, and immune suppression.

One protein of particular interest identified in these studies is BCAM, which was found to be upregulated in HGSC plasma and ascites and was associated with a poor RFS. BCAM is an adhesion molecule that plays a crucial role in the remodeling of the extracellular matrix (ECM) and has been shown to affect cancer cell migration and invasion in other malignancies. Its upregulation in HGSC plasma and ascites suggests a potential role in the metastatic process of OC [Finkernagel et al., 2019; Graumann et al., 2019].

2.4 Structural and functional features of BCAM

Basal cell adhesion molecule (BCAM), or CD239, is a type of cell adhesion molecule that carries the antigens for the Lutheran blood group system. Therefore, it is also termed "Lutheran blood group glycoprotein" [Guadall et al., 2019]. BCAM is located on chromosome 19q13.2 [Campbell et al., 1994]. It is a transmembrane protein that belongs to the immunoglobulin superfamily (IgSF) [Burton et al., 2008], characterized by their immunoglobulin (Ig)-like domains [Niu et al., 2019]. IgSF is one of the largest and most diverse protein families, including many cell-surface and soluble proteins. They are involved in numerous cellular processes [Wojtowicz et al., 2020] and have also been identified as cancer biomarkers [Wai Wong et al., 2012]. BCAM, a member of the IgSF, is expressed in different cell types and figures in multiple human diseases,

including different carcinomas, sickle cell disease, preeclampsia and glomerulonephritis [Liu et al., 2022].

BCAM consists of a cytoplasmic domain, a transmembrane domain and an extracellular domain. The cytoplasmic domain of BCAM has two variable amino acid stretches that distinguish the two BCAM isoforms: (i) BCAM1 or Lu (85 kDa), with 59 amino acids in its cytoplasmic domain, and (ii) BCAM2 or Lu(v13) (78 kDa) with 19 amino acids. In its extracellular part, BCAM has two variable (V) and three constant (C2) Ig-like domains [Kikkawa et al., 2005].

The full-length protein BCAM1 has a SH3 binding motif and potential phosphorylation sites in its cytoplasmic tail, suggesting a role in intracellular signalling pathways. In sickle red blood cells, protein kinase A-dependent (PKA) phosphorylation of BCAM1 is reported, and this phosphorylation plays a critical role in the adhesion of sickle red blood cells to LAMA5 [Gauthier et al., 2005]. BCAM2 is a shorter version of BCAM, lacking 40 amino acids in its cytoplasmic region [Gauthier et al., 2010]. Both BCAM forms (BCAM1 and BCAM2) bind to laminin $\alpha 5$ (LAMA5). This indicates that the full-length cytoplasmic domain of BCAM1 is not needed for LAMA5 binding. BCAM can also interact with the cytoskeleton protein spectrin, thereby impacting actin cytoskeleton rearrangement [Collec et al., 2011].

2.5 BCAM in Cancer

BCAM is a glycoprotein associated with poor prognosis in various cancers. Evidence suggests that BCAM is involved in many biological processes, including adhesion, migration and invasion of tumor cells, suggesting an essential role in tumor progression [Jin et al., 2020]. BCAM competes with integrins for binding to LAMA5, and this competitive interaction may enhance tumor cell migration on LAMA5 by weakening integrin binding [Kikkawa et al., 2013]. BCAM and laminin are also co-expressed in epithelial skin cancer, where BCAM has been reported to enhance the haptotactic migration of tumor cells on a laminin matrix, indicating that the interaction between BCAM and laminin may accelerate the progression of epithelial skin tumors. [Drewniok et al., 2004].

In gastric cancer (GC), BCAM expression is significantly upregulated by BCAM-sense long noncoding RNA (*BAM*) [Jin et al., 2020]. Metastasis progression and poor

prognosis of GC patients are substantially associated with elevated levels of BCAM and its lncRNA *BAN*. Genetic disruption of *BCAM* reduced GC migration and invasion, and interference with *BAN* expression inhibited GC migration and invasion, which was reversed by ectopic expression of BCAM [Jin et al., 2020].

BCAM and LAMA5 are overexpressed in KRAS-mutant colorectal cancer. Studies have shown that the interaction between BCAM and its ligand LAMA5 mediates the metastatic spread of KRAS-mutant colorectal cancer by facilitating recognition between tumor cells and TME [Bartolini et al., 2016].

In OC, elevated BCAM expression has been found to correlate with poor relapse-free survival [Finkernagel et al., 2019], but its role in OC had not been addressed prior to the present study [Sivakumar et al., 2023].

2.6 Aim of this thesis

The aim of this project was a comprehensive investigation of the role of BCAM and its different forms (BCAM1, BCAM2, sBCAM) in the metastatic spread of ovarian carcinoma (OC) within the peritoneum. The project addressed several key questions summarized below.

1. identifying the source of soluble BCAM (sBCAM) and the proteolytic enzymes responsible for its production in OC cells;
2. investigating the functional differences and commonalities of membrane-bound BCAM isoforms and sBCAM in single-cell adhesion, migration, and metastasis-related functions;
3. evaluating the impact of different BCAM forms on tumor cell spheroid compactness, spheroid dispersion in a three-dimensional (3D) collagen matrix and the clearance of mesothelial cells in vitro;
4. assessing the influence of BCAM forms on the invasion of tumor cell spheroids into omental tissue using explanted omentum and a mouse model of peritoneal colonization (collaborative work);
5. understanding the molecular mechanisms through which BCAM modulates LAMA5-integrin- β 1-dependent compaction and trans-mesothelial invasion.

These questions were addressed by a combination of biochemical, omics-based and real-time cell assays, as well as loss- and gain-of-function experiments in OC cells, explanted omentum and a mouse model of peritoneal colonization. The overarching aim of this study was to identify novel potential therapeutic options by gaining detailed insights into the role of BCAM in OC metastasis.

3.1 Basal cell adhesion molecule promotes metastasis-associated processes in ovarian cancer

Suresh Sivakumar*, Sonja Lieber, Damiano Librizzi, Corinna Keber, Leah Sommerfeld, Florian Finkernagel, Katrin Roth, Silke Reinartz, Jörg W. Bartsch, Johannes Graumann, Sabine Müller-Brüsselbach and Rolf Müller (2023). Basal cell adhesion molecule promotes metastasis-associated processes in ovarian cancer. *Clinical and Translational Medicine* 13:e1176. Doi: 10.1002/ctm2.1176

The study focused on understanding the BCAM involvement in peritoneal metastases of OC. BCAM is expressed as membrane-bound (BCAM1 and BCAM2) and cleaved (sBCAM) forms. We discovered that ADAM10 and ADAM17 are involved in BCAM shedding, with ADAM10 being the most prevalent BCAM sheddase produced by OC cells. Peritoneal dissemination of OC occurs primarily through tumor cell spheroids. This study reveals that the LAMA5–integrin- β 1 interaction is necessary for spheroid compaction and that all BCAM forms diminish spheroid compaction by preventing this necessary interaction. This results in the formation of loose spheroids promoting spheroid dispersion in a collagen matrix as well as mesothelial clearance, which in turn facilitates invasion at the site of metastasis. These findings may explain the association between BCAM and poor survival of patients with OC.

3.2 Results

3.2.1 Association of OC progression with BCAM expression and the ascites levels of its soluble form

TCGA transcriptome analysis revealed that OC has the highest *BCAM* mRNA expression compared to other cancer entities (Fig. S1A in Sivakumar et al., 2023). High *BCAM* expression correlates with poor RFS in OC, as shown by the Kaplan–Meier plot in Fig. S1C. Data obtained from PRECOG datasets demonstrated the relationship between *BCAM* expression and overall survival in all human malignancies. Increased *BCAM* expression is associated with a poor prognosis (red bars) in OC, glioma, and leukemia. In contrast, *BCAM* is associated with improved survival (blue bars) in lung adenocarcinoma (Fig. S1B). In addition, SOMAscan-based proteomic analysis of the ascites from patients with HGSC showed that increased

BCAM levels in OC ascites are associated with a poor RFS (Fig. 1C), similar to RNA expression in tumor tissue (Fig. S1C).

Immunoblot analysis was performed to determine the BCAM forms in ascites. A 95-kDa band representing membrane-associated BCAM1/2 was observed in whole-cell lysates, while a shorter BCAM form of 80 kDa (sBCAM) was present in conditioned media from BCAM-expressing cell lines. In ascites, the 80 kDa band is abundant suggesting that sBCAM form is the predominant form (Fig. 1A). Moreover, BCAM levels in ascites determined by enzyme-linked immunosorbent assay (ELISA) correlated well with immunoblot signal intensities for sBCAM. sBCAM levels in ascites from $n = 70$ patients varied over a range of 0 - 526 ng/ml, with a median level of 76 ng/ml (Fig. 1B).

3.2.2 Inhibition of OC single cell adhesion, migration, and motility by membrane-bound and soluble BCAM

BCAM is crucial for cell adhesion, migration, and motility on LAMA5 matrices in several pathological situations [Bartolini et al., 2016; Kikkawa et al., 2013; Gauthier et al., 2005]. Laminin 511 (LN-511), an ECM protein composed of three heterotrimeric subunits consisting of $\alpha 5$, $\beta 1$, and $\gamma 1$ chains. It is expressed by tumor and host cells from OC ascites and omental metastases (Fig. S3A) as well as in OVCAR cell lines (Fig. S3B). BCAM is a recognized receptor for LAMA5 and its interaction with LAMA5 plays a key role in various pathological conditions [Jin et al., 2020; Bartolini et al., 2016].

To test the effects of sBCAM, we used recombinant Fc-BCAM, a stable fusion protein consisting of the extracellular part of BCAM and the Fc portion of human IgG1 with the capacity to bind to LAMA5 [Kikkawa et al., 2013]. The real-time impedance-based system, xCELLigence, was used for adhesion and migration assays. Unidirectional cell motility was assessed by spinning disc microscopy. Live video captures of random cell movements were processed by Imaris image analysis software, and cell motility was calculated and graphed.

To compare the biological and functional properties of different BCAM forms, we analyzed their effects on cell adhesion, migration, and motility in OVCAR cells. Two BCAM isoforms, long (BCAM1) and short (BCAM2), were ectopically expressed in

OVCAR8 cells (Fig. S4) that have moderate levels of endogenous BCAM (Fig. S10B). OVCAR8 cells overexpressing BCAM1 or BCAM2 as well as wild-type cells exposed to Fc-BCAM exhibited decreased adhesion to LN-511 (Figs. 1C and 1D), whereas no significant difference was observed in collagen adhesion (Figs. S6E and S6F). In addition, migration and motility assays demonstrated a similar pattern to the adhesion assays (Figs. 1E and S8).

In agreement with these findings, *BCAM* gene disruption or inhibition by siRNA resulted in enhanced attachment and migration (Figs. S6C, S6D, and S8C). Interestingly, we observed a consistent effect on adhesion, migration, and motility by all forms of BCAM, including BCAM2 and sBCAM, which indicates that BCAM does not act as a signaling receptor to inhibit LN-511-dependent function. Our findings are consistent with a previous study proposing that BCAM competitively interferes with LAMA5–integrin binding [Kikkawa et al., 2013].

3.2.3 Expression of metalloproteinases in OC cells

Immunoblot results showed that ascites contains sBCAM (Fig. 1A). As metalloproteinases frequently participate in the shedding of membrane-bound proteins, we analyzed the protein levels of the most prevalent matrix metalloproteinases (MMPs and ADAMs) using our published dataset generated from tumor cells in OC ascites. Among all ADAMs, ADAM10 and ADAM17 were prevalent in whole-cell extracts (Fig. 2A). Moreover, secretome data revealed the highest levels for ADAM10, whereas ADAM9 and ADAM17 were present at a moderate level (Fig. S9A). Our proteome and secretome data from ascites tumor cells suggest that ADAMs may be involved in BCAM cleavage, which we addressed experimentally below.

In order to determine the suitability of using OVCAR cell lines as model systems for our experiments, we analyzed the expression of *ADAM* genes in published datasets for these cells (data from [Worzfeld et al., 2018] and [McCorkle et al., 2021]). ADAM9, ADAM10, ADAM15 and ADAM17 were strongly expressed in all four OVCAR cells (OVCAR3, OVCAR4, OVCAR5 and OVCAR8), whereas other ADAMs were weakly expressed (Fig. S9B). Furthermore, we performed immunoblotting of ADAM10 to verify the RNA sequencing results, which revealed the active form of ADAM10 in OVCAR4, OVCAR5 and OVCAR8 (Fig. S10A), consistent with our previously

described primary tumor cell proteome data (Fig. 2A). Although OVCAR5 showed the highest ADAM10 expression, it hardly expressed BCAM (Fig. S10B), which is inconsistent with the high BCAM expression in primary tumor cells (Fig. 2A). Hence, OVCAR5 was excluded from further experiments.

3.2.4 Role of ADAM10 and ADAM17 ectodomain shedding of BCAM

OVCAR4 cells exhibited the highest levels of endogenous BCAM (Fig. S10B) and sBCAM in conditioned media among all OVCAR cells (ELISA data not shown). Therefore, it was used in all subsequent experiments. Treatment with marimastat (a broad-spectrum metalloproteinase inhibitor) diminished BCAM shedding in a concentration-dependent manner (approximately 85% at 1 μ M), as confirmed by immunoblotting and ELISA (Fig. S11).

Our proteome and secretome data indicated a potential involvement of ADAM10 and ADAM17 in BCAM shedding (Figs. 2A and S9). To test this hypothesis, we used recombinant ADAM10 prodomain as a selective ADAM10 inhibitor [Moss et al., 2007]. The ADAM10 prodomain inhibited BCAM shedding by 88%. A similar effect was observed by siRNA interference with ADAM10, which inhibited BCAM shedding by 85% (Figs. 2B, 2C, 2D, and S10D). Additionally, ADAM17 siRNA significantly inhibited BCAM shedding by 35% (Figs. 2E and S10D). Our data indicate that ADAM10 and, to a lesser extent ADAM17, contribute to BCAM shedding.

3.2.5 Identification of ADAM10 cleavage sites in BCAM

We used recombinant proteins to identify the ADAM10 cleavage sites in BCAM. Human recombinant Fc-BCAM was incubated with recombinant ADAM10, which yielded two fragments. The metalloproteinase ADAM10 requires zinc for proteolytic activity. In the presence of the zinc chelator TPEN, no fragments were observed, proving the specificity of the ADAM10 cleavage reaction. The cleaved fragments were analyzed by MS, which identified three cleavage sites near the transmembrane region (Fig. 2G, red stars; sites 1, 2, and 3) and three cleavage sites in BCAM from conditioned medium of primary OC cells (Fig. 2G, black stars; sites 3, 4, and 5). A cleavage site obtained with the recombinant protein (site 3) coincided with the cleavage site of the conditioned medium from the OC cells and differs from the published cleavage site of MMP14 (Fig. 2G, a blue star).

To investigate the involvement of ADAM10 in BCAM cleavage, we attempted to align sites 1–5 with sequences known to be recognized by ADAM10. However, ADAM10 recognizes various motifs and does not have a specific consensus sequence that allows the prediction of substrate recognition and cleavage sites. We therefore used two unbiased screening approaches to identify the preferred amino acids around the ADAM10 cleavage sites [Caescu et al., 2009; Tucher et al., 2014]. The obtained data were tabulated to differentiate between weakly and strongly enriched amino acids. (Fig. S12A). Subsequently, we matched BCAM cleavage sites 1–5 with this data (Fig. S12B) and found substantial similarities between sites 3–5 and the preferred amino acids, indicating that these sites are most likely involved in ADAM10 cleavage. However, sites 4 and 5 found *in vivo* were missed in the *in vitro* study, presumably because of their location near the C-terminus which is fused to the Fc part for stability (Fig. 2G). Sites 1 and 2 weakly matched with the known amino acid preferences (Fig. S12B) and were not observed *in vivo*, suggesting that they play a minor role in BCAM shedding by ADAM10, if any. These results indicate that the major ADAM10 cleavage sites are likely the sites close to the transmembrane domain (site 3 and possibly sites 4 and 5).

Our findings and the published data indicate that BCAM is cleaved by three metalloproteinases close to the transmembrane domain (MMP14, ADAM10, and ADAM17), suggesting that sBCAM in ascites represents a mixture of different fragments of variable length and C-termini. Although the exact length of these proteins with a molecular weight of 70 kDa has not yet been determined, it is quite probable that these proteins preserve the LAMA5-binding site, which is distant from the cleavage sites and functionally important to the present investigation.

3.2.6 Immunohistochemical staining of BCAM, LAMA5 and collagens in OC metastases and matched spheroids

To unravel our understanding of OC progression and metastasis, we investigated the expression and localization of BCAM, LAMA5 and collagen I (COL1) in OC metastasis samples and their corresponding ascites tumor spheroids from eight patients by immunohistochemistry (IHC). Figures 3 and S13 depicts examples of IHC staining.

Table 2 shows a summary of the IHC staining analysis, and Table S2 lists patients' clinical details.

The summary of Figures 3, S13, and Table 2 is as follows:

- 1) BCAM was highly expressed in ascites tumor spheroids and in both the tumor and stromal regions of OC metastases (slight intersample variability is noticed).
- 2) Tumor spheroids had a significant amount of LAMA5 expression. In contrast, the stromal regions of the metastases displayed an entirely negative staining pattern. The tumor regions of metastases, except for two samples (OC84 and OC122), also lacked LAMA5 expression (Table 2).
- 3) In patient OC114, tumor cells in early metastases (recently formed tumors that remain near the surface of the tissue) were LAMA5-positive and resembled tumor spheroids more closely than tumor cells in advanced metastases (deeply invaded tumor masses), consistent with a role for spheroids in metastasis formation.
- 4) COL1 was strongly expressed in tumor spheroids and stromal regions of OC metastases.

Our results agree with the proposed role for COL1 in OC metastasis [Shen et al., 2012; Alkmin et al., 2020; Huang et al., 2020; Lyu et al., 2021], and indicate that LAMA5 may play a particular role in spheroids, with potential implications for the function of BCAM.

3.2.7 Inhibition of OC cell spheroid compaction by membrane-bound and soluble BCAM

As described above, BCAM had inhibitory effects on the adherence and migration of individual tumor cells (Figs. 1D, 1E, S6, S7, and S8), but these effects cannot explain its association with a short RFS. However, ascites-borne spheroids rather than single tumor cells are known to be pivotal in transcoelomic spreading. We therefore examined spheroids formed by OVCAR8 cells overexpressing BCAM1 and BCAM2, and observed a decrease in compactness (Fig. 4A), reduced circularity (Fig. 4B) and increased gap formation (Fig. 4C).

In agreement with these observations, the genetic disruption of BCAM in OVCAR8 cells (Fig. 4C) and the inhibition of BCAM by siRNA in OVCAR4 (Fig. 4D) and

OVCAR3 (Fig. S14) cells increased spheroid compactness. Exposure of OVCAR8 cells to Fc-BCAM yielded similar results to BCAM overexpression (OE), i.e., reduced spheroid compactness (Fig. 4E). These findings indicate that BCAM may function as a LAMA5-interacting protein in spheroid formation and dynamics. Consistent with this hypothesis, we observed deposits of LAMA5 in tumor cell spheroids from OC patients (Fig. 3).

3.2.8 Interference of BCAM with LN-511 – integrin- β 1 interaction in spheroids

In view of these results, we examined the possibility of BCAM affecting spheroid compaction by interfering with the LAMA5–integrin- β 1 interaction in spheroids. In particular, the use of an integrin- β 1-activating antibody significantly counteracted the inhibitory effects by ectopic BCAM1 or BCAM2 expression in four separate clones. Moreover, the addition of recombinant LN-511 (soluble LN-511) to the BCAM clones substantially mitigated the BCAM-induced effect, resulting in compact spheroids (Figs. 5A–F). Additionally, an integrin- β 1-blocking antibody inhibited the compaction of wild-type OVCAR8 spheroids (Figs. 5G and 5H), similar to the effect of BCAM overexpression, indicating that integrin accessibility is essential for spheroid formation. These findings imply that BCAM may regulate spheroid dynamics by impeding spheroid compaction through competing with integrin- β 1 for LAMA5 binding.

3.2.9 Promotion of spheroid dispersion and mesothelial clearance by BCAM

We next investigated the role of BCAM in spheroid dispersion in a three-dimensional COL1 matrix and disruption of a mesothelial cell monolayer, both of which mimic essential processes in peritoneal organ invasion [Kenny et al., 2011].

Our results show that OVCAR8 cells overexpressing BCAM1 and BCAM2 exhibited significantly enhanced spheroid dispersion within the collagen matrix compared to vector control cells. This effect was observed using two distinct clones for each condition (Figs. 6A and 6B). The addition of exogenous LN-511 during spheroid formation blocked BCAM-induced spheroid dispersion, suggesting that the role of BCAM in this process is related to its inhibitory impact on LAMA5-dependent spheroid compaction (Figs. 6C and 6D).

Further investigations explored the potential involvement of BCAM in mesothelial cell clearance using cocultures of spheroids with mesothelial monolayers. These studies revealed that OVCAR8 cells overexpressing BCAM1 and BCAM2 efficiently induced gaps in the mesothelial cell monolayer compared to control cells (Figs. 7A and 7B). This effect was not observed with Fc-BCAM (results not shown), indicating that the impact of BCAM on mesothelial cells likely resulted from its expression on tumor cells rather than soluble BCAM shed by these cells. Notably, adding LN-511 during spheroid formation blocked BCAM-induced mesothelial clearance, likely owing to reduced spheroid dispersion (Figs. 7C and 7D).

Taken together, these findings suggest that BCAM-mediated spheroid dispersion promotes transmesothelial invasion, possibly through weakened intraspheroidal cohesion dependent on integrin- β 1 – LAMA5 interactions. These results provide valuable insights into potential mechanisms underlying transcoelomic metastasis formation and highlight the significance of BCAM in spheroid dynamics.

3.2.10 BCAM-mediated enhancement of spheroid invasion into the omentum

To validate the *in vitro* observations on the impact of BCAM on spheroids in the context of transcoelomic metastasis, we used an adapted *ex vivo* mouse omentum model [Khan et al., 2010]. Maintaining the integrity of the organ under investigation was crucial for generating reliable data from *ex vivo* models, particularly for mesothelial cells vulnerable to activation and early senescence under stressful conditions [Książek et al., 2008].

Our experiments revealed that standard culture conditions led to an abnormal tissue state, as evidenced by the increased activation marker VCAM1 in mesothelial cells (Fig. S15A). We found that the use of delipidized serum under hypoxic conditions considerably reduced the abnormal induction of VCAM1 (Fig. S15B), and applied these optimized conditions in subsequent experiments.

Using light-sheet microscopy, we observed that OVCAR8-OE cells overexpressing BCAM1 invaded the omentum with significantly higher efficiency (approximately tenfold median) compared to control cells (Figs. 8A, 8B, and 8C). This invasion was evident in milky spots (the preferred sites of OC metastasis) [Khan et al., 2010; Platell et al., 2000], as well as areas distant from milky spots (arrows in Fig. 8B). Multiphoton

microscopy further corroborated that tumor cells invaded submesothelial collagen regions in the omentum, irrespective of milky spots (Figs. 8D and 8E). A TaqMan polymerase chain reaction-based assay confirmed a more than 10-fold stronger signal for omentum exposed to BCAM1-overexpressing OVCAR8 spheroids compared to control cell spheroids (Figs. 8F and 8G).

Finally, we used a mouse model to compare the metastatic potential of BCAM-overexpressing OVCAR8 spheroids to that of spheroids derived from control cells. Mice inoculated intraperitoneally with BCAM-overexpressing spheroids demonstrated extensive omentum colonization (Fig. 8H).

In conclusion, these findings confirm the *in vitro* observations of the role of BCAM in OC peritoneal organ invasion and provide valuable insights into potential mechanisms underlying transcoelomic metastasis formation.

3.3 Discussion

3.3.1 BCAM as a key mediator of HGSC progression in ascites

The presence of ascites in patients with HGSC is linked to a poor prognosis. Ascites is rich in tumor-promoting proteins and EVs that mirror the tumor's secretome [Worzfeld et al., 2017], which are significant in the survival of patients with HGSC [Strandmann et al., 2017]. However, the complete picture of the mediators influencing HGSC progression remains to be established [Finkernagel et al., 2019].

BCAM is a cell adhesion molecule that acts as a laminin receptor and regulates cell adhesion and migration. It is highly expressed in OC and is associated with a short RFS [Finkernagel et al., 2019]. Furthermore, OC has the highest level of *BCAM* RNA and BCAM protein expression in the Human Protein Atlas pointing to a role for this molecule in HGSC progression (Figs. 1B, 1C, and S1).

3.3.2 ADAM10 and ADAM17 mediated shedding of BCAM

Immunoblotting detected sBCAM in OC ascites, which is associated with tumor progression (Figs. 1A, 1B, and 1C). However, the origin and function of sBCAM in HGSC was unknown prior to the present study. It has been reported [Niiya et al., 2009]

that in A431 cells MMP14 is responsible for BCAM cleavage with an unknown function of the cleaved form (sBCAM). We identified ADAM10 and ADAM17 as the primary proteinases responsible for BCAM shedding in HGSC cells, with ADAM10 being the main contributor (Figs. 2B–2E). MMP14 was also detected in the proteome of ascites tumor cells, albeit at relatively low levels compared to ADAM10 and ADAM17 (Fig. 2A).

The role of ADAM10 as a BCAM-cleaving enzyme was confirmed using recombinant proteins (Fig. 2F). MS-based analysis identified cleavage sites near the transmembrane domain and the known MMP14 site (Fig. 2G). One of these cleavage sites coincided with a site observed in BCAM from the OC cell culture supernatant. These findings indicated that ADAM10 cleaves BCAM close to the plasma membrane, creating sBCAM, which is subsequently released into the TME (Fig. S12).

Given these findings, we examined and compared the function of sBCAM with those of BCAM1 and BCAM2 in the context of metastasis-related biological processes.

3.3.3 Role of BCAM in metastasis

BCAM plays different roles in metastasis, owing to the distinct biological processes underlying progression of different tumor entities. To better understand the involvement of BCAM in metastasis, we should consider its interactions with ECM components, such as laminins, and how they differ across cancer types.

In several cancer types, metastatic spread occurs predominantly through hematogenic and lymphogenic routes [Friedl et al., 2009; Janiszewska et al., 2005], including the migration of single tumor cells or groups of cells, facilitated by ECM components, such as laminins [Kikkawa et al., 1998]. LN-511, a highly adhesive and migration-promoting matrix component, is significant in integrin-dependent tumor cell migration and invasion [Kikkawa et al., 1998; Pouliot et al., 2013]. The effects of LN-511 are partially mediated through autocrine stimulation, which promotes breast cancer metastasis [Kusuma et al., 2012; Pouliot et al., 2000; Chia et al., 2007]. The inhibitory effect of BCAM on LAMA5–integrin signaling may explain its lack of association with poor survival outcomes in these cancer types (Fig. S1B).

In contrast, OC metastasis mainly occurs through transcoelomic dissemination, with cancer cells spreading *via* spheroids [Al Habyan et al., 2018; Gao et al., 2019]. In this

context, laminin–integrin interactions are crucial for compacting tumor cells within spheroids [Larson et al., 2014]. BCAM has context-dependent functions in OC cells, which can differently impact metastasis formation. For example, BCAM diminishes the adhesion of single OC cells to LN-511 (Fig. 1D), possibly by competing with integrin for laminin binding, which might have a suppressive effect on metastasis. This is consistent with findings on gastrointestinal and bladder carcinoma cells [Kikkawa et al., 2013; Chang et al., 2017]. Importantly, however, BCAM does not inhibit adhesion to COL1, a primary factor in OC metastasis (Figs. S6E–G).

Conversely, spheroids are abundant in LAMA5 (Table 2; Figs. 3 and S13), which promotes the clustering of tumor cells by binding to integrins. However, BCAM disrupts this interaction, resulting in less compact spheroids and enhanced spheroid dispersion in a 3D collagen matrix (Fig. 6). This, in turn, promotes the clearance of mesothelial cells at spheroid attachment sites and likely increases the seeding of metastatic colonies.

Moreover, BCAM promotes invasion not only into milky spots, the preferred sites of early metastasis of OC owing to their discontinuous mesothelium [Ma, X., 2020; Platell et al., 2000], but also into other areas. This observation agrees with the finding that BCAM facilitates tumor-cell-mediated clearance of a mesothelial cell monolayer (Fig. 7). Different mechanisms for mesothelium disruption by OC cells have been proposed, such as mesothelial senescence [Mikula et al., 2016], killing by secreted factors [Heath et al., 2004], and myosin-driven mechanical force exerted by tumor cells [Iwanicki et al., 2011]. Identification of the precise molecular mechanisms underlying BCAM-induced mesothelial clearance remains a topic for future investigations.

In summary, the role of BCAM in metastasis is highly context-dependent and varies across different cancer types and biological processes. Its interactions with ECM components, particularly laminins, and their effects on adhesion and invasion highlight the complexity of BCAM's involvement in cancer progression and metastasis.

3.3.4 Function of BCAM as a decoy receptor

BCAM1 (a full-length BCAM protein) is a transmembrane receptor with an intracellular domain that may be involved in signal transduction. BCAM1 is phosphorylated by various enzymes, such as glycogen synthase kinase 3 β (at serine 596), casein kinase

II (serine 598), and PKA (serine 621). The phosphorylation state of BCAM may be an essential factor for erythrocyte adhesion to LAMA5 in sickle cell anemia [El Nemer et al., 2008]. However, whether tumor cells participate in BCAM-mediated signal transduction remains unclear.

An earlier study showed that BCAM overexpression in NIH3T3 fibroblasts leads to an rearrangement of *F*-actin, a cytoskeletal protein, concomitant with enhanced Erk phosphorylation, increased RhoA activity and decreased Rac1 activity [Chang et al., 2017]. In contrast, our results indicate that BCAM is unlikely to function as a signaling receptor in the biological processes analyzed in the present study. This conclusion is based on the fact that BCAM1, BCAM2 (which lacks most of its cytoplasmic domain), and Fc-BCAM similarly affected OC cell adhesion, migration, motility, and spheroid formation.

Therefore, BCAM may operate as a competitive ligand or ligand for a signaling receptor. Our findings indicate that BCAM acts as a decoy receptor, blocking the LAMA5 – integrin- β 1 interaction, which decreases the compactness of spheroids and increases their dispersion at attachment sites. This is consistent with published studies identifying BCAM as a competitive ligand interfering with the binding of laminin to integrin- β 1 [Kikkawa et al., 2017; Godavarthy et al., 2021].

Fc-BCAM impacts OC cells in culture at a concentration equivalent to the highest levels of sBCAM in ascites (Figs. 1B, 1D, and 1E) and with similar effects as overexpressed BCAM1 or BCAM2 (Figs. 1D and 1E). Whether the effects of membrane-bound BCAM depend on its shedding remains unclear. However, it is conceivable that both membrane-bound and sBCAM contribute to regulating OC cell activities, consistent with the proposed role of BCAM as a competing ligand.

In murine glomerulonephritis, BCAM acts as a ligand for integrin α 4/ β 1 expressed on leukocytes [Huang et al., 2014]. Integrin α 4 is specifically expressed in hematopoietic cells and is almost negligible in OC cells (Fig. S16; TPM < 1), indicating that integrin α 4 may play a minor role in the latter. However, other receptors activated by BCAM or co-regulated by BCAM may exist, but have not been identified as of yet. In summary,

BCAM functions as a decoy receptor in OC by blocking LAMA5 interaction with β 1-containing integrins.

3.3.5 BCAM as a novel target for translational approaches in cancer therapy

Our study has demonstrated that membrane-bound BCAM and sBCAM, shed by ADAM10 and ADAM17, play a role in modulating metastasis-related functions, contributing to peritoneal dissemination and poor clinical outcomes in OC. This finding suggests that targeting BCAM offers novel therapeutic options for OC and other cancer types in which BCAM is overexpressed.

Supporting our argument, a group of researchers from Harvard Medical School founded a high-throughput platform for the simultaneous discovery of antibodies and targets. This platform can expedite the identification of cancer targets and antibodies, thus advancing the development of new therapeutics. They identified BCAM as a promising candidate for targeted therapy in HGSC [Schröfelbauer et al., 2023].

Antibody – drug conjugates (ADCs) targeting BCAM, named GENA-111-AF, were developed by Debiopharm International (Switzerland) and Genome & Company (Korea). GENA-111-AF exhibited significant cytotoxic activity against BCAM-expressing carcinoma cell lines, including those not responding to trastuzumab-DM1, a HER2-targeting ADC. Furthermore, GENA-111-AF induced complete remissions in a BCAM-positive human skin cancer xenograft model. These results, published as a meeting abstract, suggest that targeting BCAM using ADCs may be an effective therapeutic strategy [Yu et al., 2022].

Considering the findings from these studies, several potential strategies for targeting BCAM for therapeutic intervention can be proposed:

1. Development of ADCs: further optimization of ADCs targeting BCAM may improve treatment options for cancers with high BCAM expression.
2. Targeting the BCAM–LAMA5 interaction: as our study has demonstrated the importance of the BCAM–LAMA5 interaction in tumor progression, developing therapies that disrupt this interaction could hinder cancer cell metastasis.

3. Combination therapies: combining BCAM-targeted therapies with existing cancer treatments, such as chemotherapy or immunotherapy, could improve their efficacy and potentially enhance their ability to limit cancer progression and metastasis.

In conclusion, evidence from our work and the cited studies indicates that BCAM may be a promising target for therapeutic approaches in HGSC treatment. Its role in modulating metastasis-related functions and its overexpression in various cancer types suggest that targeting BCAM, alone or in combination with other treatments, may offer improved therapeutic options. Towards this goal, further research is needed to understand the precise role of BCAM in cancer progression and to optimize targeted therapies.

3.4 My contributions

- Generation of stable CRISPR BCAM KO clones using three different gRNAs (Fig. S5A).
- Generation of stable BCAM-overexpressing clones for long (BCAM1) and short (BCAM2) BCAM isoforms (Fig. S4).
- Immunoblot experiments (Figs. 1A, 2B, S4, S5, S10, S11, and S14C).
- Preparation of samples for ELISA (Figs. 2C, 2D, and 2E).
- xCELLigence-based real-time cell adhesion assays (Figs. 1D, S6, and S7).
- xCELLigence-based real-time cell migration assays (Figs. 1E and S8C).
- Real-time cell motility assays using a spinning disc microscope (Figs. S8D and S8E).
- Preparation of mass-spec samples for mapping ADAM10 cleavage sites in BCAM (Figs. 2G and S12).
- Verification of the *in vitro* cleavage reaction using a silver stain gel (Fig. 2F).
- Flow cytometry analysis of BCAM surface expression (Fig. S4B).
- siRNA-mediated interference of BCAM, ADAM10, and ADAM17 (Figs. S5B, S10C, and S10D).
- Spheroid formation assays (Figs. 4, 5, and S14).
- Spheroid dispersion in 3D collagen matrix assays (Fig. 6).
- Mesothelial cell clearance assays (Fig. 7).

4. List of Abbreviations

ADAM	A disintegrin and metalloproteinase
ascTU	Tumor cells from ascites
BAN	BCAM-associated long noncoding RNA
BCAM	Basal cell adhesion molecule
COL1	Collagen I
ECM	Extracellular matrix
ELISA	Enzyme-linked immunosorbent assay
GO	Gene Ontology
HGSC	High-grade serous ovarian carcinoma
Ig-like domains	Immunoglobulin-like domains
IgSF	Immunoglobulin superfamily
ITGB1	Integrin- β 1
KO	Knockout
LAMA5	Laminin α 5
LN-511	Laminin 511
lncRNA	Long noncoding RNA
Lu	Lutheran
MMPs	Matrix metalloproteinases
MS	Mass spectrometry
OC	Ovarian cancer
OE	Overexpression
PKA	Protein kinase A
RFS	Relapse-free survival
RTCA	Real-time cell analysis
sBCAM	Soluble BCAM
siRNA	Small interfering RNA
SOMAmers	Slow off-rate modified aptamers
TME	Tumor microenvironment

5. References

1. Al Habyan, Sara, et al. "Multicellular detachment generates metastatic spheroids during intra-abdominal dissemination in epithelial ovarian cancer." *Oncogene* 37.37 (2018): 5127-5135.
2. Alkmin, Samuel, et al. "Role of collagen fiber morphology on ovarian cancer cell migration using image-based models of the extracellular matrix." *Cancers* 12.6 (2020): 1390.
3. Auersperg, Nelly., et al. "The origin of ovarian carcinomas: a developmental view." *Gynecologic Oncology* 110.3 (2008): 452-454.
4. Bartolini, Alice, et al. "BCAM and LAMA5 Mediate the Recognition between Tumor Cells and the Endothelium in the Metastatic Spreading of KRAS-Mutant Colorectal Cancer BCAM in KRAS-Mutant Metastatic Colorectal Cancer." *Clinical cancer research* 22.19 (2016): 4923-4933.
5. Bowtell, David D., et al. "Rethinking ovarian cancer II: reducing mortality from high-grade serous ovarian cancer." *Nature reviews Cancer* 15.11 (2015): 668-679.
6. Burton, Nicholas M., and R. Leo Brady. "Molecular structure of the extracellular region of Lutheran blood group glycoprotein and location of the laminin binding site." *Blood Cells, Molecules & Diseases* 40.3 (2008): 446-448.
7. Buys, Sandra S., et al. "Effect of screening on ovarian cancer mortality: the Prostate, Lung, Colorectal and Ovarian (PLCO) cancer screening randomized controlled trial." *Jama* 305.22 (2011): 2295-2303.
8. Caescu, Cristina I., Grace R. Jeschke, and Benjamin E. Turk. "Active-site determinants of substrate recognition by the metalloproteinases TACE and ADAM10." *Biochemical Journal* 424.1 (2009): 79-88.
9. Campbell, Ian G., et al. "Molecular cloning of the B-CAM cell surface glycoprotein of epithelial cancers: a novel member of the immunoglobulin superfamily." *Cancer research* 54.22 (1994): 5761-5765.
10. Chia, Jenny, et al. "Evidence for a role of tumor-derived laminin-511 in the metastatic progression of breast cancer." *The American journal of pathology* 170.6 (2007): 2135-2148.

11. Collec, Emmanuel, et al. "Novel role for the Lu/BCAM–spectrin interaction in actin cytoskeleton reorganization." *Biochemical Journal* 436.3 (2011): 699-708.
12. Drewniok, Claudia, et al. "Molecular interactions of B-CAM (basal-cell adhesion molecule) and laminin in epithelial skin cancer." *Archives of dermatological research* 296 (2004): 59-66.
13. Dubeau, Louis. "The cell of origin of ovarian epithelial tumours." *The lancet oncology* 9.12 (2008): 1191-1197.
14. El Nemer, W., et al. "Role of Lu/BCAM in abnormal adhesion of sickle red blood cells to vascular endothelium." *Transfusion clinique et biologique* 15.1-2 (2008): 29-33.
15. Finkernagel, Florian, et al. "Dual-platform affinity proteomics identifies links between the recurrence of ovarian carcinoma and proteins released into the tumor microenvironment." *Theranostics* 9.22 (2019): 6601.
16. Ford, Caroline Elizabeth, et al. "The untapped potential of ascites in ovarian cancer research and treatment." *British Journal of Cancer* 123.1 (2020): 9-16.
17. Friedl, Peter, and Darren Gilmour. "Collective cell migration in morphogenesis, regeneration and cancer." *Nature reviews Molecular cell biology* 10.7 (2009): 445-457.
18. Gao, Qinglei, et al. "Heterotypic CAF-tumor spheroids promote early peritoneal metastasis of ovarian cancer." *Journal of Experimental Medicine* 216.3 (2019): 688-703.
19. Gauthier, E., et al. "PKA-dependent phosphorylation of Lu/B-CAM glycoprotein regulates cell adhesion to laminin alpha 5." *J Biol Chem* 280 (2005): 30055-30062.
20. Gauthier, Emilie, et al. "Role of the interaction between Lu/BCAM and the spectrin-based membrane skeleton in the increased adhesion of hereditary spherocytosis red cells to laminin." *British journal of haematology* 148.3 (2010): 456-465.
21. Godavarthy, Parimala Sonika, et al. "The Laminin Receptors Basal Cell Adhesion Molecule/Lutheran and Integrin $\alpha 7\beta 1$ on Human Hematopoietic Stem Cells." *Frontiers in Cell and Developmental Biology* 9 (2021): 675240.

22. Graumann, Johannes, et al. "Multi-platform affinity proteomics identify proteins linked to metastasis and immune suppression in ovarian cancer plasma." *Frontiers in oncology* 9 (2019): 1150.
23. Guadall, Anna, et al. "Dimerization and phosphorylation of Lutheran/basal cell adhesion molecule are critical for its function in cell migration on laminin." *Journal of Biological Chemistry* 294.41 (2019): 14911-14921.
24. Heath, R. M., et al. "Tumour-induced apoptosis in human mesothelial cells: a mechanism of peritoneal invasion by Fas Ligand/Fas interaction." *British journal of cancer* 90.7 (2004): 1437-1442.
25. Huang, Jin, et al. "Lutheran/basal cell adhesion molecule accelerates progression of crescentic glomerulonephritis in mice." *Kidney International* 85.5 (2014): 1123-1136.
26. Huang, Yen-Lin, et al. "Collagen-rich omentum is a premetastatic niche for integrin α 2-mediated peritoneal metastasis." *Elife* 9 (2020): e59442.
27. Iwanicki, Marcin P., et al. "Ovarian Cancer Spheroids Use Myosin-Generated Force to Clear the Mesothelium Contractile Forces Generated by Ovarian Cancer Spheroids Promote Mesothelial Clearance." *Cancer discovery* 1.2 (2011): 144-157.
28. Janiszewska, Michalina, Marina Candido Primi, and Tina Izard. "Cell adhesion in cancer: Beyond the migration of single cells." *Journal of Biological Chemistry* 295.8 (2020): 2495-2505.
29. Jin, Juan, et al. "Upregulation of BCAM and its sense lncRNA BAN are associated with gastric cancer metastasis and poor prognosis." *Molecular Oncology* 14.4 (2020): 829-845.
30. Kenny, Hilary A., et al. "The first line of intra-abdominal metastatic attack: breaching the mesothelial cell layer." *Cancer discovery* 1.2 (2011): 100-102.
31. Khan, Shaheena M., et al. "In vitro metastatic colonization of human ovarian cancer cells to the omentum." *Clinical & experimental metastasis* 27 (2010): 185-196.
32. Kikkawa, Yamato, and Jeffrey H. Miner. "Lutheran/B-CAM: a laminin receptor on red blood cells and in various tissues." *Connective tissue research* 46.4-5 (2005): 193-199.

33. Kikkawa, Yamato, et al. "The LG1-3 tandem of laminin α 5 harbors the binding sites of Lutheran/basal cell adhesion molecule and α 3 β 1/ α 6 β 1 integrins." *Journal of Biological Chemistry* 282.20 (2007): 14853-14860.
34. Kikkawa, Yamato, et al. "The Lutheran/basal cell adhesion molecule promotes tumor cell migration by modulating integrin-mediated cell attachment to laminin-511 protein." *Journal of Biological Chemistry* 288.43 (2013): 30990-31001.
35. Kikkawa, Yamato, et al. "Isolation and characterization of laminin-10/11 secreted by human lung carcinoma cells: laminin-10/11 mediates cell adhesion through integrin α 3 β 1." *Journal of Biological Chemistry* 273.25 (1998): 15854-15859.
36. Kim, Jaeyeon, et al. "High-grade serous ovarian cancer arises from fallopian tube in a mouse model." *Proceedings of the National Academy of Sciences* 109.10 (2012): 3921-3926.
37. Kleih, Markus, et al. "Direct impact of cisplatin on mitochondria induces ROS production that dictates cell fate of ovarian cancer cells." *Cell death & disease* 10.11 (2019): 851.
38. Książek, Krzysztof, et al. "Oxidative stress-mediated early senescence contributes to the short replicative life span of human peritoneal mesothelial cells." *Free Radical Biology and Medicine* 45.4 (2008): 460-467.
39. Kusuma, Nicole, et al. "Integrin-dependent response to laminin-511 regulates breast tumor cell invasion and metastasis." *International journal of cancer* 130.3 (2012): 555-566.
40. Larson, Allison R., et al. "Melanoma spheroid formation involves laminin-associated vasculogenic mimicry." *The American journal of pathology* 184.1 (2014): 71-78.
41. Lengyel, Ernst. "Ovarian cancer development and metastasis." *The American journal of pathology* 177.3 (2010): 1053-1064.
42. Lisio, Michael-Antony, et al. "High-grade serous ovarian cancer: basic sciences, clinical and therapeutic standpoints." *International journal of molecular sciences* 20.4 (2019): 952.
43. Lisio, Soochi, et al. "Ascites modulates cancer cell behavior, contributing to tumor heterogeneity in ovarian cancer." *Cancer science* 107.9 (2016): 1173-1178.

44. Liu, Min, et al. "BCAM Deficiency May Contribute to Preeclampsia by Suppressing the PIK3R6/p-STAT3 Signaling." *Hypertension* 79.12 (2022): 2830-2842.
45. Lyu, Yinfeng, and Chenchen Feng. "Collagen synthesis and gap junctions: the highway for metastasis of ovarian cancer." *Laboratory Investigation* 101.5 (2021): 540-542.
46. Ma, Xiaojing. "The omentum, a niche for premetastatic ovarian cancer." *Journal of Experimental Medicine* 217.4 (2020).
47. Matte, Isabelle, et al. "Role of malignant ascites on human mesothelial cells and their gene expression profiles." *BMC cancer* 14.1 (2014): 1-13.
48. McCorkle, J. Robert, et al. "Lapatinib and poziotinib overcome ABCB1-mediated paclitaxel resistance in ovarian cancer." *Plos one* 16.8 (2021): e0254205.
49. Mei, Shuangshuang, et al. "Tumor microenvironment in ovarian cancer peritoneal metastasis." *Cancer Cell International* 23.1 (2023): 1-13.
50. Mińska-Pietrasik, Justyna, et al. "Malignant ascites determine the transmesothelial invasion of ovarian cancer cells." *The International Journal of Biochemistry & Cell Biology* 92 (2017): 6-13.
51. Mińska-Pietrasik, Justyna, et al. "Senescent peritoneal mesothelium creates a niche for ovarian cancer metastases." *Cell death & disease* 7.12 (2016): e2565-e2565.
52. Moss, Marcia L, et al. "The ADAM10 prodomain is a specific inhibitor of ADAM10 proteolytic activity and inhibits cellular shedding events." *Journal of Biological Chemistry* 282.49 (2007): 35712-35721.
53. Niiya, Daigo, et al. "Identification and characterization of Lutheran blood group glycoprotein as a new substrate of membrane-type 1 matrix metalloproteinase 1 (MT1-MMP): a systemic whole cell analysis of MT1-MMP-associating proteins in A431 cells." *Journal of Biological Chemistry* 284.40 (2009): 27360-27369.
54. Niu, Guo-Juan, et al. "The polymeric immunoglobulin receptor-like protein from *Marsipenaes japonicus* is a receptor for white spot syndrome virus infection." *PLoS Pathogens* 15.2 (2019): e1007558.

55. Pakuła, Martyna, et al. "The epithelial-mesenchymal transition initiated by malignant ascites underlies the transmesothelial invasion of ovarian cancer cells." *International journal of molecular sciences* 20.1 (2019): 137.
56. Pasquet, Marlene, et al. "Hospicells (ascites-derived stromal cells) promote tumorigenicity and angiogenesis." *International Journal of Cancer* 126.9 (2010): 2090-2101.
57. Piché, Alain. "Malignant peritoneal effusion acting as a tumor environment in ovarian cancer progression: Impact and significance." *World Journal of Clinical Oncology* 9.8 (2018): 167.
58. Platell, Cameron, et al. "The omentum." *World Journal of Gastroenterology* 6.2 (2000): 169.
59. Pouliot, Normand, and Nicole Kusuma. "Laminin-511: a multi-functional adhesion protein regulating cell migration, tumor invasion and metastasis." *Cell adhesion & migration* 7.1 (2013): 142-149.
60. Pouliot, Normand, et al. "Colon cancer cells adhesion and spreading on autocrine laminin-10 is mediated by multiple integrin receptors and modulated by EGF receptor stimulation." *Experimental cell research* 261.2 (2000): 360-371.
61. Reid, Brett M, et al. "Epidemiology of ovarian cancer: a review." *Cancer biology & medicine* 14.1 (2017): 9.
62. Schröfelbauer, Bärbel, et al. "Discovery of antibodies and cognate surface targets for ovarian cancer by surface profiling." *Proceedings of the National Academy of Sciences* 120.1 (2023): e2206751120.
63. Shen, Yufei, et al. "Fibrillar type I collagen matrices enhance metastasis/invasion of ovarian epithelial cancer via β 1 integrin and PTEN signals." *International Journal of Gynecologic Cancer* 22.8 (2012).
64. Sivakumar, Suresh, et al. "Basal cell adhesion molecule promotes metastasis-associated processes in ovarian cancer." *Clinical and Translational Medicine* 13.1 (2023): e1176.
65. Stewart, Christine, et al. "Ovarian cancer: an integrated review." *Seminars in oncology nursing*. Vol. 35. No. 2. WB Saunders, 2019.
66. Torre, Lindsey A., et al. "Ovarian cancer statistics, 2018." *CA: a cancer journal for clinicians* 68.4 (2018): 284-296.

67. Tucher, Joanna, et al. "LC–MS Based Cleavage Site Profiling of the Proteases ADAM10 and ADAM17 Using Proteome-Derived Peptide Libraries." *Journal of proteome research* 13.4 (2014): 2205-2214.
68. von Strandmann, Elke Pogge, et al. "Tumor–host cell interactions in ovarian cancer: pathways to therapy failure." *Trends in cancer* 3.2 (2017): 137-148.
69. Wai Wong, Chee, et al. "The role of immunoglobulin superfamily cell adhesion molecules in cancer metastasis." *International journal of cell biology* 2012 (2012).
70. Wintzell, My, et al. "Protein markers of cancer-associated fibroblasts and tumor-initiating cells reveal subpopulations in freshly isolated ovarian cancer ascites." *BMC cancer* 12.1 (2012): 1-10.
71. Wojtowicz, Woj M., et al. "A human IgSF cell-surface interactome reveals a complex network of protein-protein interactions." *Cell* 182.4 (2020): 1027-1043.
72. Worzfeld, Thomas, et al. "Proteotranscriptomics reveal signaling networks in the ovarian cancer microenvironment." *Molecular & Cellular Proteomics* 17.2 (2018): 270-289.
73. Worzfeld, Thomas., et al. "The unique molecular and cellular microenvironment of ovarian cancer." *Frontiers in oncology* 7 (2017): 24.
74. Yang, Yanfei, et al. "Tumor microenvironment in ovarian cancer: function and therapeutic strategy." *Frontiers in cell and developmental biology* 8 (2020): 758.
75. Yu, Hyunkyung, et al. "The antibody-drug conjugate GENA-111 conjugated to auristatin F shows therapeutic potency in BCAM positive epithelial cancer." *Cancer Research* 82. 12_Supplement (2022): 1760 (Meeting Abstract).

6.1 All publications of the author

Sivakumar, S., Lieber, S., Librizzi, D., Keber, C., Sommerfeld, L., Finkernagel, F., Roth, K., Reinartz, S., Bartsch, J.W., Graumann, J. and Müller-Brüsselbach, S.,2023. Basal cell adhesion molecule promotes metastasis-associated processes in ovarian cancer. *Clinical and Translational Medicine*, 13(1), p.e1176

6.2 Curriculum vitae

Personal Information:

Name: Suresh Sivakumar

Date of birth: Nov. 30, 1994

Place of birth: Puducherry, India

Education:

- **PhD Student (Jan. 2019 - Present)**

Center for Tumor Biology and Immunology (ZTI), Philipps-Universität Marburg, Germany

Studying the role of BCAM in ovarian tumor microenvironment in Prof. Rolf Müller's laboratory

- **Master Thesis (2018)**

CNRS lab, University of Strasbourg, France

Investigated the binding region between I κ B α and IKK β (NF- κ B signaling pathway) in Dr. Katia Zanier's laboratory

- **Bachelor Thesis (2016)**

National University of Singapore, Singapore

Conducted research on finding potential tyrosine kinase inhibitors (small molecules) for liposarcoma in Prof. Phillip Koeffler's laboratory

- **Integrated M.Tech Biotechnology (2012 - 2018)**

Bharathidasan University, India

Experience:

- **Summer Internship (2015)**

Indian Agricultural Research Institute (IARI), India

Studied plant pathology, particularly focussed on rice crop diseases

- **Industrial Internship (2014)**

INDAM Seeds Private Limited, India

Gained experience in plant molecular biology

- **Research Trainee (2013 - 2014)**

MGDC (NCAAE), Bharathidasan University, India

Establishment of *Hydra sp.* as an alternative animal model for toxicity testing

6.3 Directory of academic teachers

- 1) Philipps-Universität Marburg - Prof. Rolf Müller and Dr. Sabine Müller-Brüsselbach
- 2) University of Strasbourg - Dr. Katia Zanier
- 3) National University of Singapore - Prof. Phillip Koeffler
- 4) Bharathidasan University - Prof. M. A. Akbarsha, Dr. M.Manickavasagam and Dr. S.Sivaramakrishnan

6.4 Acknowledgement

I would like to express my heartfelt gratitude to all those who have supported and guided me throughout my research journey and in the writing of my thesis.

First and foremost, I would like to extend my sincere thanks to Prof. Rolf Müller and Dr. Sabine Müller-Brüsselbach for their immense patience, motivation, and knowledge, and to Dr. Sonja Lieber for performing the *ex vivo* (omentum) and mouse experiments. Your expertise and guidance have been invaluable during the research process, and I have greatly benefited from your wealth of knowledge.

I am also deeply grateful for the invaluable contributions of our collaborators: Dr. Jörg W. Bartsch for his expertise in metalloproteinases, Dr. Johannes Graumann for carrying out proteomics analyses, Dr. Damiano Librizzi for performing PET/CT, Dr. Katrin Roth for help with microscopy and analysis of microscopic images, and Dr. Corinna Keber for immunohistochemistry analyses. Your support and advice have been instrumental to the success of this research.

Additionally, I would like to acknowledge the scientific support provided by Dr. Florian Finkernagel, and Dr. Silke Reinartz. Your input and guidance have been of tremendous help to me. Furthermore, I am grateful for the advice and encouragement given by Dr. Till Adhikary and the technical support provided by Margitta Alt, Klaus Weber, Traute Plaum-Allmeroth, Achim Allmeroth and Bernhard Wilke.

A special mention goes to Kaire Ojasalu for assisting me during the initial stages of my PhD journey. I am also thankful to my colleagues Dr. Mohamad Khir Hammoud, Dr. Raimund Dietze, Dr. Leah Sommerfeld, Anna Mary Steitz, and Dr. Annika Unger for their support and collaboration.

I am grateful to my friends, both here and in India, for their timely motivation and encouragement. A heartfelt thank you to Justin, Ulaga, Iccy, Ajay, Dinesh, Siddhesh, Shrey, Tek, Madhu, Netra, Reem, Prema, Harsha, and Sweetha. Your support has meant a lot to me.





Finally, I would like to express my deepest gratitude to my family - Appa, Amma, Anna, and Anni - for their unwavering love, support, and belief in me. Your presence has been a constant source of strength and inspiration.

Once again, thank you all for your invaluable contributions to my research and thesis. I am truly honored and grateful for your support.

7. Manuscript and supplementary file

RESEARCH ARTICLE

Basal cell adhesion molecule promotes metastasis-associated processes in ovarian cancer

Suresh Sivakumar¹  | Sonja Lieber¹ | Damiano Librizzi² | Corinna Keber³ | Leah Sommerfeld¹ | Florian Finkernagel^{1,4} | Katrin Roth⁵ | Silke Reinartz¹ | Jörg W. Bartsch⁶  | Johannes Graumann^{7,8}  | Sabine Müller-Brüsselbach¹ | Rolf Müller¹ 

¹Department of Translational Oncology, Center for Tumor Biology and Immunology (ZTI), Philipps University, Marburg, Germany

²Small Animal Imaging Core Facility, Center for Tumor Biology and Immunology (ZTI), Philipps University, Marburg, Germany

³Institute for Pathology, Philipps University, Marburg, Germany

⁴Bioinformatics Core Facility, Center for Tumor Biology and Immunology (ZTI), Philipps University, Marburg, Germany

⁵Cell Imaging Core Facility, Center for Tumor Biology and Immunology (ZTI), Philipps University, Marburg, Germany

⁶Clinic for Neurosurgery, Philipps University, Marburg, Germany

⁷Biomolecular Mass Spectrometry, Max Planck Institute for Heart and Lung Research, Bad Nauheim, Germany

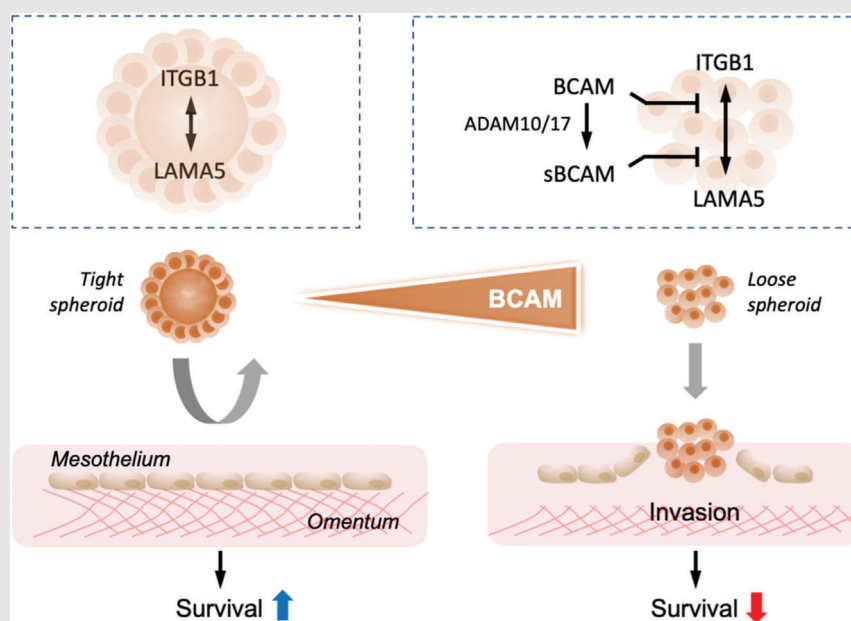
⁸Institute for Translational Proteomics, Philipps University, Marburg, Germany

Correspondence

Rolf Müller and Sabine Müller-Brüsselbach, Department of Translational Oncology, Center for Tumor Biology and Immunology (ZTI), Philipps University, 35043 Marburg, Germany.

Email: rolf.mueller@uni-marburg.de; smb@imt.uni-marburg.de





Graphical Abstract



Expression of BCAM is associated with a poor survival of ovarian cancer. BCAM reduces compaction of tumour cell spheroids, thereby facilitating their invasion of metastatic sites. Mechanistically, BCAM affects spheroid structure by blocking the interaction of laminin $\alpha 5$ (LAMA5) with integrin $\beta 1$ (ITGB1). BCAM mediates this function either as a membrane-bound protein or after shedding (sBCAM) by ADAM10 or 17

RESEARCH ARTICLE

Basal cell adhesion molecule promotes metastasis-associated processes in ovarian cancer

Suresh Sivakumar¹  | Sonja Lieber¹ | Damiano Librizzi² | Corinna Keber³ | Leah Sommerfeld¹ | Florian Finkernagel^{1,4} | Katrin Roth⁵ | Silke Reinartz¹ | Jörg W. Bartsch⁶  | Johannes Graumann^{7,8}  | Sabine Müller-Brüsselbach¹ | Rolf Müller¹ 

¹Department of Translational Oncology, Center for Tumor Biology and Immunology (ZTI), Philipps University, Marburg, Germany

²Small Animal Imaging Core Facility, Center for Tumor Biology and Immunology (ZTI), Philipps University, Marburg, Germany

³Institute for Pathology, Philipps University, Marburg, Germany

⁴Bioinformatics Core Facility, Center for Tumor Biology and Immunology (ZTI), Philipps University, Marburg, Germany

⁵Cell Imaging Core Facility, Center for Tumor Biology and Immunology (ZTI), Philipps University, Marburg, Germany

⁶Clinic for Neurosurgery, Philipps University, Marburg, Germany

⁷Biomolecular Mass Spectrometry, Max Planck Institute for Heart and Lung Research, Bad Nauheim, Germany

⁸Institute for Translational Proteomics, Philipps University, Marburg, Germany

Correspondence

Rolf Müller and Sabine-Müller-Brüsselbach, Department of Translational Oncology, Center for Tumor Biology and Immunology (ZTI), Philipps University, 35043 Marburg, Germany.
Email: rolf.mueller@uni-marburg.de; smb@imt.uni-marburg.de

Funding information

German Research Foundation, Grant/Award Number: MU601/22-1; Anneliese Pohl Stiftung, Grant/Award Number: 01-2017

Abstract

Background: Basal cell adhesion molecule (BCAM) is a laminin $\alpha 5$ (LAMA5) binding membrane-bound protein with a putative role in cancer. Besides full-length BCAM1, an isoform lacking most of the cytoplasmic domain (BCAM2), and a soluble form (sBCAM) of unknown function are known. In ovarian carcinoma (OC), all BCAM forms are abundant and associated with poor survival, yet BCAM's contribution to peritoneal metastatic spread remains enigmatic.

Methods: Biochemical, omics-based and real-time cell assays were employed to identify the source of sBCAM and metastasis-related functions of different BCAM forms. OC cells, explanted omentum and a mouse model of peritoneal colonisation were used in loss- and gain-of-function experiments.

Results: We identified ADAM10 as a major BCAM sheddase produced by OC cells and identified proteolytic cleavage sites proximal to the transmembrane domain. Recombinant soluble BCAM inhibited single-cell adhesion and migration identically to membrane-bound isoforms, confirming its biological activity in OC. Intriguingly, this seemingly anti-tumorigenic potential of BCAM contrasts with a novel pro-metastatic function discovered in the present study. Thus, all queried BCAM forms decreased the compactness of tumour cell spheroids

This is an open access article under the terms of the [Creative Commons Attribution](https://creativecommons.org/licenses/by/4.0/) License, which permits use, distribution and reproduction in any medium, provided the original work is properly cited.

© 2023 The Authors. *Clinical and Translational Medicine* published by John Wiley & Sons Australia, Ltd on behalf of Shanghai Institute of Clinical Bioinformatics.

by inhibiting LAMA5 – integrin β 1 interactions, promoted spheroid dispersion in a three-dimensional collagen matrix, induced clearance of mesothelial cells at spheroid attachment sites in vitro and enhanced invasion of spheroids into omental tissue both ex vivo and in vivo.

Conclusions: Membrane-bound BCAM as well as sBCAM shed by ADAM10 act as decoys rather than signalling receptors to modulate metastasis-related functions. While BCAM appears to have tumour-suppressive effects on single cells, it promotes the dispersion of OC cell spheroids by regulating LAMA5-integrin- β 1-dependent compaction and thereby facilitating invasion of metastatic target sites. As peritoneal dissemination is majorly mediated by spheroids, these findings offer an explanation for the association of BCAM with a poor clinical outcome of OC, suggesting novel therapeutic options.

KEYWORDS

ADAM10, BCAM, ovarian cancer, spheroids

1 | BACKGROUND

Basal cell adhesion molecule (BCAM) is a member of the immunoglobulin superfamily and is composed of five glycosylated extracellular immunoglobulin domains, a transmembrane domain and a short C-terminal cytoplasmic tail. BCAM is expressed in two membrane-bound isoforms of 628 (BCAM1) and 588 amino acids (BCAM2), respectively, that are generated by alternative splicing.¹ The longer BCAM1 isoform is also known as Lutheran blood group glycoprotein (CD239), as polymorphisms in this gene define the Lu^a/Lu^b Lutheran blood groups.² The shorter BCAM2 isoform lacks a 40-amino-acid stretch of the cytoplasmic domain including an SH3-binding domain with potential signalling function.³

BCAM is widely expressed in epithelial, endothelial, hematopoietic and other cell types and has been linked to various human diseases, including gastrointestinal and bladder carcinomas,^{4–8} sickle cell anemia,^{9,10} polycythemia vera¹¹ and glomerulonephritis.¹² BCAM was identified as a receptor for laminins in the extracellular matrix (ECM). It specifically interacts with the laminin α 5 (LAMA5) chain,^{10,13–15} which, in combination with different β and γ subunits, is a component of laminin-511 (LN-511), laminin-522 and laminin-523 trimers. In sickle cell disease, BCAM is abundant on erythrocytes, where it mediates the adhesion to LN-511-expressing endothelial cells (ECs),^{9,10} and interaction of BCAM on erythroid cells with LAMA5 on ECs has also been observed in polycythemia vera.¹¹

Understanding the role of the BCAM–LAMA5 interaction is complicated by the fact that BCAM competes with integrins (α 3 β 1, α 6 β 1, α 6 β 4) for laminin binding,⁵

functionally interacts with the LAMA5 receptor integrin α 7 β 1,¹⁶ and also functions as a ligand for the α 4 subunit of integrin α 4/ β 1 (VLA4) on hematopoietic cells.¹⁷ It therefore remains unclear whether, or under which conditions, BCAM serves as a signalling receptor, a signalling ligand or a competing molecule.

BCAM is up-regulated in multiple human tumour entities (www.proteinatlas.org) and has been associated with biological processes linked to tumour progression and metastases, including cell adhesion, motility, migration and invasion. For example, cell adhesion to laminin has been reported to be enhanced following transfection of an unspecified BCAM isoform into 3T3 fibroblasts.⁷ Furthermore, the function of BCAM may depend on the type of cancer, as ectopic expression of BCAM1 in HT1080 osteosarcoma cells decreased adhesion,⁵ while opposite observations were made for motility. Moreover, BCAM-dependent enhancement of migration was observed in gastric cancer cells,⁸ whereas a decrease was reported following the ectopic expression of BCAM1 into rat hepatoma cells¹⁸ or MDCK cells, the latter being dependent on the intracellular phosphorylation of serine-621.¹⁹ It is likely that these apparent discrepancies are due to context- and tumour-type-dependent effects. This assumption is supported by the inverse association of BCAM expression with overall survival (OS) reported for different tumour entities.²⁰

In view of its high expression in ovarian carcinoma (OC; www.proteinatlas.org), the role of BCAM in this cancer entity is of particular interest, yet its function in OC remains enigmatic. A hallmark of OC is its tumour microenvironment (TME), consisting of anatomically and functionally different compartments, that is, the solid

(metastatic) tumour masses invading host tissues and the peritoneal fluid, occurring as ascites at advanced stages.^{21–23} Due to its pivotal role in peritoneal dissemination, OC ascites differs from the effusions of other human cancers, which are often secondary or reactive. Ascites-associated cancer cells usually occur as multicellular spheroids, most likely at the root of peritoneal dissemination.²⁴

BCAM is also highly abundant as a soluble protein (sBCAM) in OC ascites, and the level of sBCAM is associated with a short relapse-free survival (RFS).²⁵ It is likely that sBCAM is generated by proteolytic cleavage of membrane-bound BCAM, possibly by matrix metalloproteinases (MMPs), as cleavage of BCAM by MMP14 has been reported.²⁶ Consistent with this notion, several members of the MMP family are found in OC ascites, including MMP14.²⁵ However, the origin and function of sBCAM in a pathophysiological context have not been addressed to date. Likewise, the role of BCAM in tumour cell spheroids despite their crucial role in OC metastasis remains unknown.

In the present study, we sought (i) to clarify the origins and structure of sBCAM in OC, (ii) to study metastasis-related functions of the soluble and the two membrane-bound isoforms of BCAM and (iii) to apply experimental models mimicking the *in vivo* situation, including tumour cell spheroids, co-cultures of tumour and mesothelial cells, explanted omentum and a mouse model of peritoneal colonisation.

2 | METHODS

2.1 | Patient samples

Ascites and greater omentum tissue with metastatic lesions were collected from patients with ovarian high-grade serous carcinoma undergoing primary surgery at the University Hospital in Marburg. Patient characteristics are summarised in Tables S1 and S2. Clinical courses were evaluated by RECIST criteria²⁷ in patients according to the recommendations by the Gynecologic Cancer Inter-Group. Tumour cell spheroids were isolated from ascites as described.^{28,29} All cell populations used for the analysis in this study had a purity of >95%, as determined by flow cytometry and RNA-sequencing.²⁸

2.2 | Cell cultures

OVCAR4, OVCAR5 and OVCAR8 cells were obtained from the NIGMS Human Genetic Cell Repository of the NIH (Bethesda, Maryland USA). All OVCAR cell lines were

cultured in RPMI 1640 (Life Technologies, Darmstadt, Germany) supplemented with 10% FBS (Capricorn Scientific, Ebsdorfergrund, Germany). Omentum co-culture was maintained in DMEM Ham's F-12 (PAN-Biotech, Aidenbach, Germany) supplemented with 20% delipidated FBS (Capricorn Scientific, Ebsdorfergrund, Germany).

Human peritoneal mesothelial cells were isolated from the omentum of OC patients by a 30-min digestion of macroscopic tumour-free omental tissue with trypsin, followed by MACS depletion of contaminating CD45⁺ and EpCAM⁺ cells, as previously described.³⁰ Mesothelial cells were cultured in OCMI/5% FCS medium³¹ for a maximum of three to five passages.

2.3 | Antibodies

Monoclonal anti-human BCAM antibody (MAB1481 was purchased from R&D Systems/Bio-Techne (Wiesbaden, Germany); polyclonal anti-human BCAM antibody (AF148) was purchased from R&D Systems/Bio-Techne; integrin β 1 activating antibody (Ultra-LEAF™ CD29 antibody; clone TS2/16, #303036) from BioLegend/Biozol (Eching, Germany); integrin β 1 blocking antibody (clone 6S6, #MAB2253) from Merck (Darmstadt, Germany); monoclonal anti-ADAM10 (ab124695) and polyclonal anti-ADAM17 (ab13535) from Abcam (Berlin, Germany); anti-CD45-PE (clone 30-F11; #553081), anti-CD45-APC (clone 30-F11; #559864), anti-CD31-PE (#553373) and anti-VCAM1/CD106 (clone 429, #561615) from BD BioSciences; anti-CD45-AlexaFluor 647 (clone 30-F11; #103124) from BioLegend. and anti-CD31-Vio 667 (clone REA784) from Miltenyi (Bergisch-Gladbach, Gerany).

2.4 | Other materials

Recombinant Fc-BCAM produced in a mouse myeloma cell line (148-BC), negative control Fc from IgG1 (110-HG) and marimastat (BB-2516; #2631) were purchased from R&D Systems/Bio-Techne and Tocris/Bio-Techne (Wiesbaden, Germany). Recombinant ADAM10 pro-domain was kindly provided by Marcia Moss (Verra Therapeutics, Lansing, NY, USA). Recombinant Human Laminin 511 was obtained from BioLamina (LN-511; Sundbyberg, Sweden) and rat tail collagen I (A1048301) from ThermoFisher Scientific (Dreiech, Germany). N'-tetrakis(2-pyridylmethyl)ethylenediamine (TPEN; sc-200131) was purchased from Santa Cruz (Heidelberg, Germany). Cell Tracker Green CMFDA (#C2925); Cell Tracker Orange CMTMR (#C2927); Cell Tracker blue CMAC (#C2110) and Cell Tracker deep red (#C34565) were from Thermo Fisher (Dreiech, Germany).

2.5 | Quantification of BCAM by flow cytometry

OVCAR cells were detached from cell culture dishes using Accutase cell dissociation solution (#A6964; Sigma-Aldrich; Taufkirchen, Germany), washed and incubated with monoclonal anti-human BCAM antibody combined with secondary FITC labelled anti-mouse IgG (eBioscience/Thermo Fisher Scientific; Dreiech, Germany). Cells were analysed by flow cytometry using a FACS Canto II instrument using Diva Software (BD Biosciences, Heidelberg, Germany). Isotype control antibodies (R&D Systems/Bio-Techne; Wiesbaden, Germany) were used. Results were calculated as percentage of positive cells and mean fluorescence intensities. Cell death was assessed by propidium iodide staining.

2.6 | Immunoblotting

Immunoblots were performed according to standard western blotting protocols using the primary antibodies described above in combination with secondary α -rabbit IgG HRP-linked polyclonal antibody (Cell Signaling Technology; #7074, RRID:AB_2099233); α -mouse IgG HRP-linked polyclonal antibody (Cell Signaling Technology; #7076, RRID: AB_330924) and α -goat IgG HRP-linked polyclonal antibody (Jackson ImmunoResearch Labs/Dianova, Hamburg, Germany). Imaging and quantification were carried out using the ChemiDoc MP system and Image Lab software version 5 (Bio-Rad; Feldkirchen, Germany). For detection of soluble BCAM, confluent cells were cultured in serum-free medium for 24 h. Conditioned media were collected and concentrated 20-fold using Vivaspin® 6 centrifugal concentrators (#512-3777; Sartorius/VWR; Göttingen, Germany) and equal amounts of proteins were mixed with SDS-PAGE sample buffer and analysed according to standard western blotting protocols. Pierce Reversible Total Protein Staining Kit (Invitrogen/Thermo Fisher Scientific; Dreiech, Germany; #24585) was used for sBCAM immunoblot normalisation.

2.7 | BCAM ELISA

OVCAR4 cells were seeded in six-well plates at 5×10^5 cells/well. The confluent cells were washed three times with PBS and serum-free medium containing either marimastat or ADAM10 prodomain was added. After 24 h, supernatants were collected and soluble BCAM was quantified using human BCAM ELISA (ELH-BCAM; Ray Biotech/BioCat; Heidelberg, Germany) according to the manufacturer's instructions.

2.8 | Mass spectrometry of in vitro generated BCAM fragments

One microgram of Fc-BCAM was incubated with 500 ng of recombinant human ADAM10 (#936-AD; R&D Systems) in activity buffer (1 mM ZnCl₂; 20 mM Tris-HCl pH 8,0; 10 mM CaCl₂; 150 mM NaCl; 0.0006% Brij-35) for 5 h at 37°C in the presence or absence of the zinc chelator TPEN (50 μ M). Samples were prepared for proteomic analysis by acetone precipitation, resolubilisation in 8 M Urea, reduction (10 mM DTT) and alkylation (55 mM iodoacetamide), followed by 2 h incubation with LysC (1:100; Wako Chemicals, Neuss, Germany), dilution to 2 M urea using 50 mM TEAB and overnight digestion using trypsin (1:50; Serva). After solid phase extraction on STAGE tips,³² LC/MS²-analysis was performed as described²⁹ and data analysed with MaxQuant using the human Uniprot database (canonical and isoforms;194237 entries; downloaded 2021/02/08). The relevant instrument as well as MaxQuant parameters are extracted using MARMoSET and included in the supplementary material.

2.9 | Protein mass spectrometry (MS) of BCAM in tumour-cell-conditioned media

For proteomic analyses of conditioned media an earlier dataset of ascites-derived tumour cells²⁹ from ovarian high-grade serous carcinoma patients was researched using a semi-specific MaxQuant search^{33,34} against the Uniprot human database (canonical and isoforms;1888349 entries; downloaded 2020/02/05). Instrument parameters used were extracted using MARMoSET³⁵ and are together with relevant MaxQuant parameters included in Supplemental Methods S1 and S2.

2.10 | siRNA-mediated interference

siRNA transfection was performed in OVCAR4 cells cultured in RPMI plus 10% FCS using the Lipofectamine 2000 (Invitrogen/Thermo Fisher Scientific; Dreiech, Germany; #11668027) reagent according to the manufacturer's protocol. BCAM, ADAM10 and ADAM17 siRNA-mediated interference was performed using three different siRNA oligonucleotides (Sigma-Aldrich; Taufkirchen, Germany): BCAM #1 (5'-GAGACUACGUGUGCGUGGU-3'), BCAM #2 (5'-GGAU UACGACGCGGCAGAU-3'), BCAM #3 (5'- CAGAGCUAAAGACAGCGGA -3');ADAM10 #1 (5'-CAGUCAUGUUAAGCGAUU-3'), ADAM10 #2 (5'-GAACUAUGGGUCUCAUGUA-3'), ADAM10 #3 (5'-CGCAUAAGAAUCAAUACAA-3');ADAM17 #1 (5'-CAUCAAGUACUGAACGUUU-3'), ADAM17 #2

(5'-CUUAGCAGAUGCUGGUCAU-3'), ADAM17 #3 (5'-CAAUCUAUAAGACCAUUGA-3'). MISSION siRNA Universal Negative Control #1 from Sigma–Aldrich (Taufkirchen, Germany) was used as a control. Cells were harvested 72 h after transfection.

2.11 | Stable BCAM overexpression in OVCAR8 cells

BCAM overexpression was achieved by transient transfection of OVCAR8 cells with BCAM1 vector (Transcript variant 1; OHu20355 – Gencript Biotech; Piscataway, NJ) or BCAM2 vector (Transcript variant 2; OHu07730 – Gencript Biotech, Piscataway, NJ) or empty pCDNA3.1 control (GenScript Biotech, Piscataway, NJ) using TransIT-X2 (MirusBio/Mobitec; Göttingen, Germany) according to the manufacturer's instructions. Cells were selected in the presence of Geneticin (G418) (Santa Cruz, Heidelberg, Germany; #sc-29065B) (0.8 mg/ml) and stable clones were analysed for BCAM expression by RT-qPCR, immunoblotting and FACS analysis using the following PCR primers (Sigma-Aldrich; Taufkirchen, Germany): 5'-TGCGCGTGGCCTATCTGGAC (forward) and 3'-CTTG-GTCCAGCGTAGGGCAGG (reverse).

2.12 | CRISPR/Cas9-mediated BCAM disruption OVCAR8 cells

The pX330-U6-Chimeric_BB-CBh-hSpCas9 vector with puromycin selection marker was a gift from Dr. Elke Pogge von Strandmann. sgRNAs targeting BCAM were cloned into linearised px330 vector. The sequences used for sgRNA are as follows:

sgRNA #1 – (5'-CACCTGCGAGCAACAGCAGCCGCG-3'),

sgRNA #2 – (5'-CACCCTGCGAGCAACAGCAGCCG-3'),

sgRNA #3 – (5'-CACCGCGCTTGTCTGTACCCCGCTGG-3').

After transfection using TransIT-X2 the OVCAR8 cells were placed into 96-well plates at the concentration of 1 cell/well. Single colonies were picked, and gene disruption was validated by immunoblot analysis. Control clones were generated by transfection of the empty px330 vector.

2.13 | xCELLigence real-time cell analysis of tumour cell adhesion and migration

Adhesion and migration assays were performed using the xCELLigence real-time cell analysis (RTCA) DP instru-

ment (ACEA Biosciences/Agilent; Waldbronn, Germany) placed in a humidified incubator at 37°C and 5% CO₂. For cell adhesion assays, E-plates-16 (ACEA Biosciences/Agilent; Waldbronn, Germany; #2801032) were used. The plates were coated with LN-511 or COL1 overnight at 4°C, washed with PBS and blocked with 1% bovine serum albumin in PBS for 1 h at 37°C. After blocking, the wells were washed, and 20,000 cells detached with Accutase solution were seeded per well. Impedance was measured every 3 min for the first 8 h, followed by every 15 min for the next 12 h. The cell index indicates the micro-electrode impedance, which corresponds to the strength of cell adhesion.

For cell migration assays, CIM-16 plates (ACEA Biosciences/Agilent; Waldbronn, Germany; #2801038) were used. These plates resemble Boyden chamber plates with upper and lower compartments separated by an 8 μm pore-containing membrane, with the impedance-measuring electrodes at the lower side. Following coating with LN-511 or COL1 overnight at 4°C, plates were washed and blocked with 1% bovine serum albumin in PBS for 1 h at 37°C. Wells were rinsed with PBS and 60,000 cells in serum-free medium were seeded into the upper compartment and allowed to migrate to the lower compartment containing medium with 10% serum. Impedance was measured every 15 min for 48 h. The cell index corresponds to the number of cells that migrated through the pores.

2.14 | Tumour cell motility

For cell motility, untreated μ slide VI uncoated 0.1 polymer coverslips (Ibidi; Gräfelfing, Germany) were coated with human recombinant laminin-511 and blocked with 1% BSA. OVCAR cells were labelled with cell tracker green CMFDA according to the manufacturer's protocol and detached with Accutase solution. Labelled cells were seeded at 20,000 cells/30 μl channel and grown for 3 h in complete medium. Cells were then incubated at 37°C in serum-free medium for 1 h in a CO₂ microscope stage incubator before monitoring cell migration by spinning-disc microscopy without medium change. Fluorescence images (488 nm laser) were taken at 10-min intervals for 12 h at 37°C and 5% CO₂ using an AxioObserver Z1 microscope and AxioVision software (Carl Zeiss). Images were processed with Imaris software (Oxford instruments; Wiesbaden, Germany), and the positions of cells were tracked using Imaris 3D tracking algorithm (Brownian motion) to quantify cell motility. For each condition, cells were tracked from 5 different fields. Trajectory plot combined with motility rate (μm/h) was plotted using Python functions.

2.15 | Spheroid formation and analysis

Spheroids were formed by seeding 2500 cells in a 96-well U-bottom cell-repellent plate (Greiner Bio-One; Frickenhäusen, Germany; #650970). For the experiments in Figure 5, spheroids were formed in the presence of 20 $\mu\text{g/ml}$ control IgG1, integrin $\beta 1$ activating antibody, 10 $\mu\text{g/ml}$ integrin $\beta 1$ blocking antibody or 10 $\mu\text{g/ml}$ LN-511. Cells were monitored with a DMI3000B microscope (Leica; Wetzlar, Germany). Images were processed using ImageJ/Fiji software. Circularity was calculated using an inbuilt feature of ImageJ software. The percentage of gaps as a reflection of spheroid compactness was calculated as (gap area of spheroid/ total area of spheroid) $\times 100$.

2.16 | Spheroid dispersion in a 3D collagen matrix

Spheroids were formed as described above. Collagen I was neutralised 1 N NaOH, adjusted to a final concentration of 2 mg/ml, added to 96-well plates (50 $\mu\text{l/well}$) and incubated for 5 min at room temperature. One spheroid was transferred to each well, incubated with 75 μl of COL1 solution for 1 h at 37°C and overlaid with 100 μl of medium. Spheroids were monitored and pictures were taken using Leica SP8i confocal microscopy (Leica; Wetzlar, Germany). Images were processed using ImageJ/Fiji software for further quantification. Percent dispersion was calculated as (area at 48 h – area at 0 h)/area at 0 h $\times 100$.

2.17 | Mesothelial cell clearance

Spheroids were generated as described above using tumour cells labelled with Cell Tracker Green. 96-well plates were coated with collagen I at a concentration of 5 $\mu\text{g/cm}^2$ for 45 min at 37°C. Mesothelial cells labelled with Cell Tracker Orange were seeded in 96-well plates (14,000 cells/well) and allowed to form a confluent monolayer. After 4 days, 1 spheroid was transferred to each well and monitored for 48 h by Leica SP8i confocal microscopy (Leica; Wetzlar, Germany). Images were processed using ImageJ/Fiji software for further quantification. Mesothelial cell clearance was calculated as cleared area at 48 h/spheroid area at 0 h.

2.18 | Immunohistochemistry of BCAM, LAMA5, COL1 and COL4

For immunohistochemistry, heat-induced epitope retrieval was performed with EDTA for LN-511 subunit LAMA5, COL1 and COL4 and with Trilogy for BCAM. Stain-

ing was performed on a DAKO autostainer plus. After blocking endogenous peroxidase, sections were incubated for 45 min with mouse monoclonal anti-BCAM antibody (1:25; R&D systems #MAB1481, clone 87207), mouse monoclonal anti-LAMA5 antibody (1:50; Atlas Antibodies # AMAb91124, clone CL3118), mouse monoclonal anti-Collagen IV antibody (1:100; Dako/Agilent; Waldbronn, Germany; #M0785, clone CIV22) or rabbit polyclonal anti-Collagen I antibody (1:200; Abcam #ab34710). Sections were washed and incubated with Dako REAL EnVision HRP Rabbit/Mouse polymer, which reacts with DAB-Chromogen, according to the manufacturer's protocol.

2.19 | Omentum model

Spheroids were generated by seeding 250,000 pre-labelled cells (0.5 μM Cell Tracker Green) in a 24-well ultra-low attachment plate (Merck; Darmstadt, Germany; #CLS3473-24EA). After 72 h spheroids of two wells were collected for each omentum. Mice were maintained and handled according to the internal approval by the local animal welfare officers. The protocol of Khan et al.³⁶ was applied with some modifications. C57Bl/6 J mice (8-12 weeks old; Charles River Laboratories, Sulzfeld, Germany) were sacrificed and the omentum, pancreas and spleen were excised *en bloc* by cutting the connections to the gastrointestinal tract and placed in ice-cold PBS, where pancreas and spleen remained at the bottom, while the adipose-rich omentum floated on the surface. By trimming its base, the omentum was separated from the surrounding organs. The omentum was placed in a reaction tube containing 3 ml of tumour cell spheroid suspension corresponding to 5×10^5 cells and kept under rotation at 37°C, 2% O₂, 93% N₂ and 5% CO₂ for 3 h. The spheroid suspension was then replaced by culture medium and the tissue was kept under rotation for an additional hour to remove loosely and non-attached cells.

Next, the omentum was attached to a Millicell culture insert (Merck Millipore, #PIC03050) using Cell-Tak Cell and Tissue Adhesive (Corning/VWR, Göttingen, Germany; #10317081). For this purpose, 7.5 μl Cell-Tak was spread evenly on the insert membrane and air-dried under laminar flow at room temperature. After two washing steps with 1 ml sterile water, the membrane was air-dried and the insert was placed in a 6-well culture plate. To allow optimal attachment, the omentum was placed on the pre-coated insert membrane without medium for 1 min. Three millilitres of culture media were pipetted into the insert and 2 ml into the surrounding well. Co-culture was carried out under hypoxic conditions³⁷ for additional 44 h at 37°C and 2% O₂, 93% N₂ and 5% CO₂. Under these conditions, a similar intensity of VCAM1 immunostaining was observed

during the observation period of the experiments, indicating that no significant activation or senescence occurred during the chosen incubation period (see *Results* section for details).³⁸

2.20 | Whole mount staining and fluorescence microscopy

After co-culture with tumour cells, whole mount staining of the omentum was performed based on a published protocol³⁹ as follows. The omentum was transferred into a 5 ml reaction tube, blocked using TruStain FcX (BioLegend; Amsterdam, Netherlands; #101320) at 10 $\mu\text{g}/\text{ml}$ in 200 μl of PBA (PBS, 1% BSA and 0.1% sodium azide) at 4°C under rotation for 10 min. Antibodies were then added directly to the tube and incubated for 2 h at 4°C under rotation (anti-CD45-PE-Vio615 6 $\mu\text{g}/\text{ml}$; anti-CD31-PE: 10 $\mu\text{g}/\text{ml}$; anti-CD45-AlexaFluor 647: 12.5 $\mu\text{g}/\text{ml}$; anti-CD45 APC 5 $\mu\text{g}/\text{ml}$). After washing in 2 ml PBA at 4°C under rotation the tissue was embedded in 1% agarose and fixed in a glass cuvette filled with PBS.

Fluorescence microscopy was performed on a Luxendo LCS SPIM light-sheet Microscope (Bruker Corp.; Billerica, MA, USA) using the following laser and filter settings: 488 nm with BP 500–530; 561 nm with BP 580–627; 642 nm with BP 655–704. Excitation and detection were performed via 4 \times objectives (excitation: Nikon, numerical aperture 0.13; detection: Olympus, numerical aperture 0.28) and images were taken in 2.2-fold magnification.

We also performed multiphoton microscopy to visualise collagen fibres by second-harmonic generation on an FVMPE-RS Multiphoton Microscope (Olympus; Hamburg, Germany) equipped with Spectra Physics pulsed laser Insight DeepSee 690 – 1300 nm and MaiTai Sa 690–1040 nm. A 25-fold magnification was achieved with a water immersion objective with a numerical aperture of 1.05. Z-stack images were taken from different regions of the omentum. For this purpose, the tissue was fixed on a cover slip (NeoLab; Heidelberg, Germany; #1-6292) by covering with 1% agarose in PBS. Image analysis was performed with Imaris software 9.9.0 (Bitplane) where fluorescently labelled tumour cells were defined and counted as spots or surfaces.

2.21 | Quantification of OVCAR8 invasion into mouse omentum by Taqman-PCR

Genomic DNA was isolated from the omentum using the NucleoSpin DNA lipid tissue kit (Macherey-Nagel; Düren, Germany; Cat# 740471.50) according to the manufacturer's instructions. Tissue lysis was performed

in Qiagen's Tissue Lyser TL at 50 Hertz for 5 min. hALU TaqMan RT-PCR was performed on a StrataGene Mx3005P real-time instrument using the forward primer 5'-GGTGAAACCCCGTCTACT-3', reverse primer 5'-GGTTCAAGCGATTCTCCTGC-3' and probe 5'-[6FAMCGCCCGGCTAATTTTTGTAT[BHQ1]-3'⁴⁰ in a total volume of 20 μl containing 10 μl TaqMan Universal Master Mix II, no UNG (Thermo Fisher; Dreiech, Germany; #10380155), 0.3 μM forward and reverse primers, 0.25 μM hydrolysis probe and the corresponding amounts of genomic DNA. The following PCR conditions were used: 1 cycle of 95°C for 10 min, followed by 50 cycles of 95°C for 15 s 56°C for 30 s and 72°C for 30 s. Control RT-PCR of murine SINEs *B2* was performed using ABsolute QPCR SYBR Green Mix (Life/ThermoFisher; Dreiech, Germany; #AB-1158B) and the primers 5'-CAATCCCAGCAACCACATG-3' (forward) and 5'-ACACACCAGAAGAGGGCATCA-3' (reverse).⁴¹ PCR conditions were one cycle at 95°C for 10 min, followed by 40 cycles at 95°C for 15 s, 56°C for 45 s and 72°C for 30 s.

2.22 | Mouse model and PET/CT imaging

Tumour cell spheroids generated as for the ex vivo model described above were injected intraperitoneally (i.p.) into immune-deficient BALB/c-nude mice (CanN.Cg-Foxn1nu/Crl; Charles River Laboratories; Sulzfeld, Germany) and the development of metastases was observed at day 28 post injection. One hour before application of 18F-FDG, mice were placed on a 37°C warm surface to minimise consumption of 18F-FDG by brown adipose tissue. To avoid interference of 18F-FDG uptake by insulin and to reduce consumption by the myocardium, animals were deprived of food for a period of 4 h before application. 18F-FDG was administered i.v. at a dose of 10 MBq in 100 μl of 0.9% NaCl solution into the tail vein 1 h prior to PET/CT imaging under isoflurane anaesthesia for maximally 60 min using a preclinical scanner from Mediso (NanoScan; Mediso Medical Imaging Systems; Budapest, Hungary). Respiration and temperature were observed during the complete acquisition period. Prior to PET a CT scan was performed for each measurement (5 min) for attenuation correction. PET data were acquired with an energy window of 400–600 keV and a coincidence time window of 5 ns. The data were reconstructed using Teratomo 3D from Mediso with a binning of 1:3. A matrix size of 212 \times 212 \times 239 (voxel: 0.4 mm) was used. CT data (50 kVp, 630 μA , 480 views over 360°) were acquired in one rotation. PET/CT images were reconstructed using a Tera-TomoTM 3D algorithm (Nucline 3.01.020.000; Mediso Medical Imaging Systems,

TABLE 1 Functional annotation of genes associated with a poor overall survival (OS) of human adenocarcinomas. Genes with a z -score > 2 (i.e., $p < .05$ and hazard ratio > 1) were retrieved from the PRECOD dataset and analysed for enrichment of GO biological processes. The table lists the top term for each instance, including the number of enriched genes, the fold enrichment and the FDR. Only terms with a fold enrichment ≥ 2.5 and an FDR < 0.01 were included. The data for OC are highlighted in red.

Entity	GO biological process	<i>n</i>	Fold	FDR
Bladder	Mitotic cell cycle	128	3.52	1.2E-26
Breast	Mitotic cell cycle	231	2.50	7.5E-22
Colon	Vasculature development	67	2.64	1.1E-08
Liver	Regulation of intrinsic apoptotic signalling pathway	23	3.59	5.5E-04
Lung	Mitotic cell cycle	206	2.64	2.8E-26
Ovarian	ECM organisation	77	2.80	2.2E-10
Pancreatic	Cellular response to DNA damage stimulus	76	2.59	8.1E-10
Prostate	Mitotic cell cycle	67	4.40	4.2E-14

Budapest, Hungary) with four iterations and six subsets. Co-registration was performed with the software InterView Fusion (Version 3.01.016.0000).

2.23 | Statistical analysis of experimental data and functional annotations

Comparative data were statistically analysed by paired or unpaired Student's t -test (two-sided, unequal variance), as indicated in the figure legends. Statistical significances are indicated as follows: * $p < .05$; ** $p < .01$; *** $p < .001$; **** $p < .0001$. Box plots with medians, upper and lower quartiles, range and outliers were constructed using the Seaborn boxplot function with Python. Functional annotations by gene ontology enrichment analysis or PANTHER classification⁴² were performed using the online tool at <http://geneontology.org>. Reactome analysis was carried out at <https://reactome.org>.

3 | RESULTS

3.1 | A specific role for BCAM in OC

Analysis of the published TCGA transcriptome dataset⁴³ revealed that OC exhibits the highest expression of *BCAM* mRNA of all human malignancies (Figure S1A). Expression of *BCAM* mRNA is associated with both a poor OS (Figure S1B) and RFS (Figure S1C). Intriguingly, *BCAM* expression is significantly associated with a short OS of only two other cancers among the 39 entities in the PRECOG database (Figure S1B; red bars), pointing to a specific role for BCAM in OC. Gene ontology enrichment analysis of genes associated with a poor OS of different human adenocarcinoma revealed ECM organisation and integrin signalling as the most significant term specifically for OC (Table 1), as did Reactome analysis ($p = 1.9 \times 10e17$).

PANTHER classification⁴² of the same gene set identified integrin signalling as the most significant pathway for OC ($p = 4.9 \times 10e-9$). Taken together with the published observations on BCAM-LAMA5-integrin interactions,⁵ these data point to a potential connection between a poor clinical outcome of OC and a role for BCAM in ECM-mediated signalling.

3.2 | Characterisation of soluble BCAM in OC ascites

The source and potential functions of soluble BCAM in cancer are unknown. To elucidate the nature of ascites-associated BCAM in OC patients we performed immunoblotting experiments, which revealed only traces of, if any, BCAM1/2 with an apparent molecular mass of 95 kDa, while a shorter BCAM form of approximately 80 kDa was abundant (Figure 1A). Consistent with these findings, a short BCAM form of very similar length was observed in conditioned medium from OVCAR4 cells, while BCAM1/2 was detected exclusively in whole cell extracts (Figure 1A, rightmost lanes). The signal intensities for the shorter BCAM form in ascites correlated well with the BCAM levels measured by ELISA (Figure 1A, bottom). We will henceforth refer to this shorter soluble BCAM form in ascites and conditioned medium as sBCAM. ELISA measurements of $n = 70$ ascites samples of a high-grade serous OC patient cohort²⁵ revealed a wide concentration range for sBCAM of 0–520 ng/ml with a median level of 76 ng/ml (Figure 1B), and ascites levels of sBCAM were significantly associated with a short RFS (Figure 1C), consistent with a previous aptamer-based analysis.²⁵ Correlation analyses showed a link between the levels of BCAM protein in tumour cells from ascites²⁹ (ascTU) and the level of sBCAM in ascites (Spearman $\rho = 0.78$; $p = .014$), suggesting that the expression level

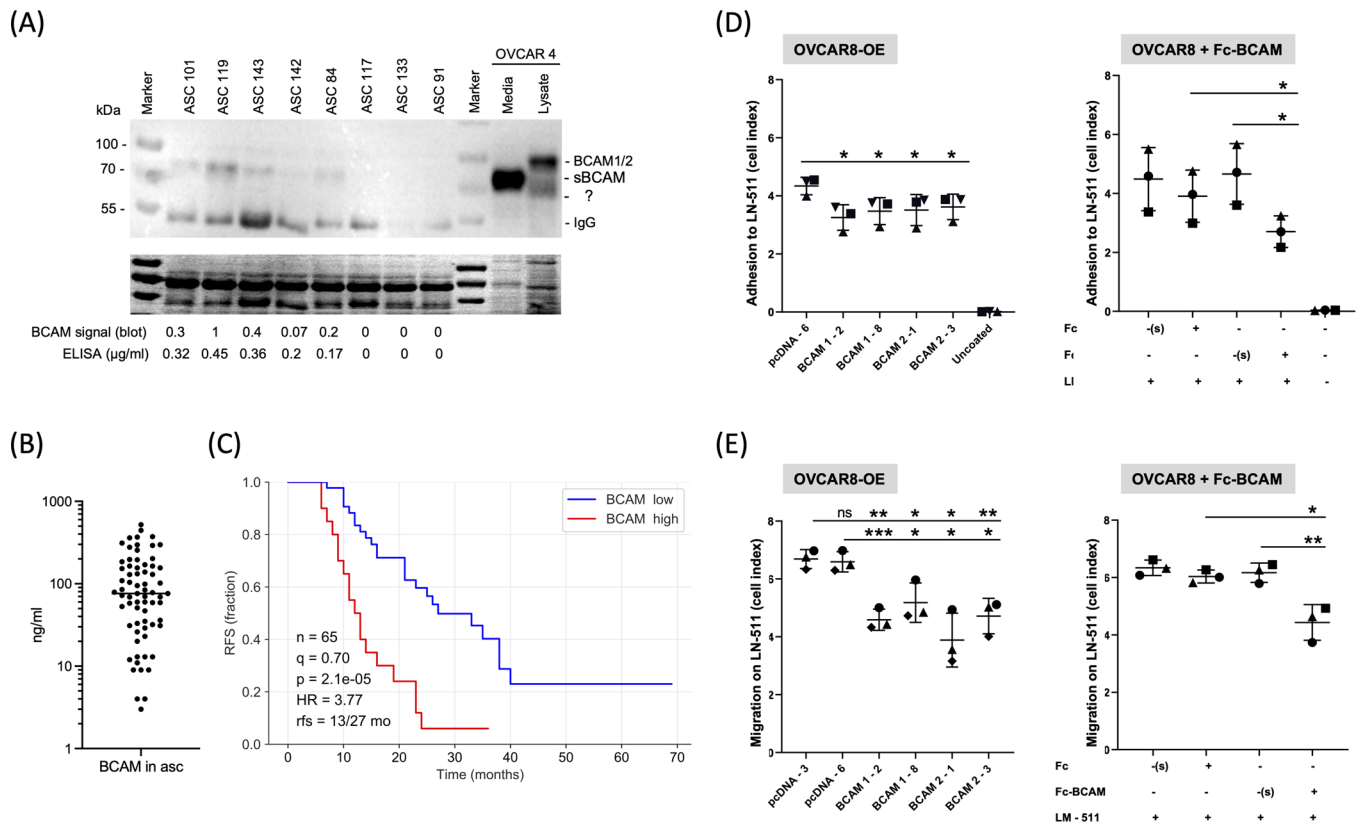


FIGURE 1 Analysis of BCAM in OC ascites and comparative functional analysis of membrane-bound and soluble BCAM. (A) Immunoblot of BCAM in eight different cell-free ascites samples. For comparison, conditioned medium (containing sBCAM) and lysate from OVCAR4 cell was included (right-most lanes). Quantitation of relative signal intensities as well as BCAM levels in ascites samples measured by ELISA are shown at the bottom. The band labelled with "?" denotes an unspecific background band. The bottom panel shows the membrane after staining with the Pierce Reversible Total Protein Stain Kit as loading control. (B) Concentration of BCAM protein in the ascites from $n = 70$ high-grade serous OC patients determined by ELISA. (C) Kaplan–Meier plot analysing the relapse-free survival (RFS) of $n = 65$ evaluable patients analysed in panel B. Groups were split at the $q = 0.7$ quantile (best-fit); p : logrank p value; HR: median hazard ratio; rfs: months to 50% RFS for patients with high/low BCAM levels. (D) Effect of BCAM on OC cell adhesion to LN-511 on non-adhesive microplates coated with LN-511. Cell adhesion was quantified by RTCA. Left: BCAM-overexpressing OVCAR8 cells (OVCAR8-OE). Clones stably transfected with BCAM1 or BCAM2 (Figure S4) were compared with cells transduced with the empty expression vector (pcDNA-6). Right: Adhesion of OVCAR8 cells was analysed in the presence of Fc-BCAM or negative control (Fc) at equimolar concentration (1 µg/ml of Fc-BCAM; 0.33 µg/ml of Fc). (s): solvent for Fc or Fc-BCAM. (E) Effect of BCAM on two-dimensional OC cell migration under the same conditions as in panel D, except that a further control clone (pcDNA3) was included. Transwell-chamber microplates were coated with LN-511 and cell migration was quantified by RTCA. The data in D and E are based on $n = 3$ biological replicates. * $p < .05$; ** $p < .01$; *** $p < .001$; ns, not significant by unpaired t test.

of BCAM, besides shedding proteases, is one of the factors determining the concentration of sBCAM. In tumour cells from ascites, *BCAM1* RNA was the predominant form in most samples, with a highly variable *BCAM1/BCAM2* ratio ranging from 0.8 to 50 (Figure S2).

3.3 | Comparative functional analysis of membrane-bound and soluble BCAM

Previous studies with 3T3 fibroblasts,⁷ HT1080 osteosarcoma cells,⁵ gastric cancer cells,⁸ rat hepatoma cells¹⁸ and MDCK cells¹⁹ showed that BCAM can modulate cell adhe-

sion and migration on LN-511 matrices (see *Background* for details). To compare the biological properties of the BCAM forms we therefore analysed their effect on the adhesion and migration of OC cells. LN-511 deserves particular attention due to its prominence in the OC TME, as suggested by the high RNA expression of its subunits in tumour and/or tumour-associated cells³⁰ (Figure S3A), which is mirrored by OVCAR cell lines (Figure S3B).

As a source of soluble BCAM protein for functional assays, we used recombinant Fc-BCAM expressed in mammalian cells. Fc-BCAM is composed of a fragment lacking the transmembrane and the intracellular domains fused to an Fc fragment. Importantly, Fc-BCAM retains an intact

LAMA5 binding site.¹⁵ Fc-BCAM was used at a concentration of 1 $\mu\text{g}/\text{ml}$, which approximately corresponds to the highest molar concentration of sBCAM in ascites (Figure 1B). The impact of different BCAM forms on matrix adhesion was quantified by xCELLigence-based RTCA.⁴⁴ Overexpression of BCAM1 or BCAM2 (Figure S4A; cell surface localisation verified in Figure S4B) or exposure to Fc-BCAM resulted in an inhibition of adhesion to LN-511 (Figure 1D). As reduced adhesion of BCAM-overexpressing cells was observed as soon as attachment was detectable (~ 15 min after plating; Figure S7), it is likely that non-cleaved, membrane-bound BCAM contributes to the inhibitory effect. Consistent with gain-of-function experiments in Figure 1D, BCAM gene disruption (Figure S5A) or inhibition of BCAM expression by siRNA-mediated interference (Figure S5B) enhanced adhesion (Figures S6C and D).

Analysis of adhesion to LN-511 of 3 additional vector control clones and wildtype OVCAR8 cells (not shown) yielded results identical to the control clone used in Figure 1D (pcDNA-6), thus strongly reducing the probability of experimental artefacts due to clonal selection. Moreover, no significant effects of BCAM were observed on the adhesion of OC cells to COL1 (Figure S6E–G), which may be relevant with respect to its known role in OC cell invasion.^{45–50}

Similar to its effect on adhesion, overexpression or the addition of Fc-BCAM (Figure 1E) inhibited migration, while BCAM disruption resulted in enhanced migration (Figure S8C). Furthermore, real-time microscopic analyses of undirected motility of BCAM-overexpressing and Fc-BCAM-treated OVCAR8 cells revealed a clear inhibitory effect on both cases (Figures S8D and E).

Our findings are consistent with the known interaction of BCAM with LAMA5 (the LN-511 alpha subunit), which has been proposed to interfere with LAMA5 binding to integrins.⁵ Importantly, BCAM1 and BCAM2, the latter lacking most of the intracellular domain, showed nearly identical effects, suggesting that BCAM does not act as a signalling receptor to mediate inhibition of LN-511-dependent adhesion. This conclusion is supported by the remarkably similar effect of Fc-BCAM and the membrane-associated BCAM proteins.

3.4 | Metalloproteinases produced by OC cells

The data in Figure 1A suggest that sBCAM may be generated by shedding through proteolytic cleavage of the membrane-bound forms. To identify candidate BCAM sheddases, we analysed our published proteomics datasets²⁹ of tumour cells from OC ascites for expression

of metalloproteinases of the ADAM and MMP families. As shown in Figure 2A, four ADAMs (ADAM9, 10, 15, 17) and three MMPs (MMP8, 9, 14) were identified in whole cell proteomes. The highest expression levels were observed for ADAM10 and ADAM17, raising the possibility that they might represent BCAM-cleaving proteases. In agreement with this result, ADAM9, 10 and 17 were also found in the secretome of these cell types, with the highest expression levels observed for ADAM10 (Figure S9A).

To gauge the suitability of OC cell lines as experimental models we analysed the expression of ADAM genes in OVCAR3, OVCAR4, OVCAR5 and OVCAR8. As shown in Figure S9B, all four cell lines expressed ADAM9, ADAM10, ADAM15 and ADAM17 at levels of ~ 40 –370 TPM, while transcripts from all other ADAM genes were much lower or undetectable. This pattern is consistent with the proteome data for primary tumour cells described above (Figure 2A), particularly for OVCAR4, OVCAR5 and OVCAR8 (low ADAM15 expression). These three cell lines also expressed the active form of ADAM10 (Figure S10A). However, OVCAR5 cells exhibited barely detectable expression of BCAM protein (Figure S10B), which is inconsistent with the *in vivo* findings (Figure 2A), and were therefore excluded from further analyses.

3.5 | Identification of ADAM10 as the major BCAM sheddase of OC cells

Production of sBCAM by OVCAR-4 cells was strongly inhibited by the broad-spectrum metalloproteinase inhibitor marimastat in a concentration-dependent fashion, as shown by immunoblotting and ELISA (Figures S11A and B) of conditioned medium (85% inhibition at 1 μM). A similar pattern was observed with a recombinant ADAM10 prodomain, a specific inhibitor of ADAM10⁵¹ (Figures 2B and C; 88% inhibition at the lowest dilution), pointing to a significant role for ADAM10 in shedding BCAM from OC cells. This was confirmed by siRNA-mediated interference with ADAM10 expression (Figures 2D and S10C), showing 85% inhibition similar to the ADAM10 prodomain. Interference with ADAM17 expression also significantly inhibited the release of sBCAM but to a considerably lower extent (35% inhibition; Figures 2E and S10D). These data strongly suggest that both ADAM10 and ADAM17 contribute to BCAM shedding, with ADAM10 as the major contributor.

3.6 | ADAM10 cleavage sites in BCAM protein

Cleavage of BCAM by ADAM10 was reproduced using recombinant proteins. As shown in Figure 2F and

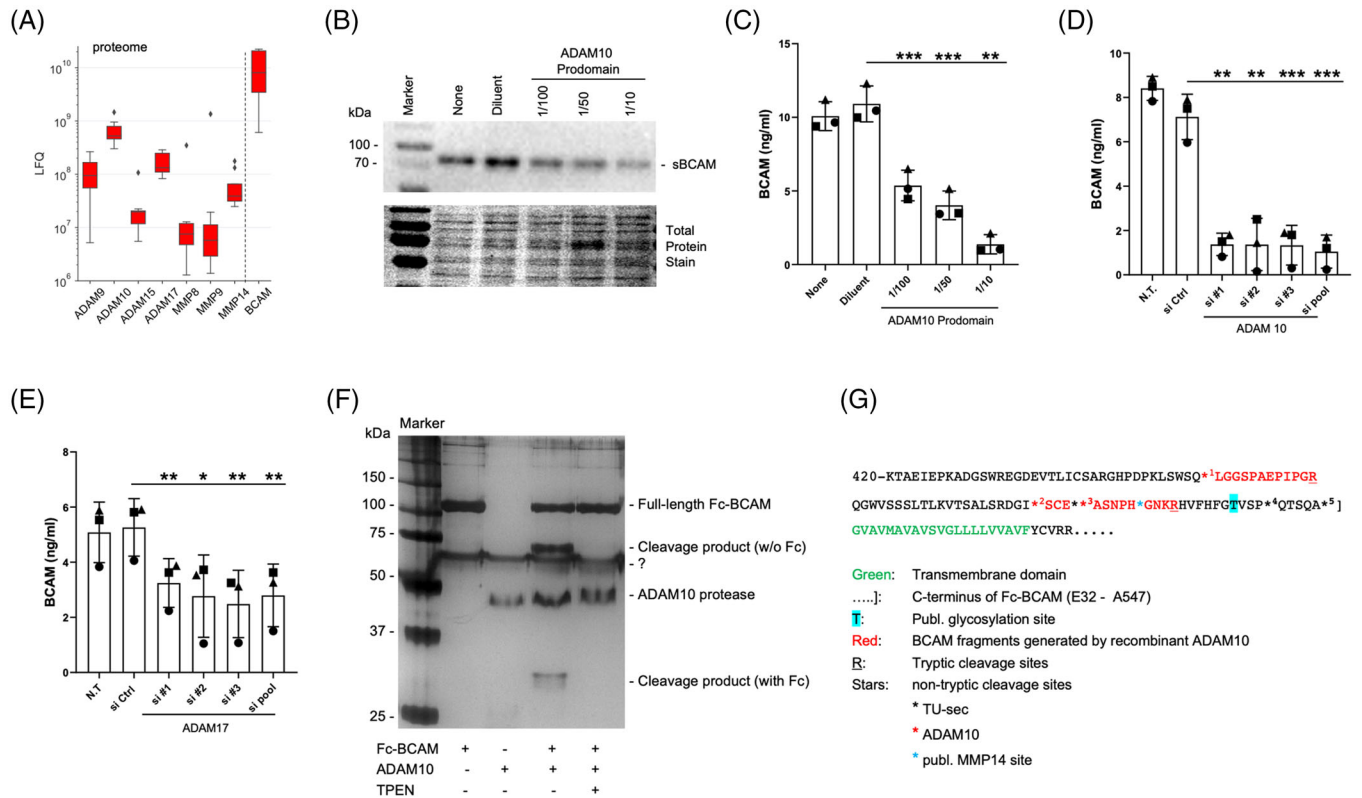


FIGURE 2 Role of ADAM10 in the generation of sBCAM and identification of cleavage sites. (A) Distribution of BCAM and metalloproteinase expression in tumour cells from $n = 9$ OC patients, based on a previously published dataset obtained by MS-based proteomic analysis.⁵ Signal intensities reflect LFQ values. Boxplots show medians (line), upper and lower quartiles (box), ranges (whiskers) and outliers (diamonds). (B) Immunoblot of medium from OVCAR4 cells cultured in the presence of different concentrations of the ADAM10 prodomain (selective ADAM10 inhibitor)⁵¹ for 24 h. The panel below the immunoblot show the respective membranes stained with the Pierce Reversible Total Protein Stain Kit. (C) ELISA-based quantification of sBCAM secretion by OVCAR4 cells treated as in panel B. (D) Analysis of BCAM release by OVCAR4 cells treated with three different siRNAs targeting ADAM10 (si#1, si#2, si#3), a pool of all three siRNAs (si pool) or negative control siRNA (si Ctrl). The leftmost bar represents non-transfected cells (NT). Cell culture media were analysed by ELISA as in panel C. (E) Analysis of OVCAR4 cells as in panel D but treated with ADAM17-targeting siRNAs. * $p < .05$; ** $p < .01$; *** $p < .001$ by unpaired t -test. (F) Silver-stained PAGE gel of recombinant Fc-BCAM after digestion with recombinant ADAM10 and in the absence or presence of the zinc chelator TPEN. '?' denotes an unspecific background band. (G) Schematic representation of the C-terminal amino acid sequence of BCAM, including the ADAM10 cleavage sites in recombinant BCAM identified in panel F (Table S3), the cleavage sites found in the secretome of tumour cells from OC ascites (TU-sec; Table S4) and the previously published MMP14 cleavage site.²⁶

Tables S2 and S3, incubation of recombinant Fc-BCAM (see Figure 2G for details) with recombinant ADAM10 yielded two fragments, which disappeared in the presence of the zinc chelator and ADAM10 inhibitor TPEN, indicating the specificity of the observed cleavage. Mass spectrometry (MS) identified three cleavage sites near the transmembrane domain (red stars in Figure 2G; sites 1, 2 and 3). MS analysis also identified three cleavage sites in BCAM in the conditioned medium from primary OC cells (black stars in Figure 2G; sites 3, 4 and 5), one of which (site 3) coincides with a cleavage site found with recombinant ADAM10. A published MMP14 cleavage site²⁶ is also indicated (blue star in Figure 2G).

To gain further insight into the role of ADAM10 in BCAM cleavage we sought to align sites 1–5 with known

ADAM10-targeted motifs. As ADAM10 activity is highly promiscuous, a clear consensus sequence of its targeted cleavage sites has not been defined. We therefore made use of two published unbiased screening approaches identifying preferred amino acids surrounding ADAM10 cleavage sites.^{52,53} We combined these datasets to compile the table in Figure S12A, which also distinguishes between strongly and weakly enriched amino acids. Figure S12B shows alignments of cleavage sites 1–5 in BCAM with these published data. Sites 3–5 show considerable matches, consistent with ADAM10-mediated cleavage. It is possible that sites 4 and 5, which are cleaved in vivo, are missing in the in vitro experiment, as they are located close to the C-terminus of the BCAM fragment and the Fc fusion (see Figure 2G). By contrast, sites 1 and 2 identified in cleaved

TABLE 2 Summary of immunohistochemical analysis of BCAM, LAMA5, COL1 and COL4 in matched samples of OC metastases (Met) and spheroids from ascites (Asc). Staining intensities were classified as follows: Negative (0, black), weak (1, blue), moderate (2, brown) and strong (3, red). Metastatic sites analysed are listed in Table S2. Examples are shown in Figures 3 and S13

Patient ID	BCAM			Laminin α 5 (LAMA5)			Collagen I (COL1)			Collagen IV (COL4)		
	Met tumour	Met stroma	Asc spheroid	Met tumour	Met stroma	Asc spheroid	Met tumour	Met stroma	Asc spheroid	Met tumour	Met stroma	Asc spheroid
OC26	3	2	3	0	0	3	1	2	3	0	1	0
OC27	3	2	3	0	0	1	1	2	2	0	1	0
OC54	1	1	2	0	0	2	1	2	2	0	1	0
OC66	1	1	3	0	0	2	0	1	2	0	1	0
OC67	2	2	3	0	0	2	1	1	2	0	1	0
OC84	3	2	3	3	0	2	1	3	2	0	1	1
OC114*	1	1	3	0	0	2	0	1	3	0	1	0
OC122	2	2	3	2	0	1	1	2	2	0	1	0

*Small metastases from patient OC114 were positive of LAMA5 (score 2; see Figure 3).

Fc-BCAM barely matching the published amino acid preferences (Figure S12B) were not found in vivo and therefore likely play a minor role, if any, in the shedding of BCAM by ADAM10. This suggests that the sites proximal to the transmembrane domain (site 3 and possibly 4 and 5) are the major sites cleaved by ADAM10 to produce sBCAM from OC cells.

Our findings together with published data indicate that BCAM is cleaved by at least three proteases (ADAM10, ADAM17, MMP14) at multiple adjacent sites, suggesting that sBCAM in ascites (Figure 1A) represents a mixture of fragments with different C-termini. Although the exact lengths of these proteins with a relative molecular mass of 70 kDa are not known, it is highly likely that they retain the LAMA5-binding site, which is located far away from the cleavage sites and functionally relevant in the context of our study.

3.7 | Immunohistochemical visualisation of BCAM and matrix proteins in OC metastasis and spheroids from OC ascites

To be able to interpret the results obtained in the present study in the context of OC metastasis we analysed BCAM, the LN-511 α -subunit LAMA5 and COL1 in metastases and ascites spheroids from eight patients (clinical data in Table S2) by immunohistochemistry. The results of this analysis are summarised in Table 2 and examples are presented in Figures 3 and S13 and can be summarised as follows:

1. BCAM is expressed in tumour and stroma compartments of metastasis as well as in spheroids, albeit at varying levels;

2. LAMA5 expression is observed in all spheroids in contrast to metastases (two out of eight positives in tumour compartment; stroma compartment negative in all samples except for a few small areas with positive cells in two cases; see Table 2);
3. Tumour cells in early metastases (small and near the surface) from patient OC114 are LAMA5-positive, and in this respect resemble spheroids more closely than advanced metastases, supporting the notion that LAMA5 protein or accessibility may be regulated during metastatic growth in some cases;
4. COL1 is clearly expressed in the stroma compartments of all tumour samples and all spheroids; expression is weaker in the tumour cell compartments.

COL1 and LAMA5 were found majorly as deposits around cells, particularly in spheroids, while BCAM antibodies stained both the plasma membrane and cytoplasm, albeit with inter-sample variability (Figure S13). These results agree with the proposed essential role for COL1 in OC metastasis.^{45–50} The data also reveal a potential role for LAMA5 selectively in spheroids with implications for BCAM. For comparison, we also analysed the expression of the basal membrane protein collagen IV (COL4), which was not detectable in the tumour compartment of all metastases and spheroids (examples in Figure S13 and Table 2).

3.8 | Impact of BCAM on OC spheroid formation

The inhibitory effects of BCAM on known functions of tumour cells, that is, adherence and migration of single cells (Figures 1D, 1E, S6–S8), cannot explain its

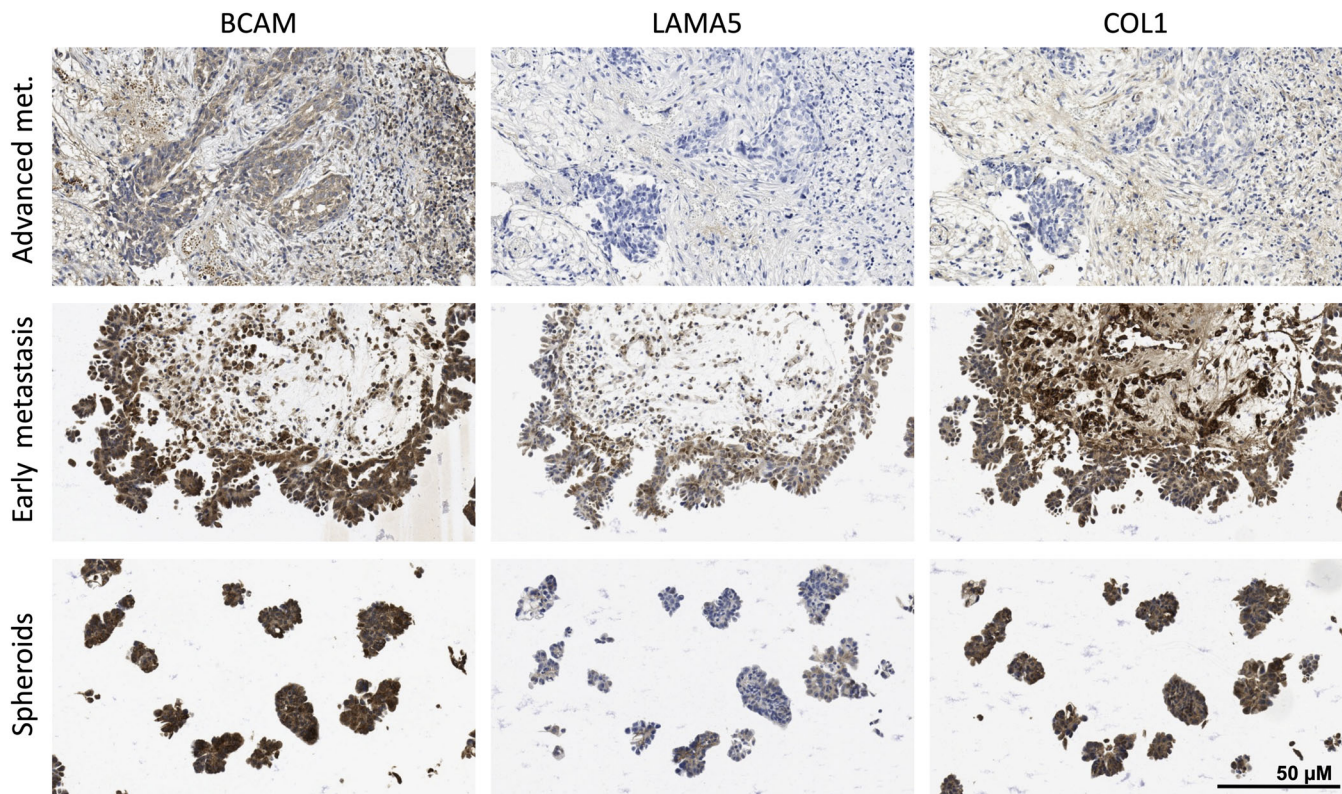


FIGURE 3 Immunohistochemical analysis of BCAM, LAMA5 and COL1 in matched samples of OC metastases and spheroids from ascites. Paraffin sections from metastases at different stages (early metastases: tumour cells still near the surface; advanced metastases: deeply invading larger tumour masses) and spheroids from ascites were stained by immunohistochemistry as described in *Materials and Methods*. A quantification of the images is shown in Table 2 (patient OC114). Further examples are depicted in Figure S13 and quantified in Table 2. Scale bar: 50 μm

association with a poor clinical outcome (Figures 1C and S1). In view of the known pivotal role of spheroids rather than single tumour cells in transcoelomic spreading and the observed deposition of LAMA5-containing laminin in spheroids (Figure 3), we investigated a potential function of BCAM as a laminin-interacting protein in spheroid formation and dynamics. Figure 4A depicts the morphology of OVCAR8 spheroids derived from BCAM1- and BCAM2-overexpressing OVCAR8 cells (OVCAR8-OE) compared with control cells. It is obvious that expression of both BCAM isoforms decreased the compactness of spheroids. This conclusion was confirmed by image analysis of 4 different clones, revealing a significantly decreased circularity (“roundness”) and clearly increased gap formation in spheroids (Figure 4B). In agreement with these observations, genetic disruption (KO) of BCAM in OVCAR8 cells (Figure 4C; OVCAR8-KO) and BCAM siRNA treatment of OVCAR4 cells (Figure 4D) had the opposite effect. To confirm the role of BCAM in spheroid formation, we tested a third cell line, OVCAR3, which expresses BCAM at a similar level to OVCAR8 (Figure S10B). Consistent with the OVCAR4 data, siRNA-mediated inhibition of BCAM expression in OVCAR3 cells resulted in a strongly

increased compaction of spheroids (Figure S14). Finally, exposure of OVCAR8 cells to Fc-BCAM emulated the effect of BCAM overexpression, leading to a significant decrease of spheroid compactness (Figure 4E), analogous to our observations in other functional assays described above.

3.9 | Role of LN-511 and integrin $\beta 1$ in BCAM-regulated spheroid compaction

Considering the results described above we asked whether BCAM might exert its effect on spheroid compaction by interfering with the LAMA5–integrin $\beta 1$ interaction in spheroids. Several lines of experimental evidence support this notion. As shown in Figures 5A–F, an integrin- $\beta 1$ -activating antibody significantly alleviated the inhibitory effect of ectopic BCAM1 or BCAM2 expression in four independent clones in contrast to a control antibody (~3-fold increase in circularity) after a 48-h culture period. Likewise, the addition of soluble LN-511 also significantly reduced the BCAM-mediated effect. Furthermore, an integrin- $\beta 1$ -blocking antibody inhibited the compaction

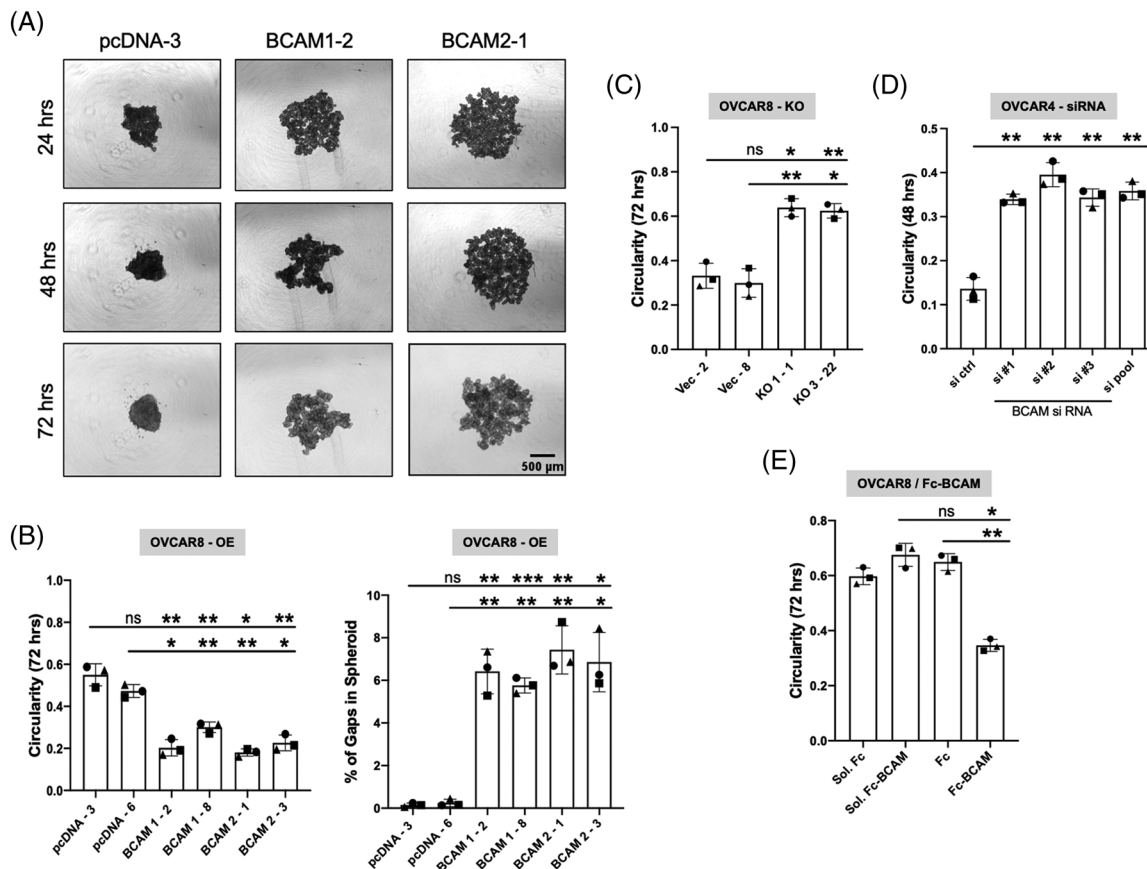


FIGURE 4 Impact of BCAM on OC cell spheroid formation. (A) Morphology of spheroids derived from BCAM-overexpressing OVCAR8 clones (BCAM1-2, BCAM2-1) compared with cells transduced with the empty pcDNA-3 vector (representative examples). Scale bar: 500 μ m. (B) Circularity of spheroids and percentage of gaps in spheroids as in panel A. The plot shows quantifications for two different clones in each case. (C) OVCAR8 cells with disrupted BCAM (OVCAR8-KO) compared with cells transduced with the empty vector (clones Vec-2, Vec-8). The plot shows circularities for two different clones in each case. (D) OVCAR4 cells transfected with control-siRNA (si ctrl), three different BCAM-siRNAs (#1, #2, #3) or pooled siRNAs (pool). (E) Spheroids from OVCAR8 cells formed in the presence of Fc-BCAM or Fc control at equimolar concentration (1 μ g/ml of Fc-BCAM; 0.33 μ g/ml of Fc). Sol: solvent for Fc or Fc-BCAM. Each plot is based on $n = 3$ biological replicates. * $p < .05$; ** $p < .01$; *** $p < .001$; ns: not significant by unpaired t -test

of wild-type OVCAR8 spheroids (Figures 5G and H) similar to BCAM overexpression (Figures 4A and B), indicating that integrin accessibility is essential for spheroid formation. These observations strongly suggest that BCAM reduces the compaction of spheroids by competing with integrin $\beta 1$ for interaction with LAMA5.

3.10 | Impact of BCAM on spheroid dispersion and mesothelial clearance

We next addressed the potential relevance of BCAM's effect on spheroids in the context of transcoelomic metastasis formation. Invasion of peritoneal organs has been described to be critically dependent on spheroid dispersion and clearance of the mesothelial cell layer at attachment sites.⁵⁴ As shown in Figures 6A and B, both BCAM1 and BCAM2 overexpressing OVCAR8-OE

cells showed clearly enhanced dispersion in a collagen matrix compared with vector control cells using 2 different clones for each condition (>100% enlargement of area relative to the initial spheroid after 48 h versus 10–20%). Moreover, exogenous LN-511 added to developing spheroids blocked BCAM-induced spheroid dispersion (Figures 6C and D), suggesting that the role of BCAM in spheroid dispersion is related to its inhibitory impact on LAMA5-dependent spheroid compaction shown in Figure 5.

Mesothelial cell clearance is a step strongly associated with the adhesion to and invasion of peritoneal organs. We therefore addressed the potential role of BCAM in this process using co-cultures of spheroids with mesothelial monolayers. As shown in Figure 7A, both BCAM1- and BCAM2-overexpressing OVCAR8-OE cells (labelled green) efficiently induced gaps in the mesothelial cell monolayer (labelled red) in contrast to control (pcDNA)

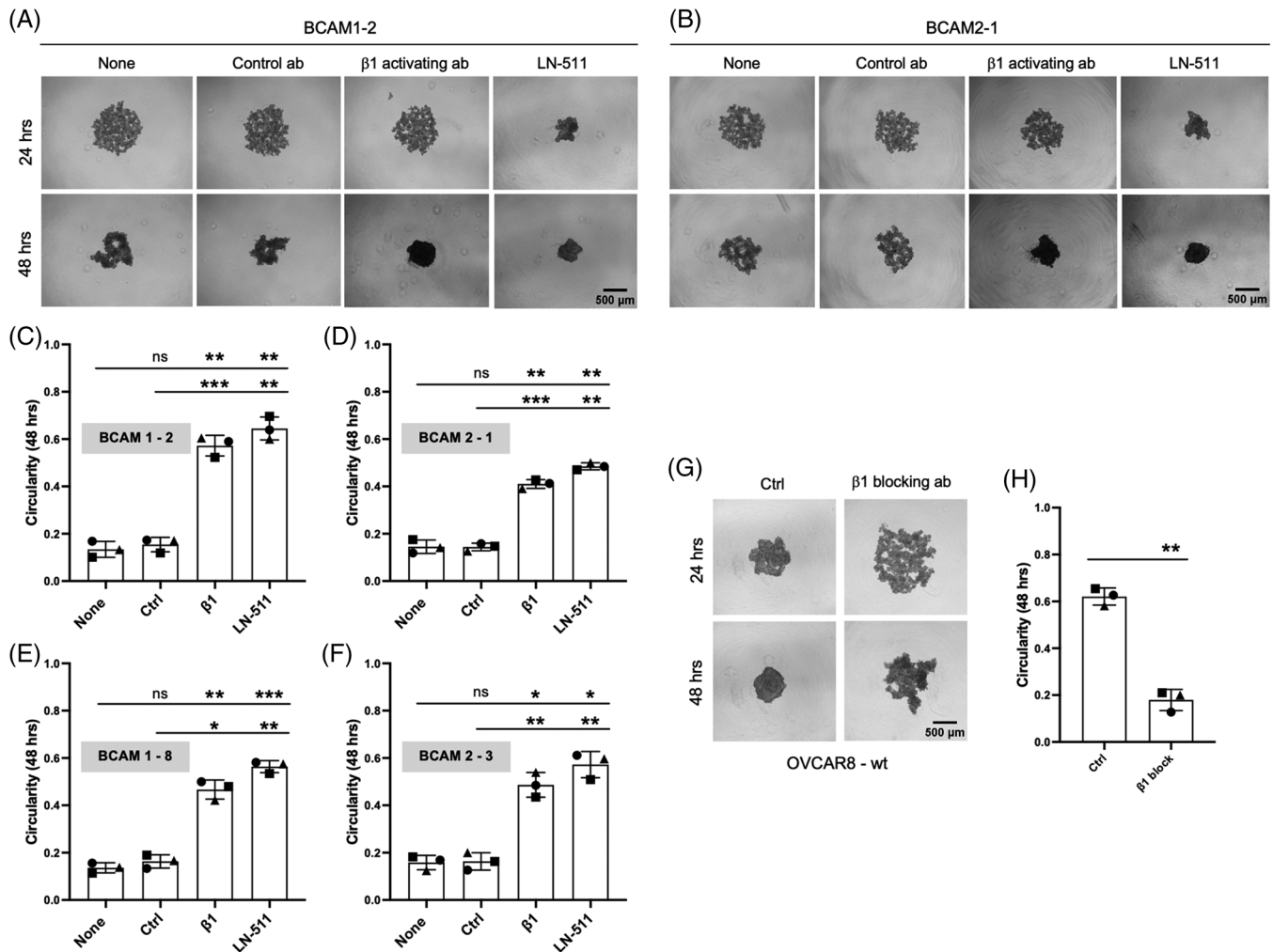


FIGURE 5 Role of LN-511 and integrin $\beta 1$ in BCAM-regulated spheroid compaction. (A, B) Morphology of spheroids derived from BCAM-overexpressing OVCAR8 clones (BCAM1 in panel A; BCAM-2 in panel B) cultured in the presence of an integrin- $\beta 1$ activating antibody, a control antibody or exogenous LN-511 (representative examples). None: untreated cells. Scale bar: 500 μm . (C, D) Quantification of circularity of spheroids in panels A and B ($n = 3$ biological replicates each). (E, F) Circularity of spheroids from two additional BCAM-overexpressing clones ($n = 3$ replicates). (G) Morphology of spheroids derived from OVCAR8 cells in the presence of an integrin- $\beta 1$ blocking antibody or a control antibody (Ctrl). Scale bar: 500 μm . (H) Quantification of circularity of spheroids in panels G. Data are shown for $n = 3$ biological replicates in panels C–F and H. * $p < .05$; ** $p < .01$; *** $p < .001$; ns: not significant by unpaired t -test

cells. Very similar results were obtained with two independent clones for each condition (Figure 7B). To exclude potential effects of soluble BCAM shed from BCAM-OE cells, we also tested the effect of Fc-BCAM on mesothelial cells, which did not induce any detectable changes (data not shown). Finally, addition of LN-511 during spheroid formation blocked BCAM-induced mesothelial clearance (Figures 7C and D), presumably as a consequence of diminished spheroid dispersion (Figure 6).

Taken together, these observations strongly suggest that BCAM-mediated dispersion of spheroids promotes trans-mesothelial invasion, probably due to weakening of integrin- $\beta 1$ -LAMA5-mediated intraspheroidal cohesion of tumour cells.

3.11 | Effect of BCAM on OC cell invasion into the omentum

To validate the in vitro observations described above we used an ex vivo model of mouse omentum adapted from Khan and colleagues.³⁶ A prerequisite for obtaining conclusive data from ex vivo models is the integrity of the organ under investigation during the observation period. This applies particularly to mesothelial cells which are prone to activation and premature senescence under stress conditions.⁵⁵ We found that under standard culture conditions the activation marker VCAM1 strongly and steadily increased in the mesothelial cells of mouse omentum cultured ex vivo for 1–5 days (Figure S15A), indicating

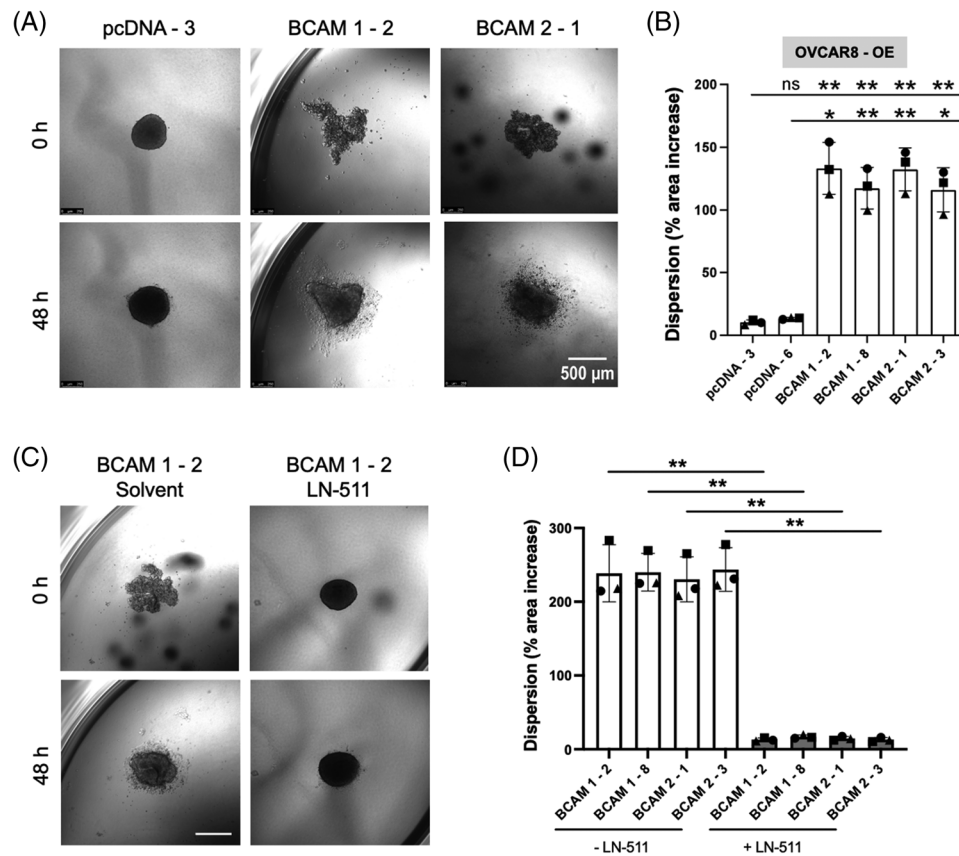


FIGURE 6 Effect of BCAM on spheroid dispersion. (A) Spheroids of BCAM-overexpressing OVCAR8 clones (BCAM1-2, BCAM2-1) and cells transduced with the empty vector (pcDNA-3) were embedded in a 3D collagen matrix for 48 h. The photomicrographs show a clear dispersion only for the BCAM-overexpressing cells. Scale bar: 500 μ m. (B) Quantification of dispersion of spheroids in panel A plus one additional clone for each condition ($n = 3$ biological replicates each). * $p < .05$; ** $p < .01$; *** $p < .001$; ns: not significant by unpaired t -test. (C) Spheroids were generated from BCAM-overexpressing BCAM1-2 cells in the presence or absence of exogenous LN-511 (10 μ g/ml) as in panel A. Pictures were taken at times 0 and 48 h after embedding. (D) Quantification of dispersion of spheroids generated from four different BCAM-overexpressing and four control clones in the presence or absence of exogenous LN-511 as in panel C ($n = 3$ biological replicates each). ** $p < .01$ by paired t -test

an aberrant state of the tissue. It has been shown that advanced glycation end-products (AGEs) induce VCAM1 in mesothelial cells by binding to their receptor RAGE.³⁸ AGEs are formed under hyperoxic conditions⁵⁶ such as those in regular cell culture. We therefore tested the effect of delipidised serum instead of regular FCS under hypoxic conditions. As shown in Figure S15B, the aberrant induction of VCAM1 was strongly diminished under these conditions, which were therefore used in all subsequent experiments.

As demonstrated by light-sheet microscopy of whole omentum specimens, BCAM1-overexpressing OVCAR8-OE cells invaded the omentum with an efficiency clearly exceeding that of OVCAR8 control cells (Figures 8A and B) by a median of approximately 10-fold (Figure 8C). Milky spots are morphologically distinct areas in the omentum, which are characterised by a dense microvasculature, an abundance of immune cells and a discontinuous mesothe-

lial layer, making milky spots preferred sites of early OC metastasis.^{36,57,58} Importantly, BCAM1-overexpressing OVCAR8-OE cells invaded not only milky spots but also areas distant to milky spots (arrows in Figure 8B), which is consistent with the observed BCAM-dependent clearance of a mesothelial cell monolayer by tumour cells in vitro (Figure 7). Further analyses by multi-photon microscopy confirmed that the invading tumour cells were homing to the sub-mesothelial collagen areas of the omentum independent of the presence of milky spots (milky spot area in Figure 8D; area distant from milky spots in Figure 8E).

To allow for an independent quantification of tumour cells invading the omentum, we developed a Taqman-PCR-based assay for the specific detection of human tumour cell DNA. As shown in the validation experiment in Figure 8F, the assay faithfully reflected the number of tumour cells in a mixed population with mouse cells with a linear increase over a range of $>10^4$. Using this assay, we found

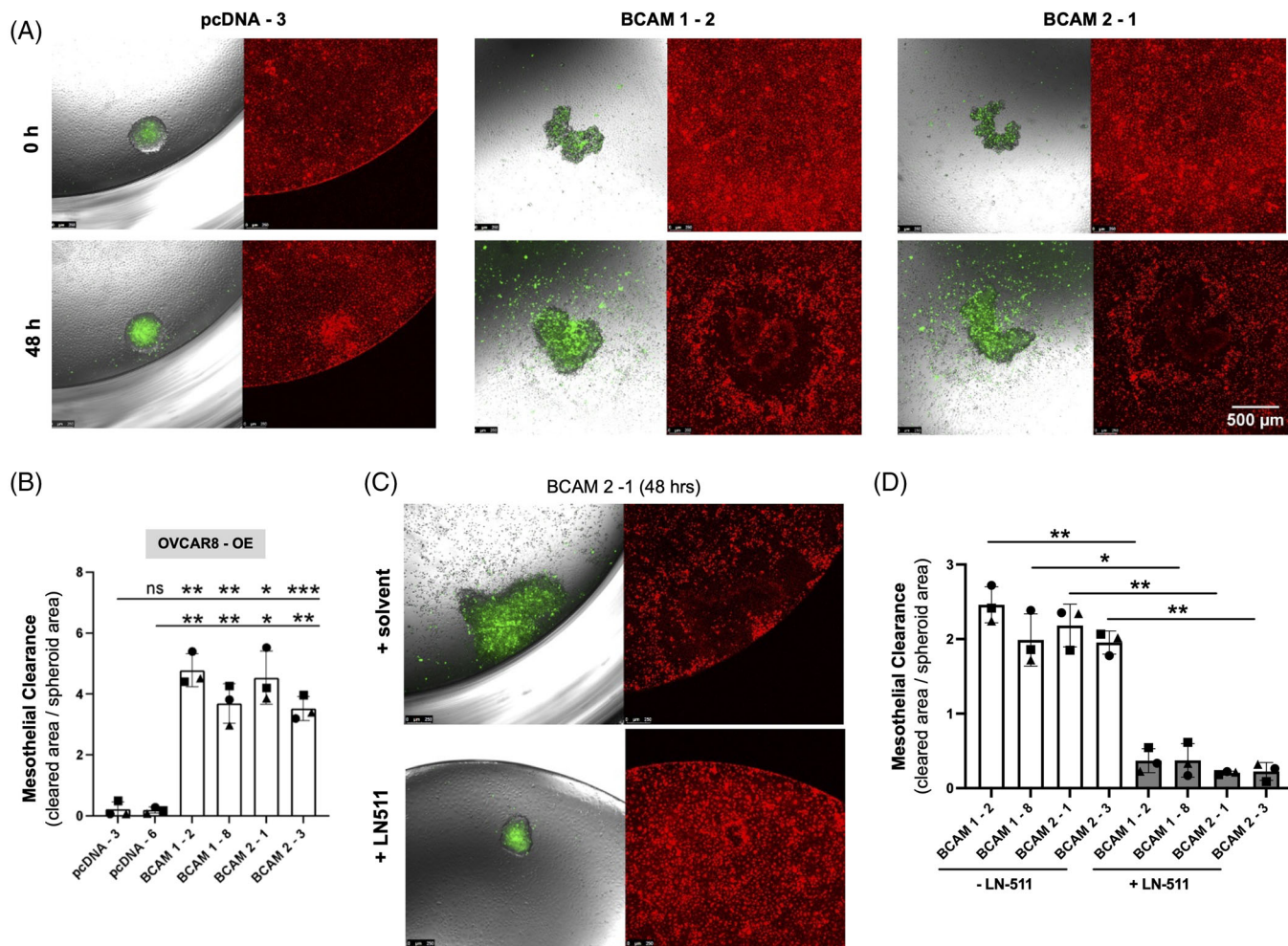


FIGURE 7 Effect of BCAM on clearance of a mesothelial monolayer. (A) The same clones as in Figure 6 (labelled with Cell Tracker green) were plated on a confluent monolayer of omental mesothelial cells (Cell Tracker orange) and mesothelial cell clearance was observed after 48 h. Scale bar: 500 μ m. (B) Quantification of mesothelial cell clearance by clones in panel A plus one additional clone for each condition ($n = 3$ biological replicates each). * $p < .05$; ** $p < .01$; *** $p < .001$; ns: not significant by unpaired t -test. (C) Spheroids were generated from BCAM-overexpressing BCAM2-1 cells in the presence or absence of exogenous LN-511 (10 μ g/ml) as in panel A and analysed after 48 h. (D) Quantification of mesothelial cell clearance by spheroids generated from four different BCAM-overexpressing and four control clones in the presence or absence of exogenous LN-511 as in panel C ($n = 3$ biological replicates each). * $p < .05$; ** $p < .01$ by paired t -test

a >10-fold stronger signal (approximately 4 Ct difference) for omentum exposed to BCAM1-overexpressing OVCAR8 spheroids compared with spheroids from control cells (Figure 8G), confirming the microscopic enumeration of tumour cells above (Figure 8C).

Finally, we tested the metastatic potential of BCAM-overexpressing OVCAR8 spheroids compared with spheroids derived from control cells in a mouse model. To this end, spheroids were injected i.p. and formation of tumour masses was observed for a period of 28 days by 18F-FDG PET/CT imaging. As shown in Figure 8H, clearly elevated PET signals in the upper abdominal region harbouring the omentum were detected consistently with spheroids derived from two different clones of BCAM1-overexpressing cells relative to corresponding control spheroids. Post-mortem dissection confirmed massive

colonisation of the omentum in mice inoculated with BCAM-overexpressing spheroids (shown for BCAM1-8 in Figure 8H), corroborating the observations made with the ex vivo model described above.

4 | DISCUSSION

The present study provides new insights into the role of BCAM in the context of OC, which include the mechanism of BCAM shedding from tumour cells to release sBCAM, the hitherto unknown impact of sBCAM on metastasis-related biological processes, a comparative functional analysis of sBCAM, BCAM1 and BCAM2 and the discovery of novel functions for BCAM with implications for peritoneal metastasis, including spheroid compaction/dispersion and

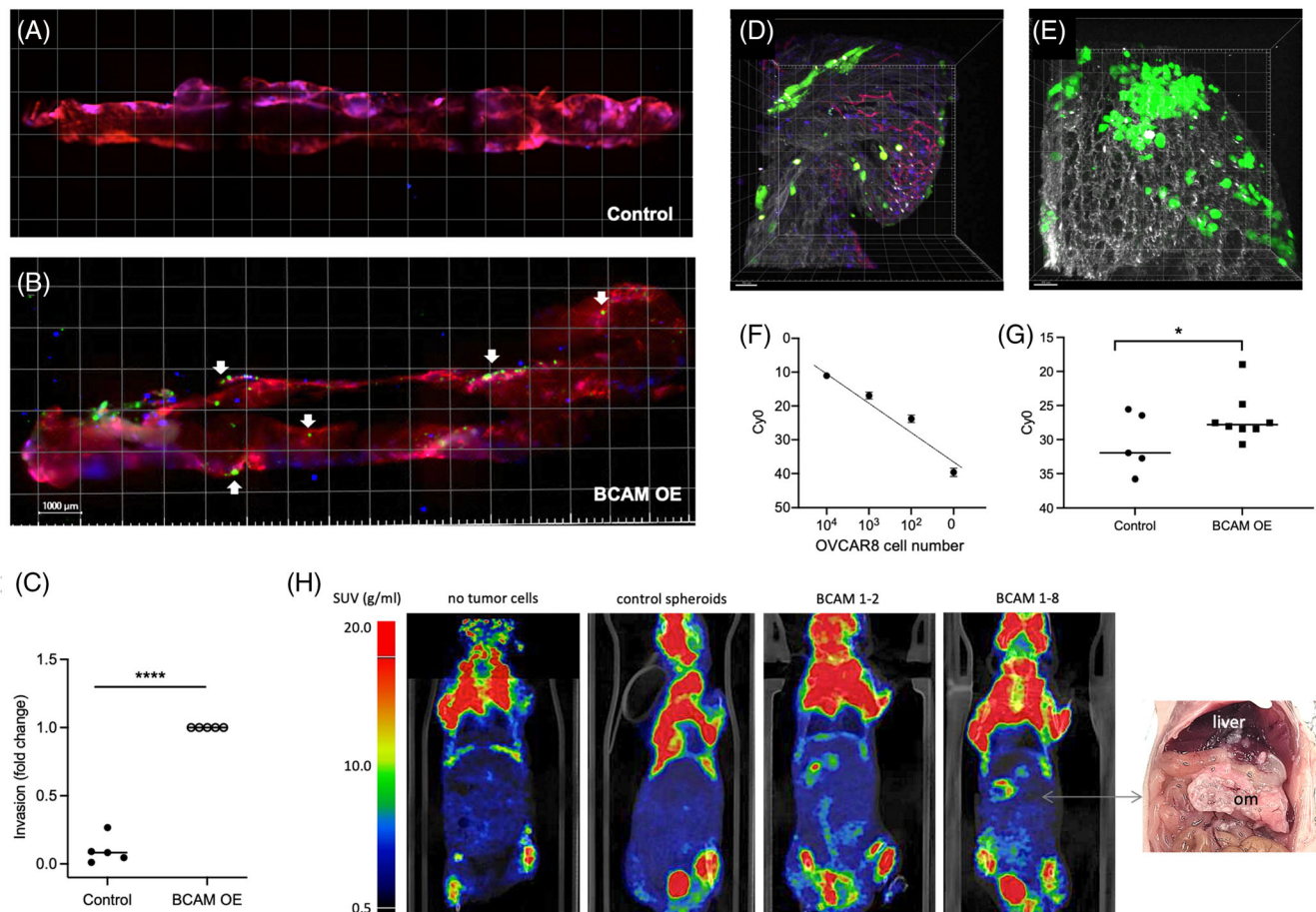


FIGURE 8 Effect of BCAM on invasion of mouse omentum by tumour cell spheroids. (A, B) Representative light-sheet microscopic images showing the invasion of explanted mouse omentum ex vivo by spheroids derived from control (A) and BCAM1-overexpressing (B) OVCAR8 cells pre-labelled with Cell Tracker Green. Spheroids derived from equal numbers of cells were added to freshly resected omentum and co-cultured for 48 h. Thereafter, the omentum was stained for immune cells (CD45; blue) and microvessels (CD31; red) and observed by light-sheet microscopy. Arrows point to areas of tumour cells that are not in the vicinity of milky spots (examples). These areas are characterised by the absence of CD45+ cell clusters (blue), which appear purple if co-localising with CD31+ endothelial cells. Scale bar: 1000 μ m. The sharp blue spots represent staining artefacts. (C) Quantification of the number of invaded cells analysed as in panels A and B for $n = 5$ biological replicates. **** $p < .0001$ by t test. (D, E) Multiphoton microscopy of tumour cells from BCAM-overexpressing OVCAR8 spheroids pre-labelled with Cell Tracker Green. Collagen fibres are visualised in white by second-harmonic generation. Panel D shows the area below a milky spot, panel E an area distant from milky spots. Scale bar: 50 μ m. (F) Validation of Taqman-PCR for the quantification of tumour cell invasion into omentum. Genomic DNA from human OVCAR8 cells and mouse omentum (100 pg) were mixed at the indicated ratios and the signal for human DNA (hAlu sequences) was determined. The plot shows a linear relationship between signal intensity and the amount of human DNA. (G) Quantification by Taqman-PCR of human DNA in omentum samples after incubation with spheroids generated from control and BCAM1-overexpressing OVCAR8 cells as in panels A–E. The plot shows the data for $n = 5$ –8 biological replicates as indicated by symbols. * $p < .05$; by t -test. (H) Longitudinal ^{18}F -FDG PET/CT images of mice 28 days after i.p. injection of spheroids derived from OVCAR8 control cells and from two different clones of BCAM-overexpressing OVCAR8 cells. Leftmost image: mouse not inoculated with tumour cells for comparison. The picture on the right shows large space-occupying BCAM1-8 tumour masses in the omentum (om) displacing the liver and other organs.

mesothelial clearance. These results are summarised in the Graphical Abstract and discussed in detail below.

4.1 | Role of ADAM10 in BCAM shedding

The origin and function of sBCAM in the tumour have not been addressed prior to the present study. BCAM in

OC ascites is associated with a poor RFS (Figures 1C), but its source and function in OC progression were not investigated. Niiya and colleagues identified BCAM as a substrate of MMP14 in human epidermoid carcinoma A431 cells to produce a cleavage product of unknown function.²⁶ We also detected MMP14 in the proteome of ascTU cells, but at low levels relative to several ADAM proteases (Figure 2A). Consistent with these observations,

analyses using proteinase inhibitors and MMP-specific siRNAs clearly identified ADAM10 and ADAM17 as the proteinases majorly responsible for BCAM shedding, with ADAM10 playing a key role (Figures 2B–E).

The role of ADAM10 as a BCAM-cleaving enzyme was confirmed using recombinant proteins (Figure 2F). MS-based analysis identified cleavage sites in BCAM near the transmembrane domain and in the vicinity of the published MMP14 site (Figure 2G). One of these sites (site 3; Figure 2G) overlapped with a cleavage site found in BCAM from the culture supernatant of OC cells, and fitted the motifs of preferred amino acids at ADAM10 cleavage sites defined in previous studies^{52,53} (Figure S12). These findings indicate that ADAM10 cleaves BCAM close to its insertion point in the plasma membrane to produce a soluble form (sBCAM) released into the TME. This conclusion was confirmed by immunoblotting identifying sBCAM rather than the longer membrane-associated forms in OC ascites (Figure 1A). Based on these results, we analysed the function of sBCAM in comparison with BCAM1 and BCAM2 in metastasis-related biological processes as discussed in the following sections.

4.2 | Metastasis-related functions of BCAM

Literature reports on the role of BCAM in cancer progression do not provide a consistent picture describing both tumour-promoting and suppressive functions and clinical associations (see *Background*; Figure S1). As discussed in the following, these seemingly contradictory findings may be due to tumour-entity-related differences in the biology of tumour progression, which also have implications for interpreting the results of the present study.

In most cancer types, metastatic spread via blood or lymphatic vessels is mediated by migrating single tumour cells or groups of cells.^{59,60} Components of the ECM, including laminins, are instrumental in processes involved in hematogenic and lymphogenic spreading, such as intravasation, extravasation and tissue invasion by cancer cells. LN-511 is one of the most potent adhesive and migration-promoting matrix components.⁶¹ It promotes integrin-dependent tumour cell migration and invasion and exerts its effects partly via autocrine stimulation,^{61–63} which has been described for the promotion of breast cancer metastasis.^{64,65} The inhibitory effect of LAMA5-integrin signaling⁵ may therefore provide an explanation why BCAM expression is not associated with the short survival of these cancer entities (Figure S1B).

This contrasts with OC, where transcoelomic dissemination of cancer cells, particularly via spheroids,

is the main route of metastasis.^{23,66–68} Laminin-integrin interactions have been reported to play a crucial role in compacting tumour cells in spheroids. For example, laminin networks mimicking a vasculogenic environment were found to be integral to the extracellular architecture and thereby the formation of melanoma spheroids *in vitro*.⁶⁹ Likewise, ECM-triggered ITGB1 signalling, including the addition of exogenous laminin (from Engelbreth–Holm–Swarm murine sarcoma basement membrane), promoted the formation and adhesion of OC spheroids.^{70,71}

Our own data points to context-dependent functions for BCAM in OC cells differing in their potential impact on metastasis formation. On the one hand, BCAM inhibits the adhesion of single OC cells to LN-511 (presumably by competing for integrin binding), which may have an inhibitory impact on metastasis, consistent with studies of gastrointestinal and bladder carcinoma cells.^{5,7} However, BCAM does not inhibit adhesion to COL1 (Figures S6E–G), which is relevant given the crucial role of collagen in OC metastasis.^{48,50,72} On the other hand, spheroids are rich in LAMA5, (Table 2; Figures 3 and S13), which presumably provides a scaffold for OC cell adhesion via integrin binding. This interaction is prone to perturbation by BCAM,⁵ reducing the compactness of spheroids (Figure 5), promoting their dispersion in a 3D collagen matrix (Figure 6) and the clearance of mesothelial cells at spheroid attachment sites (Figure 7), which in turn likely enhances the seeding of metastatic colonies. Thus, the final consequences of the interaction of BCAM and LAMA5 and the ensuing inhibition of laminin-dependent adhesion, depend on the precise scenario considered.

Milky spots are the preferred sites of early OC metastasis due to their discontinuous mesothelium,^{36,57,58} However, cancer cell invasion into serous membranes also occurs outside milky spots, where the mesothelial layer needs to be disrupted by the adhering tumour cells to initiate invasion, and this mode of metastatic seeding increases with disease progression. Our data obtained with explanted omentum suggest that BCAM promotes invasion into areas outside of milky spots, without detectable effects on invasion into milky spots (Figure 8B). This is in perfect agreement with our finding that tumour-cell-mediated clearance of a mesothelial cell monolayer is promoted by BCAM (Figure 7). Different mechanisms mediating disruption of the mesothelium by OC cells have been proposed, including mesothelial senescence⁷³ and killing by secreted factors⁷⁴ as well as myosin-driven mechanical force exerted by tumour cells.⁷⁵ In view of these complexities, the molecular mechanism(s) underlying BCAM-induced mesothelial clearance have to remain the subject of future investigations.

4.3 | Molecular basis of LAMA5-dependent functions of BCAM

The full-length BCAM isoform, BCAM1, is a transmembrane receptor for LAMA5 with an intracellular domain with potential signal transducing functions. It has been reported that overexpression of BCAM in NIH3T3 fibroblasts leads to F-actin rearrangement via increased Erk phosphorylation, increased RhoA and decreased Rac1 activity, but the relevance of these findings in an endogenous context remains unclear. BCAM1 has also been shown to be phosphorylated by glycogen synthase kinase 3 β , casein kinase II and PKA at serines 596, 598 and 621, respectively and the phosphorylation state of BCAM might be a critical factor for adhesion of erythrocytes to LAMA5 in sickle cell anemia.⁷⁶ In tumour cells, BCAM-mediated signal transduction has not been investigated to date.

Our data clearly suggest that BCAM exerts its biological functions in OC described in the present study not as a signalling receptor. This conclusion is based on the observations that BCAM1, BCAM2 and Fc-BCAM had identical effects on OC cell adhesion, migration, motility and spheroid formation (Figures 1C, 1D, 4 and S8). BCAM2 lacks most of the cytoplasmic domain, presumably impairing its signalling potential. Taken together with the data obtained with Fc-BCAM, a function for BCAM as a signalling receptor in the context of the biological effects observed in the present study can be ruled out.

It is therefore more likely that BCAM acts by competing with another ligand for a signalling receptor or by interacting as a ligand or auxiliary protein with another receptor. BCAM has been reported to compete with β 1-containing integrins for laminin binding.^{5,16} Our data strongly support the conclusion that a similar mechanism applies to the BCAM-mediated inhibition of LN-511-dependent OC cell adhesion as well as spheroid compaction and dispersion. Thus, the effect of BCAM was counteracted by an integrin β 1 activating antibody or by the addition of excess LN-511 (Figures 5A–F and 6C and D). Furthermore, an integrin β 1 blocking antibody had a similar effect as BCAM (Figures 5G and H). These observations strongly suggest that BCAM acts as a non-signalling decoy receptor blocking the interaction of LAMA5 with β 1-containing integrins to diminish the attachment of single tumour cells to a matrix on the one hand, and to decrease the compactness of spheroids and enhance their dispersion at attachment sites on the other.

Soluble BCAM (as recombinant Fc-BCAM) affects tumour cells in culture at a concentration corresponding to the highest sBCAM levels in ascites (Figures 1B, D and E), strongly supporting a role in the OC TME. Our data also indicate that Fc-BCAM and overexpressed BCAM1 or BCAM2 are functionally similar (Figures 1D

and E), raising the question as to whether the effect of membrane-bound BCAM depends on its shedding. While cleavage of overexpressed BCAM is likely to contribute to the observed functions, kinetic experiments suggest that membrane-bound forms play a role (Figure S7). Thus, cells overexpressing BCAM1 or BCAM2 showed clearly decreased adhesion to LN-511 within less than 20 min after plating the cells, which is unlikely to suffice for the accumulation of a functionally relevant level of sBCAM. It thus appears that both membrane-bound and soluble BCAM figure in modulating OC cell functions, consistent with the proposed role as a competing ligand. BCAM shedding nevertheless may be of particular importance to increase the pool of sBCAM in the TME. This is suggested by the observation that tumour-associated host cells also express elevated levels of BCAM and/or BCAM-cleaving proteases. This is documented in Figure S17, showing high expression of BCAM in mesothelial cells, ADAM10 and ADAM17 in CAF and MMP14 in tumor-associated macrophages (TAM) and carcinoma-associated fibroblasts (CAF).

BCAM has also been identified as a ligand for integrin α 4/ β 1 on leukocytes in murine glomerulonephritis,¹² but an impact on signal transduction has not been investigated. Moreover, integrin α 4 is selectively expressed in hematopoietic cells, and its expression is barely detectable in OC cells (TPM < 1; Figure S16), suggesting a minor role, if any, as a signalling receptor bound by BCAM. It is, however, possible that other unidentified receptor(s) exist that are activated by BCAM or co-regulated by BCAM.

4.4 | Translational perspectives

The association of an unfavourable clinical outcome with both BCAM RNA expression (Figure S1C) and ascites levels of sBCAM (Figure 1C), in conjunction with its prometastatic function uncovered in the present study, suggests that BCAM may represent a novel therapeutic target in OC. Although such considerations remain hypothetical at present, several options can be devised and tested in future studies. A promising approach appears to be to prevent BCAM from its interaction with LAMA5. In this context, it is noteworthy that KRAS-mutated colon carcinoma cells express high levels of BCAM and efficiently form hepatic metastases in mice, which is inhibited by BCAM-mimetic peptides blocking LAMA5–BCAM interaction.⁶ Alternatively, it could be envisaged to develop molecules targeting BCAM to block its interaction interface, which is likely to result in lesser side-effects than blocking LAMA5, which is essential for numerous crucial physiological functions.⁷⁷ In this scenario, the development of small molecule drugs, particularly PROTACs,⁷⁸ may represent a successful strategy. Furthermore, BCAM is a potential

candidate for targeted immunotherapies, which could address both membrane-bound and soluble BCAM. Preventing the production of sBCAM by blocking ADAM10 and/or other relevant metalloproteinases may also represent an option, but is less likely to succeed in view of the failure of marimastat in clinical trials, including ovarian cancer.^{79,80} Even though BCAM-directed approaches may not be suitable for the treatment of established metastatic lesions, they could provide invaluable tools to prevent de novo metastasis formation in an adjuvant scenario.

5 | CONCLUSIONS

The role of BCAM in cancer progression is controversial and has not been addressed for OC to date, including the origin and potential function of soluble BCAM abundant in the OC microenvironment. In the present study we show that BCAM negatively regulates the compactness of LAMA5-rich tumour cell spheroids, and consequently triggers the dispersion of spheroids in a collagen matrix, facilitates the clearance of mesothelial cells at spheroid attachment sites and promotes the trans-mesothelial invasion of tumour cell spheroids into omental tissue.

We also present compelling evidence suggesting that BCAM acts as a decoy rather than a signalling receptor to modulate metastasis-related functions on OC cells. This conclusion is supported by the observation that full-length BCAM1 and the truncated isoform BCAM2 lacking most of the cytoplasmic domain with potential signalling function had the same effect in different biological assays. Furthermore, we have identified ADAM10 as a major BCAM sheddase produced by OC cells and identified proteolytic cleavage sites yielding a soluble BCAM isoform exclusively composed of the extracellular domain. Recombinant soluble BCAM mimicking this isoform had the same effect as the membrane-bound BCAM proteins.

Mechanistically, all BCAM forms interfered with interaction of LAMA5 and integrin- β 1. On the one hand, this results in decreased adhesion of single cells to a LN-511 matrix, potentially representing an anti-metastatic function. However, according to previous studies adhesion of OC cells to collagen rather than laminin drives peritoneal dissemination.⁴⁵⁻⁵⁰ Importantly, BCAM has no detectable effect on adhesion to COL1, suggesting that the observed inhibitory effect of BCAM on the single-cell adhesion to LN-511 is of minor significance in this context. On the other hand, BCAM loosens the structure of spheroids, where LAMA5-integrin β 1 interaction is essential to maximise compaction, thereby promoting the dispersion of cancer cell spheroids at target sites, which in turn is likely to contribute to peritoneal metastatic spread. This conclusion is consistent with the observed colonisation-enhancing

effect of BCAM in both explanted omentum and a mouse model, as well as the highly significant association of BCAM with a poor clinical outcome of OC. Our data not only provide new mechanistic insights into OC biology, but may also pave the way for therapeutic strategies impacting peritoneal metastasis formation.

ACKNOWLEDGEMENTS

We are grateful to the Anneliese Pohl Stiftung for sponsoring the Distinguished Senior Professorship for Translational Oncology held by R.M., to Marcia Moss (Verra Therapeutics, Lansing, NY, USA) for kindly providing recombinant ADAM10 pro-domain, to Elke Pogge von Strandmann for sharing the pX330-U6-Chimeric_BB-CBh-hSpCas9 vector and to J. Kirch-Heber, T. Plaum, A. Allmeroth and M. Alt for expert technical assistance.

Open access funding enabled and organized by Projekt DEAL.

CONFLICT OF INTEREST

The authors declare no competing financial interests.


ETHICS STATEMENT

All experiments were carried out with informed consent by the patients and approval by the ethics committee of Marburg University (205/10). All patients have agreed in writing to the publication of pseudonymized data derived from clinical materials.

ORCID

Suresh Sivakumar  <https://orcid.org/0000-0002-5711-0871>

Jörg W. Bartsch  <https://orcid.org/0000-0002-2773-3357>

Johannes Graumann  <https://orcid.org/0000-0002-3015-5850>

Rolf Müller  <https://orcid.org/0000-0003-3339-4248>

REFERENCES

- Rahuel C, Le Van Kim C, Mattei MG, Cartron JP, Colin Y. A unique gene encodes spliceforms of the B-cell adhesion molecule cell surface glycoprotein of epithelial cancer and of the Lutheran blood group glycoprotein. *Blood*. 1996;88:1865-1872.
- Nemer El, W R, Colin Y, et al. Organization of the human LU gene and molecular basis of the Lu(a)/Lu(b) blood group polymorphism. *Blood*. 1997;89:4608-4616.
- Gauthier E, Nemer El, Wautier MP, et al. Role of the interaction between Lu/BCAM and the spectrin-based membrane skeleton in the increased adhesion of hereditary spherocytosis red cells to laminin. *Br J Haematol*. 2010;148:456-465.
- Kikkawa Y, Sudo R, Kon J, et al. Laminin alpha 5 mediates ectopic adhesion of hepatocellular carcinoma through integrins and/or Lutheran/basal cell adhesion molecule. *Exp Cell Res*. 2008;314:2579-2590.
- Kikkawa Y, Ogawa T, Sudo R, et al. The lutheran/basal cell adhesion molecule promotes tumor cell migration by

- modulating integrin-mediated cell attachment to laminin-511 protein. *J Biol Chem.* 2013;288:30990-31001.
6. Bartolini A, Cardaci S, Lamba S, et al. BCAM and LAMA5 mediate the recognition between tumor cells and the endothelium in the metastatic spreading of KRAS-mutant colorectal cancer. *Clin Cancer Res.* 2016;22:4923-4933.
 7. Chang HY, Chang HM, Wu T, et al. The role of Lutheran/basal cell adhesion molecule in human bladder carcinogenesis. *J Biomed Sci.* 2017;24:61.
 8. Jin J, Xie S, Sun Q, et al. Upregulation of BCAM and its sense lncRNA BAN are associated with gastric cancer metastasis and poor prognosis. *Mol Oncol.* 2020;14:829-845.
 9. Udani M, Zen Q, Cottman M, et al. Basal cell adhesion molecule/lutheran protein. The receptor critical for sickle cell adhesion to laminin. *J Clin Invest.* 1998;101:2550-2558.
 10. Kikkawa Y, Miner JH. Review: lutheran/B-CAM: a laminin receptor on red blood cells and in various tissues. *Connect Tissue Res.* 2005;46:193-199.
 11. Wautier MP, Nemer El, Gane P, et al. Increased adhesion to endothelial cells of erythrocytes from patients with polycythemia vera is mediated by laminin alpha5 chain and Lu/BCAM. *Blood.* 2007;110:894-901.
 12. Huang J, Filipe A, Rahuel C, et al. Lutheran/basal cell adhesion molecule accelerates progression of crescentic glomerulonephritis in mice. *Kidney Int.* 2014;85:1123-1136.
 13. Zen Q, Cottman M, Truskey G, Fraser R, Telen MJ. Critical factors in basal cell adhesion molecule/lutheran-mediated adhesion to laminin. *J Biol Chem.* 1999;274:728-734.
 14. Parsons SF, Lee G, Spring FA, et al. Lutheran blood group glycoprotein and its newly characterized mouse homologue specifically bind alpha5 chain-containing human laminin with high affinity. *Blood.* 2001;97:312-320.
 15. Kikkawa Y, Sasaki T, Nguyen MT, et al. The LG1-3 tandem of laminin alpha5 harbors the binding sites of Lutheran/basal cell adhesion molecule and alpha3beta1/alpha6beta1 integrins. *J Biol Chem.* 2007;282:14853-14860.
 16. Godavarthy PS, Walter CB, Lengerke C, Klein G. The laminin receptors basal cell adhesion molecule/lutheran and integrin alpha7beta1 on human hematopoietic stem cells. *Front Cell Dev Biol.* 2021;9:675240.
 17. Nemer El, W W, Rahuel C, et al. Endothelial Lu/BCAM glycoproteins are novel ligands for red blood cell alpha4beta1 integrin: role in adhesion of sickle red blood cells to endothelial cells. *Blood.* 2007;109:3544-3551.
 18. Akiyama H, Iwahana Y, Suda M, et al. The FBI1/Akirin2 target gene, BCAM, acts as a suppressive oncogene. *PLoS One.* 2013;8:e78716.
 19. Guadall A, Cochet S, Renaud O, et al. Dimerization and phosphorylation of Lutheran/basal cell adhesion molecule are critical for its function in cell migration on laminin. *J Biol Chem.* 2019;294:14911-14921.
 20. Gentles AJ, Newman AM, Liu CL, et al. The prognostic landscape of genes and infiltrating immune cells across human cancers. *Nat Med.* 2015;21:938-945.
 21. Lengyel E. Ovarian cancer development and metastasis. *Am J Pathol.* 2010;177:1053-1064.
 22. Ahmed N, Stenvers KL. Getting to know ovarian cancer ascites: opportunities for targeted therapy-based translational research. *Front Oncol.* 2013;3:256.
 23. Worzfeld T, Strandmann P, Huber M, et al. The unique molecular and cellular microenvironment of ovarian cancer. *Front Oncol.* 2017;7:24.
 24. Liao J, Qian F, Tchabo N, et al. Ovarian cancer spheroid cells with stem cell-like properties contribute to tumor generation, metastasis and chemotherapy resistance through hypoxia-resistant metabolism. *PLoS One.* 2014;9:e84941.
 25. Finkernagel F, Reinartz S, Schuldner M, et al. Dual-platform affinity proteomics identifies links between the recurrence of ovarian carcinoma and proteins released into the tumor microenvironment. *Theranostics.* 2019;9:6601-6617.
 26. Niiya D, Egawa N, Sakamoto T, et al. Identification and characterization of Lutheran blood group glycoprotein as a new substrate of membrane-type 1 matrix metalloproteinase 1 (MT1-MMP): a systemic whole cell analysis of MT1-MMP-associating proteins in A431 cells. *J Biol Chem.* 2009;284:27360-27369.
 27. Rustin GJ, Timmers P, Nelstrop A, et al. Comparison of CA-125 and standard definitions of progression of ovarian cancer in the intergroup trial of cisplatin and paclitaxel versus cisplatin and cyclophosphamide. *J Clin Oncol.* 2006;24:45-51.
 28. Reinartz S, Finkernagel F, Adhikary T, et al. A transcriptome-based global map of signaling pathways in the ovarian cancer microenvironment associated with clinical outcome. *Genome Biol.* 2016;17:108.
 29. Worzfeld T, Finkernagel F, Reinartz S, et al. Proteotranscriptomics reveal signaling networks in the ovarian cancer microenvironment. *Mol Cell Proteomics.* 2018;17:270-289.
 30. Sommerfeld L, Finkernagel F, Jansen JM, et al. The multicellular signalling network of ovarian cancer metastases. *Clin Transl Med.* 2021;11:e633.
 31. Reinartz S, Lieber S, Pesek J, et al. Cell-type-selective pathways and clinical associations of lysophosphatidic acid biosynthesis and signaling in the ovarian cancer microenvironment. *Mol Oncol.* 2019;23:185-201.
 32. Rappsilber J, Ishihama Y, Mann M. Stop and go extraction tips for matrix-assisted laser desorption/ionization, nanoelectrospray, and LC/MS sample pretreatment in proteomics. *Anal Chem.* 2003;75:663-670.
 33. Cox J, Mann M. MaxQuant enables high peptide identification rates, individualized p.p.b.-range mass accuracies and proteome-wide protein quantification. *Nat Biotechnol.* 2008;26:1367-1372.
 34. Cox J, Neuhauser N, Michalski A, et al. Andromeda: a peptide search engine integrated into the MaxQuant environment. *J Proteome Res.* 2011;10:1794-1805.
 35. Kiweler M, Looso M, Graumann J. MARMoSET - extracting publication-ready mass spectrometry metadata from RAW files. *Mol Cell Proteomics.* 2019;18:1700-1702.
 36. Khan SM, Funk HM, Thiollay S, et al. In vitro metastatic colonization of human ovarian cancer cells to the omentum. *Clin Exp Metastasis.* 2010;27:185-196.
 37. Grayson WL, Zhao F, Bunnell B, Ma T. Hypoxia enhances proliferation and tissue formation of human mesenchymal stem cells. *Biochem Biophys Res Commun.* 2007;358:948-953.
 38. Boulanger E, Wautier MP, Wautier JL, et al. AGEs bind to mesothelial cells via RAGE and stimulate VCAM-1 expression. *Kidney Int.* 2002;61:148-156.
 39. Gerber SA, Rybalko VY, Bigelow CE, et al. Preferential attachment of peritoneal tumor metastases to omental immune

- aggregates and possible role of a unique vascular microenvironment in metastatic survival and growth. *Am J Pathol.* 2006;169:1739-1752.
40. Funakoshi K, Bagheri M, Zhou M, et al. Highly sensitive and specific Alu-based quantification of human cells among rodent cells. *Sci Rep.* 2017;7:13202.
 41. Janssens J, Crans RAJ, Van Craenenbroeck K, et al. Evaluating the applicability of mouse SINEs as an alternative normalization approach for RT-qPCR in brain tissue of the APP23 model for Alzheimer's disease. *J Neurosci Methods.* 2019;320:128-137.
 42. Mi H, Ebert D, Muruganujan A, et al. PANTHER version 16: a revised family classification, tree-based classification tool, enhancer regions and extensive API. *Nucleic Acids Res.* 2021;49:D394-D403.
 43. The Cancer Genome Atlas Research Network. Integrated genomic analyses of ovarian carcinoma. *Nature.* 2011;474:609-615.
 44. Dowling CM, Herranz Ors C, Kiely PA. Using real-time impedance-based assays to monitor the effects of fibroblast-derived media on the adhesion, proliferation, migration and invasion of colon cancer cells. *Biosci Rep.* 2014;34.
 45. Shen Y, Shen R, Ge L, Zhu Q, Li F. Fibrillar type I collagen matrices enhance metastasis/invasion of ovarian epithelial cancer via beta1 integrin and PTEN signals. *Int J Gynecol Cancer.* 2012;22:1316-1324.
 46. Alkmin S, Brodziski R, Simon H, et al. Role of collagen fiber morphology on ovarian cancer cell migration using image-based models of the extracellular matrix. *Cancers (Basel).* 2020;12.
 47. Huang YL, Liang CY, Ritz D, et al. Collagen-rich omentum is a premetastatic niche for integrin alpha2-mediated peritoneal metastasis. *Elife.* 2020;9.
 48. Lyu Y, Feng C. Collagen synthesis and gap junctions: the high-way for metastasis of ovarian cancer. *Lab Invest.* 2021;101:540-542.
 49. Valmiki S, Aid MA, Chaitou AR, et al. Extracellular matrix: a treasure trove in ovarian cancer dissemination and chemotherapeutic resistance. *Cureus.* 2021;13:e13864.
 50. Sarwar M, Sykes PH, Chitcholtan K, Evans JJ. Collagen I dysregulation is pivotal for ovarian cancer progression. *Tissue Cell.* 2022;74:101704.
 51. Moss ML, Bomar M, Liu Q, et al. The ADAM10 prodomain is a specific inhibitor of ADAM10 proteolytic activity and inhibits cellular shedding events. *J Biol Chem.* 2007;282:35712-35721.
 52. Caescu CI, Jeschke GR, Turk BE. Active-site determinants of substrate recognition by the metalloproteinases TACE and ADAM10. *Biochem J.* 2009;424:79-88.
 53. Tucher J, Linke D, Koudelka T, et al. LC-MS based cleavage site profiling of the proteases ADAM10 and ADAM17 using proteome-derived peptide libraries. *J Proteome Res.* 2014;13:2205-2214.
 54. Kenny HA, Nieman KM, Mitra AK, Lengyel E. The first line of intra-abdominal metastatic attack: breaching the mesothelial cell layer. *Cancer Discov.* 2011;1:100-102.
 55. Ksiazek K, Mikula-Pietrasik J, Jorres A, Witowski J. Oxidative stress-mediated early senescence contributes to the short replicative life span of human peritoneal mesothelial cells. *Free Radic Biol Med.* 2008;45:460-467.
 56. Taneja S, Vetter SW, Leclerc E. Hypoxia and the receptor for advanced glycation end products (RAGE) signaling in cancer. *Int J Mol Sci.* 2021;22.
 57. Platell C, Cooper D, Papadimitriou JM, Hall JCT. *World J Gastroenterol.* 2000;6:169-176.
 58. Ma X. The omentum, a niche for premetastatic ovarian cancer. *J Exp Med.* 2020;217.
 59. Friedl P, Gilmour D. Collective cell migration in morphogenesis, regeneration and cancer. *Nat Rev Mol Cell Biol.* 2009;10:445-457.
 60. Janiszewska M, Primi MC, Izard T. Cell adhesion in cancer: beyond the migration of single cells. *J Biol Chem.* 2020;295:2495-2505.
 61. Kikkawa Y, Sanzen N, Sekiguchi K. Isolation and characterization of laminin-10/11 secreted by human lung carcinoma cells. laminin-10/11 mediates cell adhesion through integrin alpha3 beta1. *J Biol Chem.* 1998;273:15854-15859.
 62. Pouliot N, Connolly LM, Moritz RL, Simpson RJ, Burgess AW. Colon cancer cells adhesion and spreading on autocrine laminin-10 is mediated by multiple integrin receptors and modulated by EGF receptor stimulation. *Exp Cell Res.* 2000;261:360-371.
 63. Pouliot N, Kusuma N. Laminin-511: a multi-functional adhesion protein regulating cell migration, tumor invasion and metastasis. *Cell Adh Migr.* 2013;7:142-149.
 64. Kusuma N, Denoyer D, Eble JA, et al. Integrin-dependent response to laminin-511 regulates breast tumor cell invasion and metastasis. *Int J Cancer.* 2012;130:555-566.
 65. Chia J, Kusuma N, Anderson R, et al. Evidence for a role of tumor-derived laminin-511 in the metastatic progression of breast cancer. *Am J Pathol.* 2007;170:2135-2148.
 66. Shield K, Ackland ML, Ahmed N, Rice GE. Multicellular spheroids in ovarian cancer metastases: biology and pathology. *Gynecol Oncol.* 2009;113:143-148.
 67. Al Habyan S, Kalos C, Szyzborski J, McCaffrey L. Multicellular detachment generates metastatic spheroids during intra-abdominal dissemination in epithelial ovarian cancer. *Oncogene.* 2018;37:5127-5135.
 68. Gao Q, Yang Z, Xu S, et al. Heterotypic CAF-tumor spheroids promote early peritoneal metastasis of ovarian cancer. *J Exp Med.* 2019;216:688-703.
 69. Larson AR, Lee CW, Lezcano C, et al. Melanoma spheroid formation involves laminin-associated vasculogenic mimicry. *Am J Pathol.* 2014;184:71-78.
 70. Casey RC, Skubitz AP. CD44 and beta1 integrins mediate ovarian carcinoma cell migration toward extracellular matrix proteins. *Clin Exp Metastasis.* 2000;18:67-75.
 71. Casey RC, Burleson KM, Skubitz KM, et al. Beta 1-integrins regulate the formation and adhesion of ovarian carcinoma multicellular spheroids. *Am J Pathol.* 2001;159:2071-2080.
 72. Burleson KM, Hansen LK, Skubitz AP. Ovarian carcinoma spheroids disaggregate on type I collagen and invade live human mesothelial cell monolayers. *Clin Exp Metastasis.* 2004;21:685-697.
 73. Mikula-Pietrasik J, Uruski P, Sosińska P, et al. Senescent peritoneal mesothelium creates a niche for ovarian cancer metastases. *Cell Death Dis.* 2016;7:e2565.
 74. Heath RM, Jayne DG, O'Leary R, Morrison EE, Guillou PJ. Tumour-induced apoptosis in human mesothelial cells: a mechanism of peritoneal invasion by Fas Ligand/Fas interaction. *Br J Cancer.* 2004;90:1437-1442.
 75. Iwanicki MP, Davidowitz RA, Ng MR, et al. Ovarian cancer spheroids use myosin-generated force to clear the mesothelium. *Cancer Discov.* 2011;1:144-157.

76. El Nemer W, Gauthier E, Wautier MP, et al. Role of Lu/BCAM in abnormal adhesion of sickle red blood cells to vascular endothelium. *Transfus Clin Biol.* 2008;15:29-33.
77. Miner JH, Cunningham J, Sanes JR. Roles for laminin in embryogenesis: exencephaly, syndactyly, and placentopathy in mice lacking the laminin alpha5 chain. *J Cell Biol.* 1998;143:1713-1723.
78. Bekes M, Langley DR, Crews CM. PROTAC targeted protein degraders: the past is prologue. *Nat Rev Drug Discov.* 2022;21:181-200.
79. Steward WP. Marimastat (BB2516): current status of development. *Cancer Chemother Pharmacol.* 1999;43:S56-60.
80. Marimastat. *Drugs R&D* 2003;4:198-203.

SUPPORTING INFORMATION

Additional supporting information can be found online in the Supporting Information section at the end of this article.

How to cite this article: Sivakumar S, Lieber S, Librizzi D, et al. Basal cell adhesion molecule promotes metastasis-associated processes in ovarian cancer. *Clin Transl Med.* 2023;13:e1176. <https://doi.org/10.1002/ctm2.1176>

SUPPLEMENTAL FIGURES

Basal cell adhesion molecule (BCAM) promotes metastasis-associated processes in ovarian cancer

Suresh Sivakumar, Sonja Lieber, Damiano Librizzi, Corinna Keber, Leah Sommerfeld, Florian Finkernagel, Katrin Roth, Silke Reinartz, Jörg Bartsch, Johannes Graumann, Sabine Müller-Brüsselbach and Rolf Müller

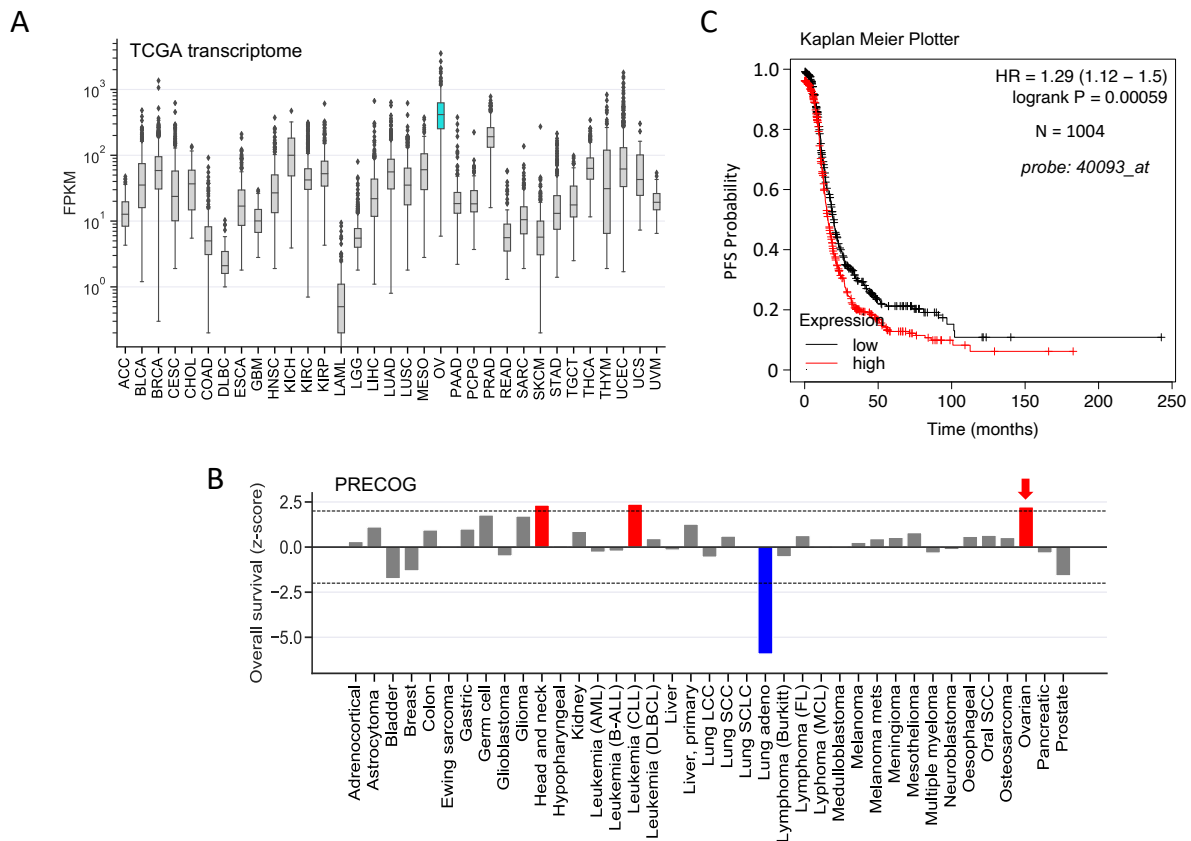


Figure S1: Expression of *BCAM* mRNA and association with overall survival (OS) in different cancer entities and assoc.

(A) Data were retrieved from the TCGA transcriptome dataset (TCGA Research Network, 2011). Boxplots show medians (horizontal line in boxes), upper and lower quartiles (box), and range (whiskers). **(B)** Data retrieved from the PRECOG dataset (Gentles et al., 2015). Positive and negative z-scores indicate $HR > 1$ and $HR < 1$, respectively. A z-score of $|1.96|$ corresponds to a logrank p-value of 0.05. Red: significant association with a short OS; blue: significant association with a long OS. **(C)** Association of *BCAM* RNA expression with relapse-free survival (RFS) of OC. The plot was generated by the Kaplan-Meier Plotter online tool (Gyorffy et al., 2012) using the following settings: Jet set best probe; auto-select best cutoff; histology: serous; all other parameters: default).

ACC: Adrenocortical carcinoma; BLCA: Bladder Urothelial Carcinoma; BRCA: Breast invasive carcinoma; CESC: Cervical squamous cell carcinoma and endocervical adenocarcinoma; CHOL: Cholangiocarcinoma; COAD: Colon adenocarcinoma; DLBC: Lymphoid Neoplasm Diffuse Large B-cell Lymphoma; ESCA: Esophageal carcinoma; GBM: Glioblastoma multiforme; HNSC: Head and Neck squamous cell carcinoma; KICH: Kidney Chromophobe; KIRC: Kidney renal clear cell carcinoma; KIRP: Kidney renal papillary cell carcinoma; LAML: Acute Myeloid Leukemia; LGG: Brain Lower Grade Glioma; LIHC: Liver hepatocellular carcinoma; LUAD: Lung adenocarcinoma; LUSC: Lung squamous cell carcinoma; MESO: Mesothelioma; OV: Ovarian serous cystadenocarcinoma; PAAD: Pancreatic adenocarcinoma; PCPG: Pheochromocytoma and Paraganglioma; PRAD: Prostate adenocarcinoma; READ: Rectum adenocarcinoma; SARC: Sarcoma; SKCM: Skin Cutaneous Melanoma; STAD: Stomach adenocarcinoma; TGCT: Testicular Germ Cell Tumors; THCA: Thyroid carcinoma; THYM: Thymoma; UCEC: Uterine Corpus Endometrial Carcinoma; UCS: Uterine Carcinosarcoma; UVM: Uveal Melanoma.

References:

The Cancer Genome Atlas (TCGA) Research Network. Integrated genomic analyses of ovarian carcinoma. *Nature* 474, 609–615 (2011).

Gentles, A.J. et al. The prognostic landscape of genes and infiltrating immune cells across human cancers. *Nat Med* 21, 938–945 (2015).

Gyorffy, B., Lanczky, A. & Szallasi, Z. Implementing an online tool for genome-wide validation of survival-associated biomarkers in ovarian-cancer using microarray data from 1287 patients. *Endocr Relat Cancer* 19, 197–208 (2012). Website: <http://kmplot.com/analysis/index.php?p=service&cancer=ovar>

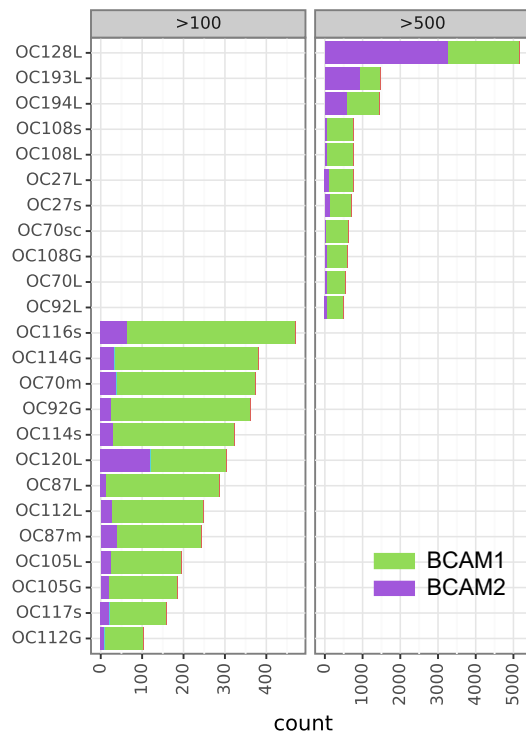


Figure S2: Expression of *BCAM1* versus *BCAM2* mRNA in tumor cells from ascites.

The plot is based on exon spanning reads from RNA-Seq data published in Sommerfeld et al. (2021).

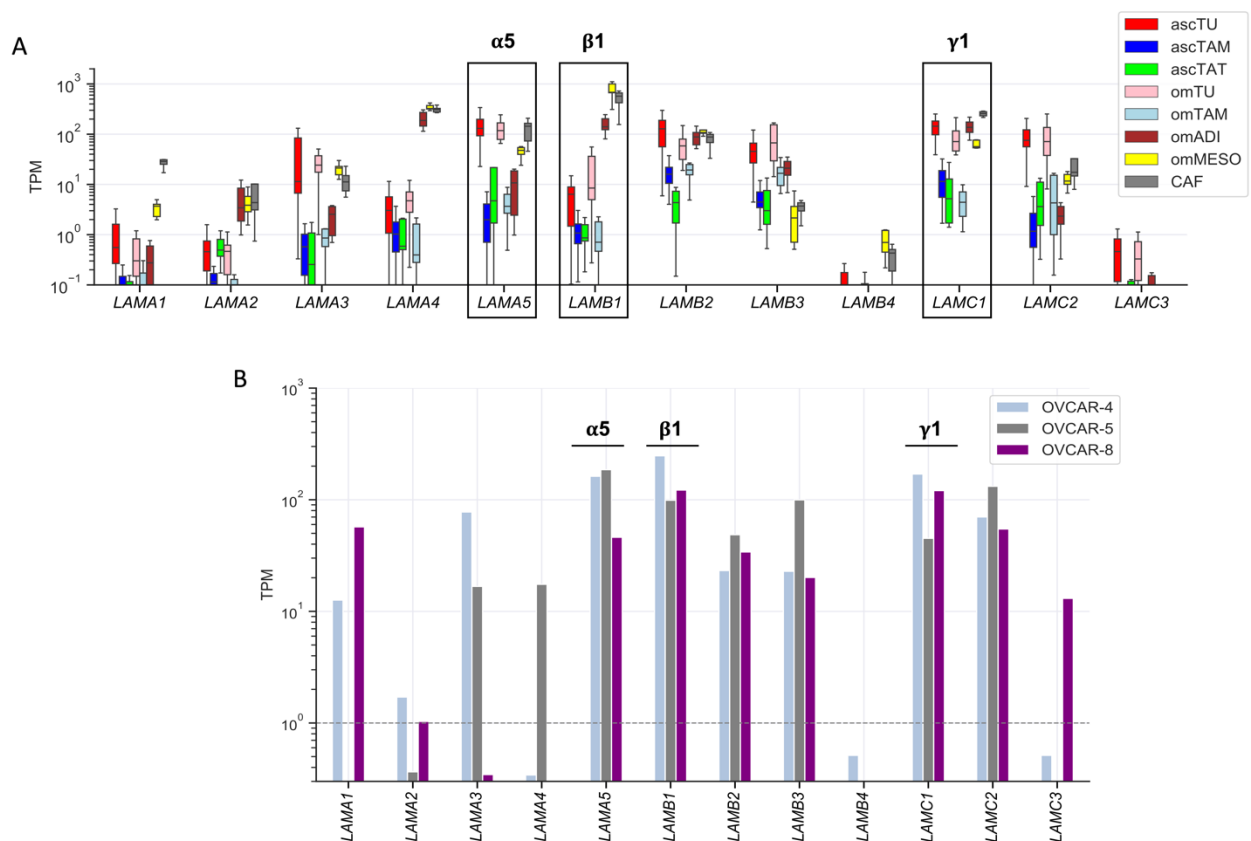


Figure S3: Expression of genes coding for laminin family members in cells of the OC TME and in OVCAR cell lines based on RNA-Seq data.

(A) Expression in tumor and host cells in OC ascites and omental metastases. The plot is based on RNA-Seq data retrieved from Sommerfeld et al. (2021). asc: ascites-derived; om: isolated from omental metastases; TU: tumor cells; TAM: tumor-associated macrophages; TAT: tumor-associated T cells; ADI: adipocytes; MESO: mesothelial cells; CAF: fibroblasts. Boxplots show medians (horizontal line in boxes), upper and lower quartiles (box), and range (whiskers).

(B) Expression in OVCAR4, OVCAR5 and OVCAR8 cells. Data for were generated by RNA-Seq as described in Sommerfeld et al. (2021).

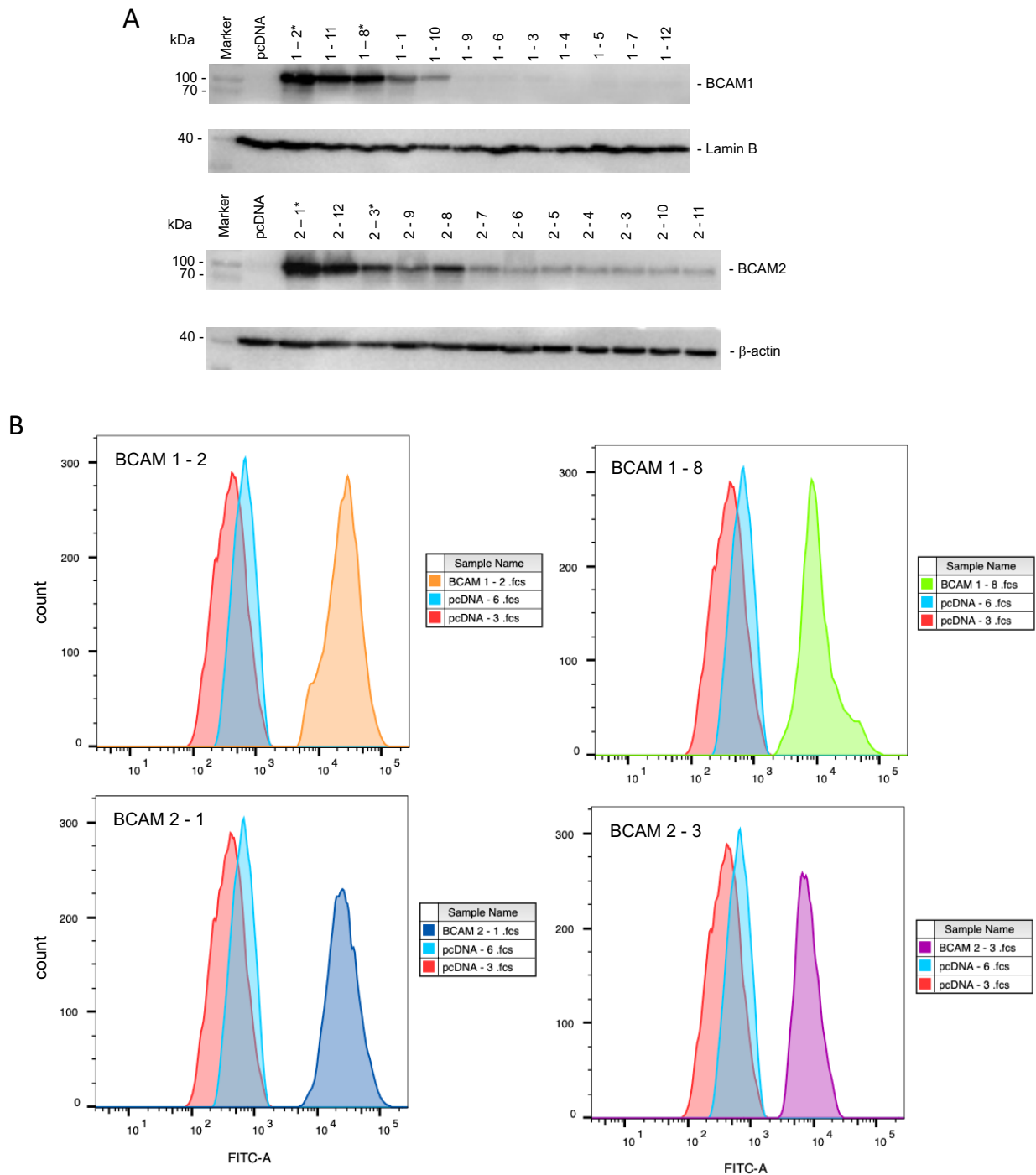


Figure S4: BCAM expression in OVCAR8 clones stably expressing ectopic BCAM1 or BCAM2.

(A) Immunoblot analysis of BCAM. β -actin was included as loading control. *clones used for functional experiments in the present study.

(B) Flow cytometric analysis of BCAM surface expression in OVCAR8 clones stably expressing ectopic BCAM1 or BCAM2. Experimental details were as described in the main text.

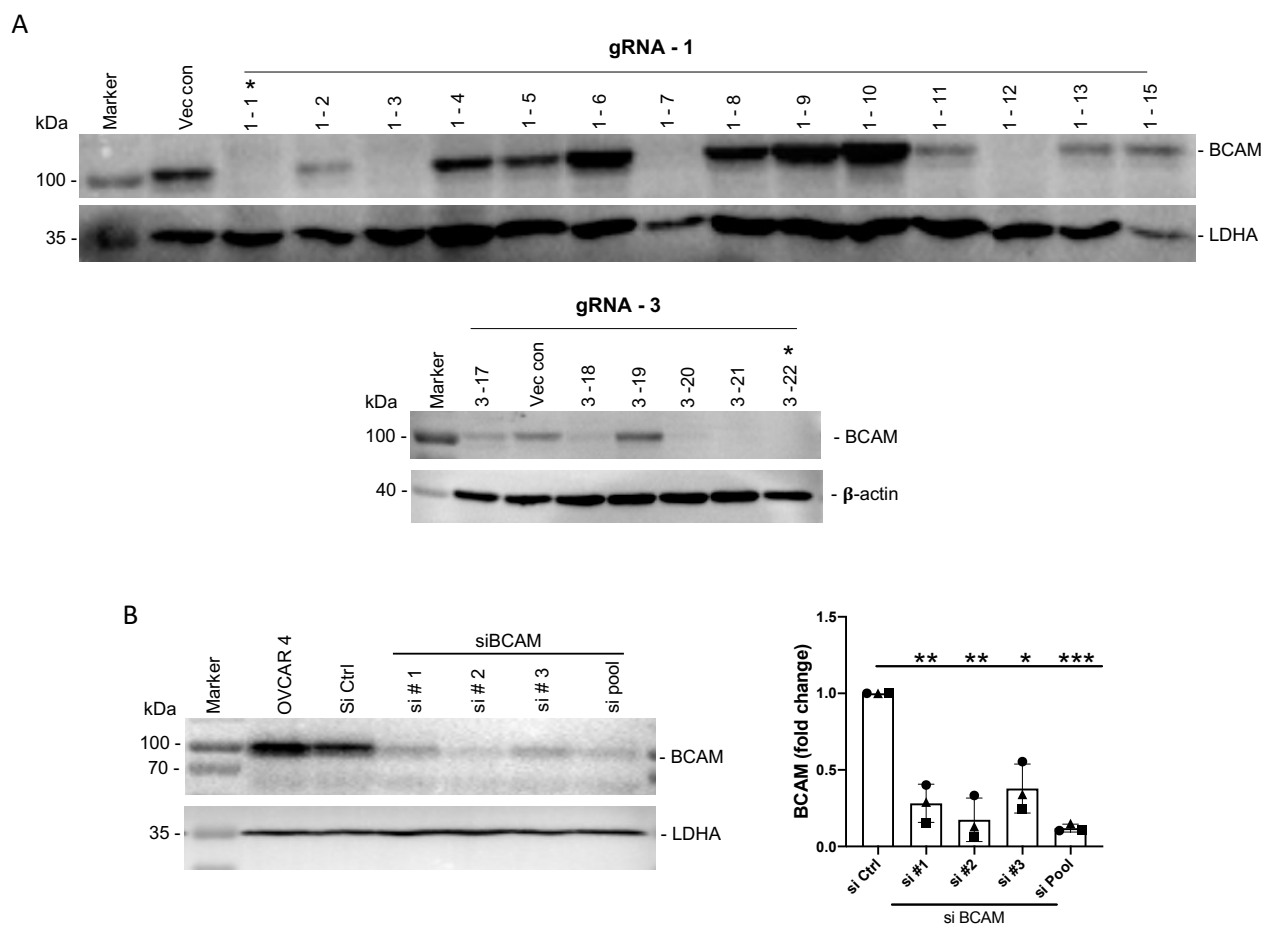


Figure S5: Immunoblot verification of *BCAM* gene disruption and *BCAM* targeting siRNA.

(A) Immunoblot verification of CRISPR-Cas9-mediated *BCAM* disruption in individual OVCAR8 clones. β -actin and LDHA were included as loading controls. Vec con: empty vector control. *clones used for functional experiments in the present study.

(B) Immunoblot analysis of siRNA-mediated inhibition of *BCAM* in OVCAR4 cells. Different siRNAs (si #1, #2, #3) were tested both individually and pooled. si Ctrl: unrelated control siRNA. α -tubulin and LDHA were included as loading controls.

Experimental details were as described in the main text.

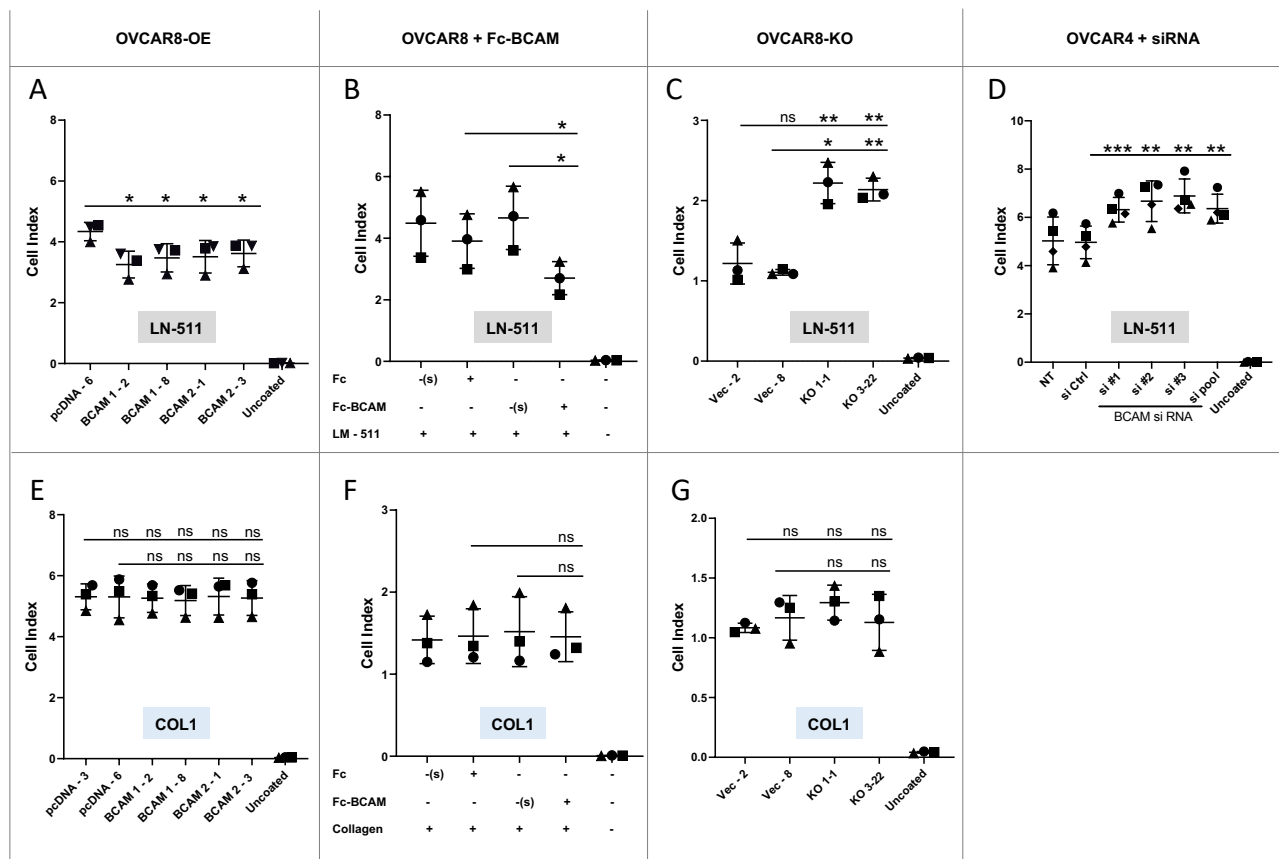


Figure S6. Effect of BCAM on OC cell adhesion to LN-511 and COL1.

Cells were seeded on non-adhesive microplates coated with LN-511 (panels A-D) or COL1 (panels E-G) and cell adhesion was quantified by RTCA.

NOTE: Panels A and B are identical to Fig. 1D. They are included here to allow for a better comparison

(A, E) BCAM-overexpressing OVCAR8 cells (OVCAR8-OE). Clones stably transfected with BCAM1 or BCAM2 (Fig. S4) were compared to cells transduced with the empty expression vectors (pcDNA-3, pcDNA-6).

(B, F) OVCAR8 cells were analyzed in the presence of Fc-BCAM or negative control (Fc). (s): solvent for Fc or Fc-BCAM. The data are based on n=3 biological replicates. *p<0.05; **p<0.01; ***p<0.001; ns, not significant by unpaired t test.

(C, G) OVCAR8 cells with disrupted BCAM gene (OVCAR8-KO) compared to cells transduced with the empty vector (clones Vec-2, Vec-8).

(D) OVCAR4 cells transfected with control-siRNA, 3 different BCAM-siRNAs (#1, #2, #3) or pooled siRNAs (pool). NT: non-transfected cells. Uncoated: cells plated on uncoated dishes.

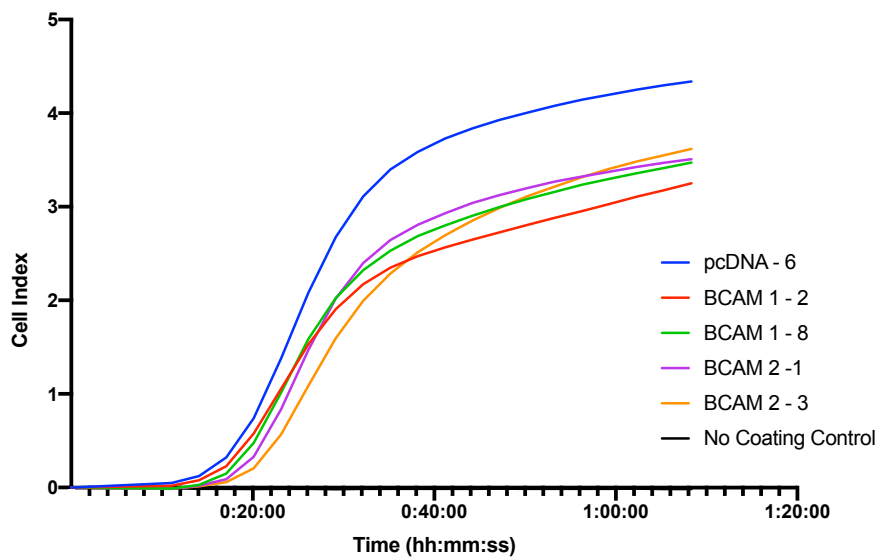


Figure S7. Kinetics of OVCAR8 cell adhesion to LN-511.

Cells were seeded on non-adhesive microplates coated with LN-511 (or uncoated control plates) and cell adhesion was quantified by RTCA as in Fig. S6. Clones overexpressing BCAM1 or BCAM2 were compared to cells transduced with the empty expression vector (pcDNA-6).

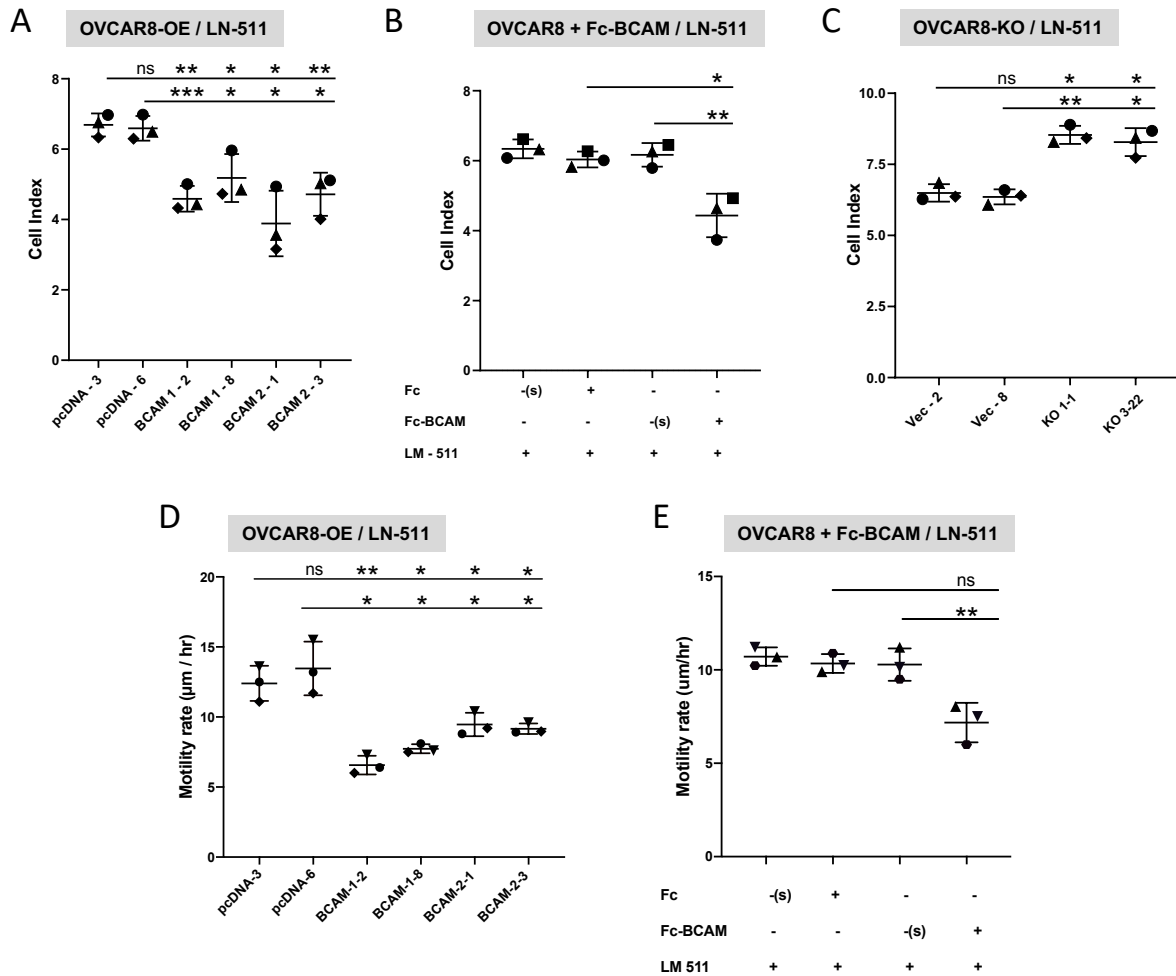


Figure S8. Effect of BCAM on two-dimensional OC cell migration and motility.

NOTE: Panels A and B are identical to Fig. 1E. They are included her to allow for a better comparison.

(A-C) Quantification of cell migration. Cells were seeded on transwell-chamber microplates coated with LN-511 and cell migration was quantified by RTCA.

(A) BCAM-overexpressing OVCAR8 cells (OVCAR8-OE; 2 BCAM1 and 2 BCAM2 clones) compared to cells transduced with the empty vector (2 clones).

(B) OVCAR8 cells analyzed in the presence of negative control (Fc) or Fc-BCAM and plated on LN-511. The data are based on n=3 biological replicates.

(C) OVCAR8 cells with disrupted BCAM (OVCAR8-KO) compared to cells transduced with the empty vector.

(D, E) Quantification of cell motility. The plots show quantifications of non-directional movement of OVCAR8 cells overexpressing BCAM1 or BCAM2 in panel D, or exposed to Fc or Fc-BCAM in panel E. Fluorescently labeled cells were observed for 12 hrs. Positions of cells were tracked to quantify cell motility. For each condition, trajectories were tracked in 5 different fields. “(s)” in panels C and E: solvent for Fc or Fc-BCAM. Data are shown for n=3 biological replicates in each panel. *p<0.05; **p<0.01; ***p<0.001; ns, not significant by unpaired t test.

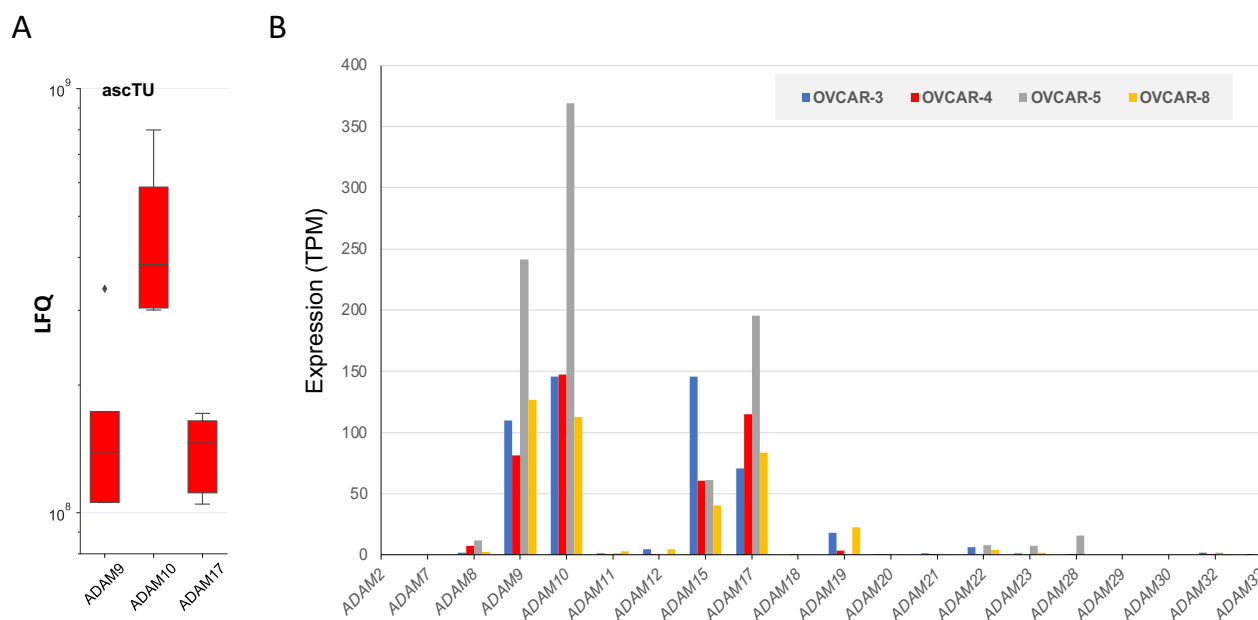


Figure S9: Release of ADAMs by ascTU cells and expression of ADAM genes in OVCAR cell lines.

(A) Proteomic analysis of ADAM proteins in the secretome of ascTU cells (conditioned medium after short-term culture) as previously described (Worzfeld et al., 2018).

(B) Data for OVCAR4, OVCAR5 and OVCAR8 cells were generated by RNA-Seq as described in Sommerfeld et al. (2021). Data for OVCAR3 cells were retrieved from the literature (McCorkle et al., 2021) and included after re-processing of original data, and are therefore not directly comparable to the other datasets.

References:

Worzfeld, T., Finkernagel, F., Reinartz, S., Konzer, A., Adhikary, T., Nist, A., et al. Proteotranscriptomics Reveal Signaling Networks in the Ovarian Cancer Microenvironment. *Mol Cell Proteomics* 2018;17:270-289.

McCorkle JR, Gorski JW, Liu J, Riggs MB et al. Lapatinib and poziotinib overcome ABCB1-mediated paclitaxel resistance in ovarian cancer. *PLoS One* 2021;16(8):e0254205.

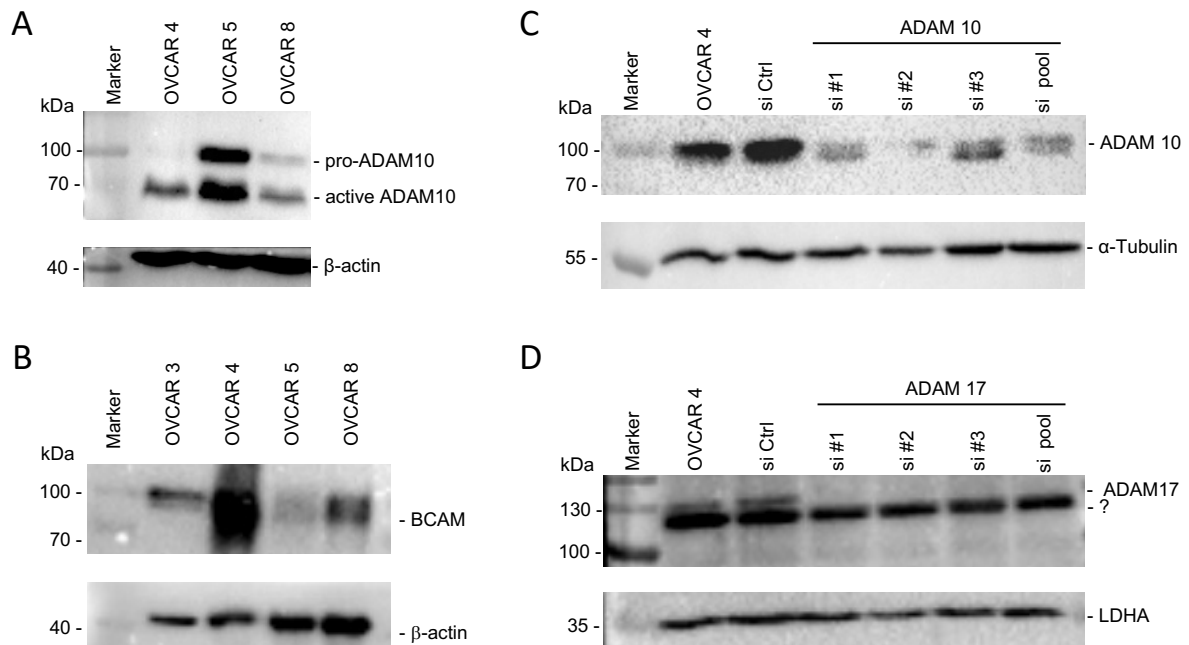


Figure S10: Immunoblot analysis of ADAM10, ADAM17 and BCAM in OVCAR cell lines.

(A) Immunoblot analysis of ADAM10 in OVCAR cell lines. β-actin was included as loading control

(B) Immunoblot analysis of BCAM in OVCAR cell lines. β-actin was included as loading control.

(C, D) Immunoblot analysis of siRNA-mediated inhibition of ADAM10 and ADAM17 in OVCAR4 cells. Different siRNAs (si #1, #2, #3) were tested both individually and pooled. siCtrl: unrelated control siRNA. α-tubulin and LDHA were included as loading controls.

Experimental details were as described in the main text.

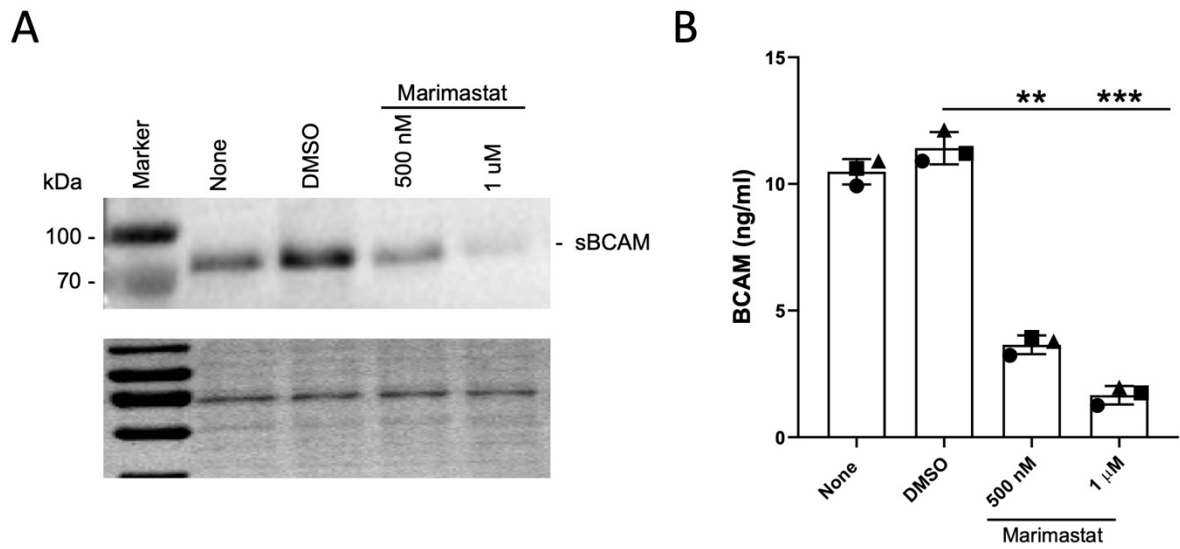


Figure S11: Effect of marimastat on sBCAM production.

(A) Immunoblot of medium from OVCAR4 cells cultured in the presence of different concentrations of marimastat for 24 hrs. The bottom panel shows the membrane after staining with the Pierce Reversible Total Protein Stain Kit as loading control. **(B)** Analysis of BCAM release by OVCAR4 cells treated as in panel A. Cell culture media were analyzed by ELISA 24 hrs after medium change. The plot shows the results of 3 independent experiments. * $p < 0.05$; ** $p < 0.01$; *** $p < 0.001$ by unpaired t test.

A

	enriched 1-2x	enriched >2x
P5	AGQS	CHPY
P4	ACEHIKQRSVY	TW
P3	CFKNPQSV	AHMTY
P2	EHLQS	ACM
P1	CEFHKM	APRY
P1'	FIMQRV	CHLWY
P2'	AIKLQRSTVY	HM
P3'	ADLMQRSTY	GW
P4'	ACEGHPQRST	D
P5'	ADGHLMNPQY	R

B

Site 1 (rec-ADAM10)

L S W S Q * L G G S P
 • • + + • •

Site 2 (rec-ADAM10)

S R D G I * S C E A S
 • • •

Site 3 (TU-sec & rec-ADAM10)

G I S C E * A S N P H
 • • • + • • • •

Site 4 (TU-sec, close to TM-domain)

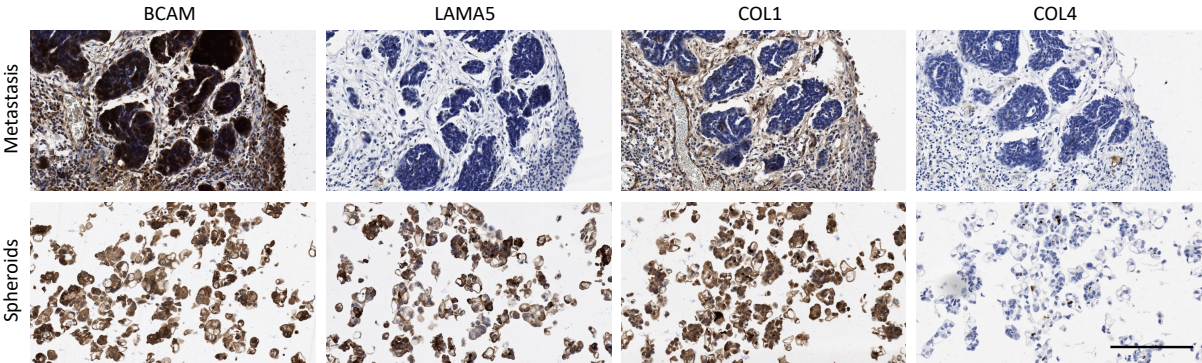
G T V S P * Q T S Q A
 • + • • + • • • • •

Site 5 (TU-sec, next to TM-domain)

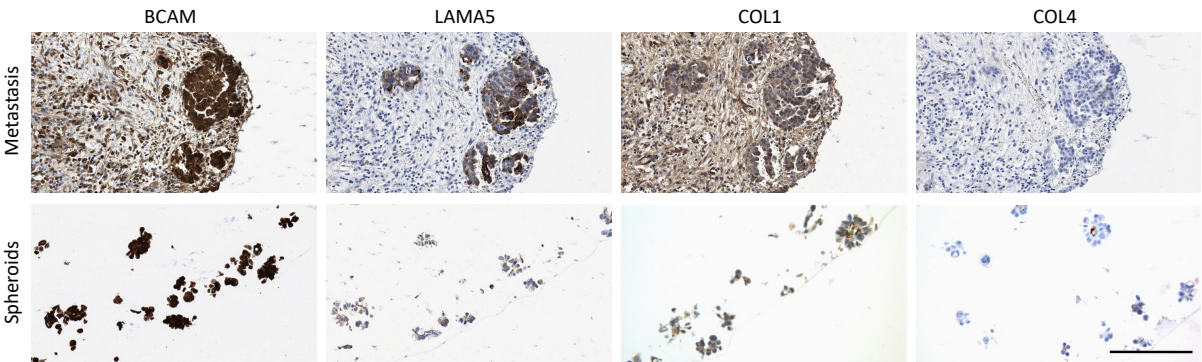
Q T S Q A * G V A V M
 • + • • + • • •

Figure S12: Analysis of ADAM10 cleavage sites in BCAM protein. (A) Preferential amino acids around ADAM10 cleavage sites (between positions -5 and 5). The table integrates data from two published studies using unbiased screening approaches (Caescu et.al. 2009; Tucher et al., 2014) and distinguishes strongly enriched (>2x) and weakly enriched (1-2x) amino acids. **(B)** Matches of cleavage sites 1-5 (see Fig. 2G) with the consensus motif in panel A. +, match with strongly enriched amino acid; •, match with weakly enriched amino acid (as defined in panel A). Note that cleavage at sites 4 and 5 was not observed in the Fc-BCAM fusion protein, probably due to steric hindrance in the hinge region between BCAM and Fc tag.

Patient OC26



Patient OC84



Patient OC122

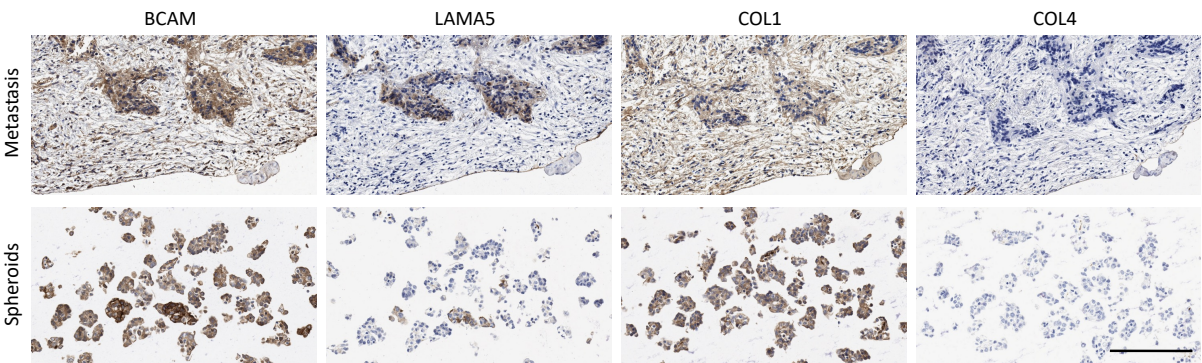


Figure S13: Immunohistochemical analysis of BCAM, LAMA5, COL1 and COL4 in matched samples of metastases and spheroids from ascites of 3 different OC patients.

Paraffin sections from metastases and spheroids from ascites were stained by immunohistochemistry as described in Materials and Methods. Quantifications of the images are shown in Table 2. Scale bar: 200 μ m .

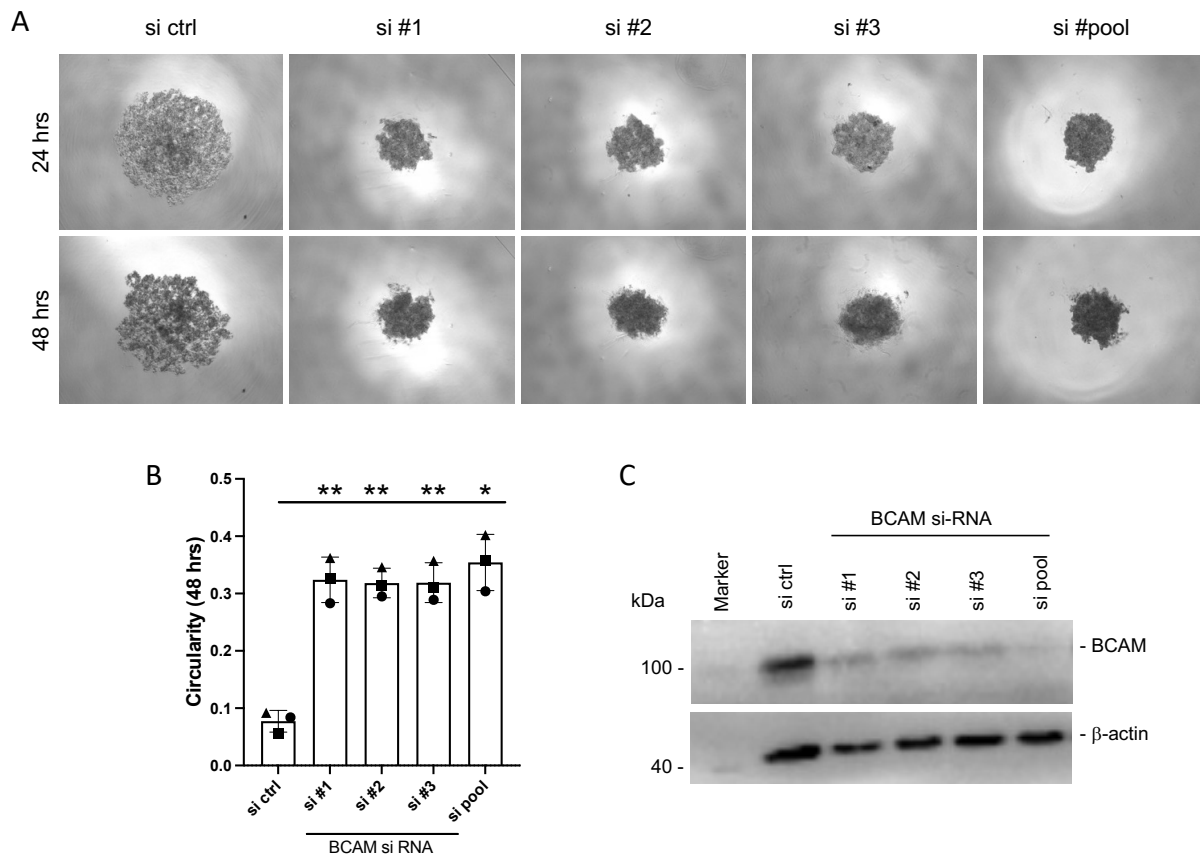


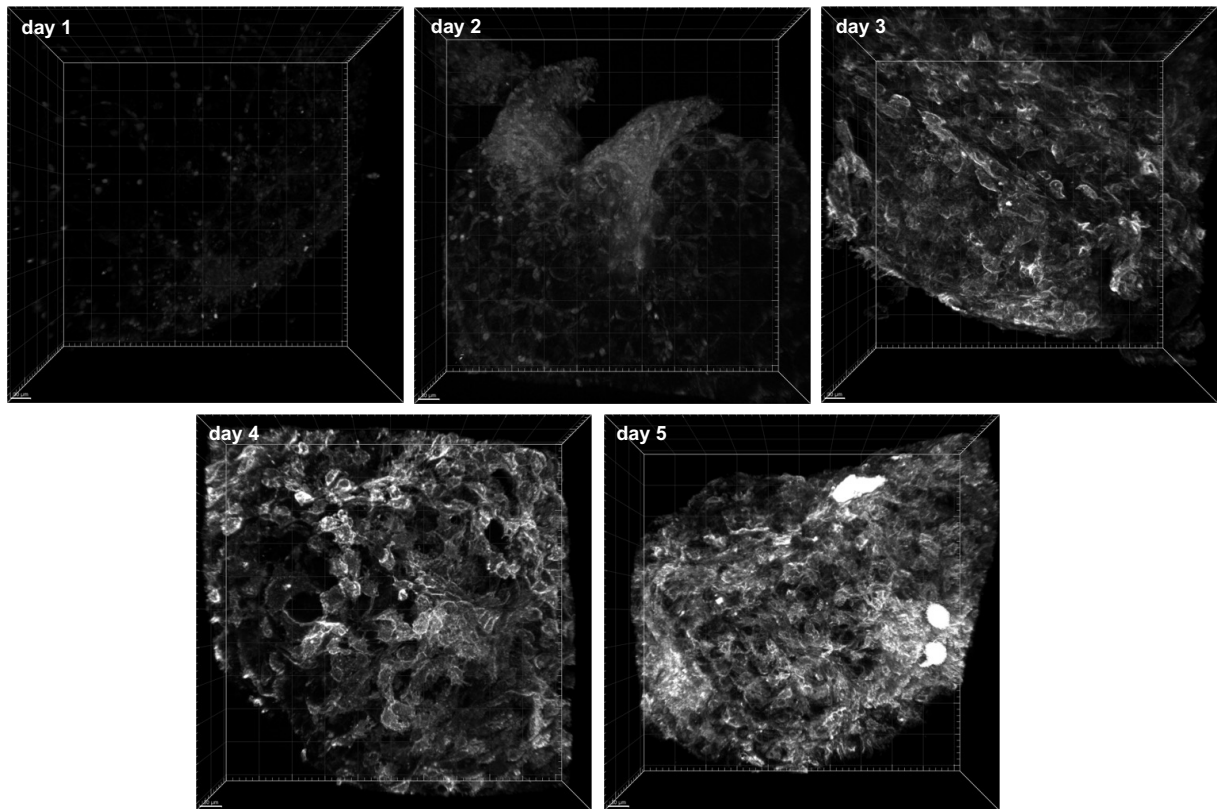
Figure S14: Impact of siRNA-mediated inhibition of BCAM expression on OVCAR3 spheroid formation.

(A) Morphology of spheroids derived from OVCAR3 cells transfected with control-siRNA (si ctrl), 3 different BCAM-siRNAs (#1, #2, #3) or pooled siRNAs (pool).

(B) Quantification of 3 independent experiments. * $p < 0.05$; ** $p < 0.01$ by unpaired t test.

(C) Immunoblot analysis of siRNA-mediated inhibition of BCAM expression in OVCAR3 cells. Different siRNAs (si #1, #2, #3) were tested both individually and pooled. si ctrl: unrelated control siRNA. Experimental details were as described in the main text. β -actin was included as loading control

A



B

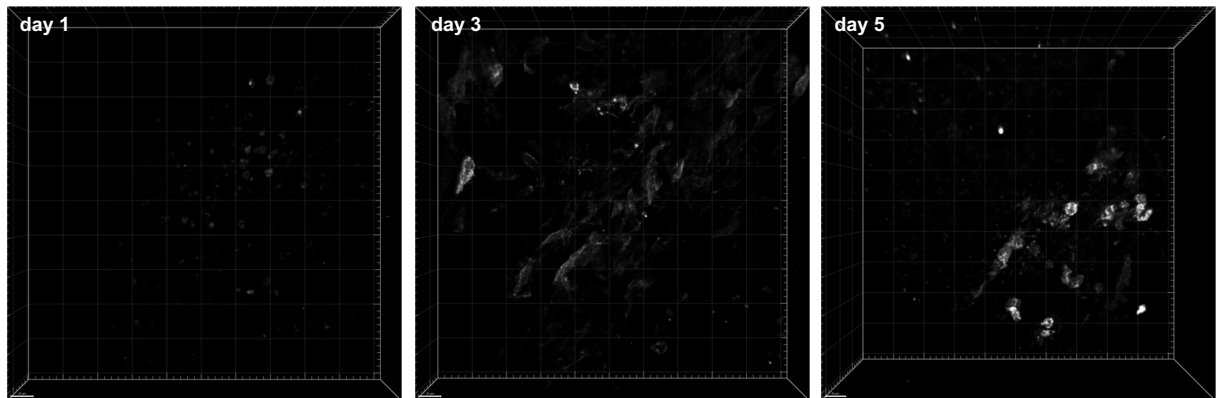


Figure S15: Expression of VCAM1 in mouse omentum at different times of culture *ex vivo* under different culture conditions.

(A) Culture *ex vivo* under standard culture conditions (hyperoxia, 5% regular FCS).

(B) Culture *ex vivo* under adapted culture conditions (hypoxia, delipidized FCS).

VCAM1 (CD106) was visualized (white) by immunostaining followed by multiphoton microscopy as described in Materials and Methods.

Scale bar: 30 μ M.

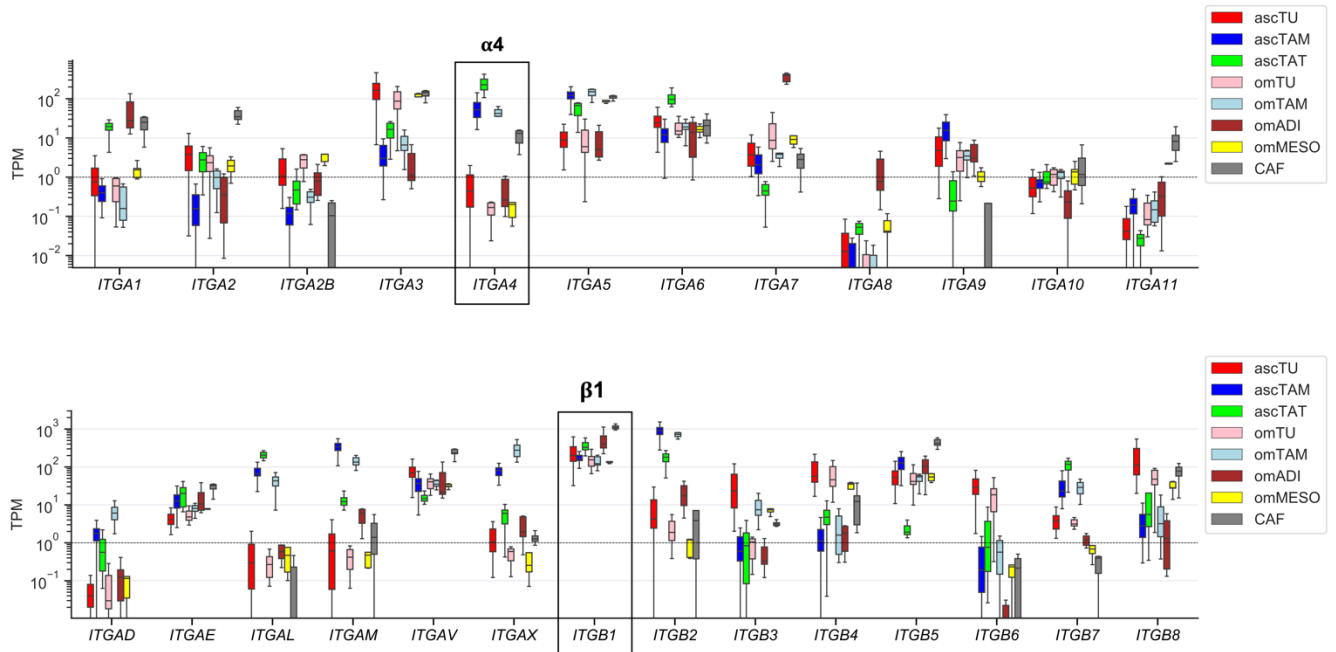


Figure S16: Expression of genes coding for integrin subunits in tumor and host cells of the OC TME.

The plot is based on RNA-Seq data from Sommerfeld et al. (2021)

Framed: integrin $\alpha 4/\beta 1$ (BCAM receptor) subunits.

asc: ascites-derived; om: isolated from omental metastases; TU: tumor cells; TAM: tumor-associated macrophages; TAT: tumor-associated T cells; ADI: adipocytes; MESO: mesothelial cells; CAF: fibroblasts.

Boxplots show medians (horizontal line in boxes), upper and lower quartiles (box), and range (whiskers).

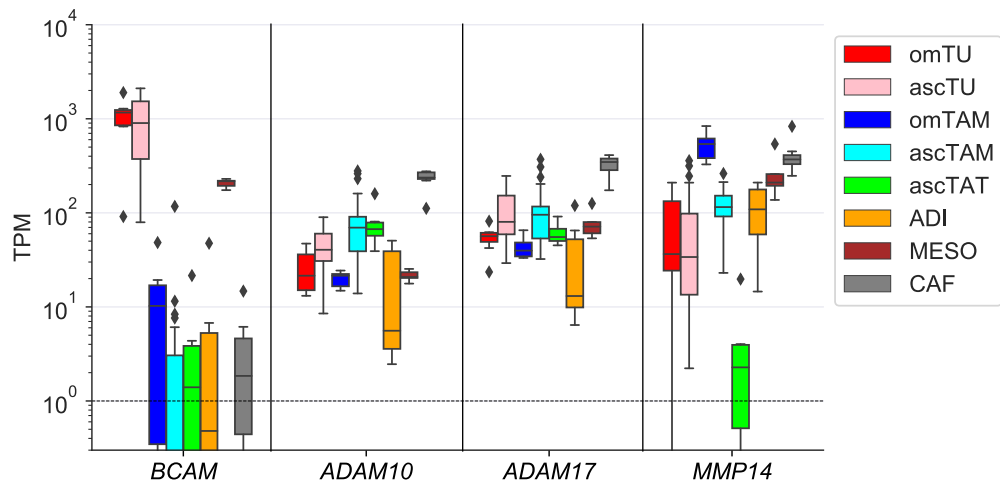


Figure S17: Expression of BCAM and metalloprotease genes in tumor and host cells of the OC TME.

The plot is based on RNA-Seq data from Sommerfeld et al. (2021)

asc: ascites-derived; om: isolated from omental metastases; TU: tumor cells; TAM: tumor-associated macrophages; TAT: tumor-associated T cells; ADI: adipocytes; MESO: mesothelial cells; CAF: fibroblasts.

The plot shows medians (horizontal line in boxes), upper and lower quartiles (box), and range (whiskers).